

# **The practicability of multimodal data fusion for simultaneous EEG-fMRI demonstrated on a cognitive control task**

Submitted for the attainment of the academic degree Master of Science (M.Sc.)  
at the Department of Psychology and the Department of Medicine (Philipps  
University of Marburg)

by: **Malte Rudo Güth** (B.Sc.)

Marburg, May 2018

**Matriculation number:** 2521067

**E-Mail:** maltegueth@gmail.com

**First Instructor:** Dr. Dipl.-Phys. Jens Sommer

(Core Facility for Brainimaging, Department of  
Medicine, Philipps University of Marburg)

**Second Instructor:** Prof. Dr. Dr. Martin Peper

(Neuropsychology Section, Department of  
Psychology, Philipps University of Marburg)

## Abstract

Objective: Multimodal data fusion (e.g., joint Independent Component Analysis, Multiway Partial Least Squares) is a promising approach for the analysis of simultaneously recorded EEG and fMRI data. It allows experimenters to examine common features and adapt multiple perspectives on brain activity. Therefore, data fusion can be applied to provide more convincing results for testing hypotheses. For example, proactive control and early decision-making is often associated with increased efforts for active maintenance of context information in the dorsolateral prefrontal cortex (DLPFC). Yet, optimal performance is often thought to be reached by automatizing behavior and by reducing cognitive effort. Method: To investigate which spatio-temporal signal sources in EEG and fMRI best represent proactive control, this study utilized simultaneous EEG-fMRI recordings and multimodal data fusion to join both methods. Thirteen healthy participants performed an adaptation of the Dot Pattern Expectancy (DPX) task. Results: We found significant activations in a prefrontal-parietal cognitive control network, accompanied by late frontoparietal positivity as well as synchronized theta and alpha oscillations in the EEG. Signal components reflecting frontoparietal positivity following imperative context cues were related to a decrease in voxel clusters in the DLPFC. Moreover, theta oscillations in particular yielded strong co-variation with activation increases in both medial PFC and posterior parietal cortex Discussion: Findings suggest coupling of the BOLD signal and oscillatory as well as amplitude changes triggered by proactive control. This neurovascular coupling and decoupling aided testing the postulated hypotheses. Thus, data fusion was successfully applied to improve interpretations of experimental results and their validity.

## Table of Contents

<b>Acknowledgements .....</b>	V
<b>List of Abbreviations.....</b>	VI
<b>1. Theoretical Background and Aims.....</b>	7
1.1 Promoting psychological research with simultaneous EEG-fMRI .....	7
1.1.1 The benefits of combining EEG and fMRI .....	7
1.1.2 Cognitive efforts of proactive control and optimal performance .....	13
1.2 Multivariate and asymmetric EEG and fMRI data integration .....	16
1.3 Approaches for multimodal data fusion .....	19
1.3.1 Joint and Parallel Independent Component Analysis .....	19
1.3.2 Multiway Partial Least Squares for EEG and fMRI.....	22
1.3.3 Mixed-effects modeling with multimodal regressors.....	23
1.4 Aims of this study.....	24
1.4.1 Investigating mechanisms of cognitive control with EEG-fMRI.....	24
1.4.2 The practicability of multimodal data fusion .....	26
<b>2. Methods.....</b>	28
2.1 Data and code availability statement.....	28
2.2 Participants .....	28
2.3 Experimental Design and Setup .....	29
2.3.1 General Procedure .....	29
2.3.2 DPX Paradigm.....	31
2.4 Data acquisition.....	33
2.4.1 Materials and software .....	33
2.4.2 Experimental protocol for simultaneous recordings .....	35
2.4.3 Recording parameters for EEG and fMRI.....	36
2.5 Unimodal data analysis .....	37
2.5.1 Behavioral Data.....	37
2.5.2 fMRI pre-processing.....	38
2.5.3 EEG pre-processing.....	39
2.5.4 Time-frequency and Parallel Factor analysis .....	42
2.6 Multimodal data analysis.....	43
2.6.1 Asymmetric data integration .....	43
2.6.2 Joint and Parallel ICA .....	45
2.6.3 Multiway Partial Least Squares.....	46

2.6.4	Mixed-effects modeling with multimodal regressors.....	47
3.	Results .....	50
3.1	Unimodal results.....	50
3.1.1	Behavioral results .....	50
3.1.2	EEG results.....	51
3.1.3	fMRI results.....	55
3.2	Multimodal results.....	57
3.2.1	Asymmetric integration.....	57
3.2.2	Joint and parallel ICA.....	59
3.2.3	Multiway Partial Least Squares.....	62
3.2.4	Multimodal mixed-effects modeling .....	63
4.	Discussion .....	65
4.1	General findings .....	65
4.2	A multimodal perspective on the DPX task and proactive control .....	70
4.3	Insights from data integration and fusion.....	71
4.4	Limitations.....	73
4.5	Conclusions .....	75
5.	References .....	77
	Appendix A: Forms and participant information.....	LXXXIX
	Appendix B: Interviews, protocol and pretest .....	XCV
	Appendix C: Behavioral data.....	CI
	Appendix D: Supplementary ERP data .....	CIV
	Appendix E: Supplementary multimodal correlations .....	CVI

## Acknowledgements

First and foremost, I want to thank José C. García Alanis and Peer Herholz. Both of them have been training me for years not just in their respective fields, but in many disciplines of scientific research including psychology, cognitive neuroscience, EEG, MRI, statistics and programming. This project, which fittingly is about bringing together two of the major methodologies in cognitive neuroscience, was only possible, because of the time, trust and energy you invested in me. If it were not for you, I would have missed out on amazing opportunities like visiting conferences, joining an open science community, not to mention my PhD student position. My application would have read remarkably worse if you had not stayed up until early in the morning to proofread my writing. You have been and to some extent will always remain my mentors.

Next, I want to thank my instructors on this thesis, Jens Sommer and Martin Peper. Like Peer and José, you have been teaching me for years and trusted me with this task, although the idea might have seemed farfetched or too extensive. I would have failed early on if you had not given me access to your labs. More than that, in almost any project you involved me in one of your primary concerns was to provide me learning opportunities. Thank you for your advice, especially when it was time to draw a line and finish this thesis.

I also want to extend my gratitude to the students of the cognitive and computational auditory neuroscience group as well as Christoph Vogelbacher and Jan Thiele. Jan has been a great supporter and knew how to keep me motivated. Christoph was always generous with his time when I needed help and proved his patience during my beginnings in learning how to program. So did the others when they endured sitting through the prolonged talks I gave on this project in our weekly meetings and when they offered valuable feedback. Thanks to you my work hopefully has become more structured and comprehensible. Thank you, Rebekka, Mirjam, Bene, Cecilia, Klara, Caro, Jan Otto, Jacky, Chrissi, Marie and Michael. I'm looking forward to reading all of your theses.

## List of Abbreviations

<b>ACC</b>	anterior cingulate cortex
<b>AIC</b>	Akaike Information Criterion
<b>AX-CPT</b>	AX continuous performance task
<b>BCG</b>	ballistocardiogram
<b>BEM</b>	boundary element method
<b>BOLD</b>	blood oxygenation level dependent
<b>DLPFC</b>	dorsolateral prefrontal cortex
<b>DMC</b>	Dual Mechanisms of Cognitive Control
<b>DPX</b>	dot pattern expectancy
<b>ECG</b>	electrocardiography
<b>EEG</b>	electroencephalography
<b>ER</b>	error rate
<b>ERP</b>	event-related potential
<b>ERSP</b>	event-related spectral perturbation
<b>EPI</b>	echo-planar imaging
<b>fMRI</b>	functional magnetic resonance imaging
<b>FWE</b>	familywise error
<b>GA</b>	gradient artefact
<b>GFP</b>	global field power
<b>GLM</b>	general linear model
<b>HRF</b>	hemodynamic response function
<b>ICA</b>	independent component analysis
<b>IFG</b>	inferior frontal gyrus
<b>jICA</b>	joint independent component analysis
<b>LFP</b>	local field potential
<b>MFG</b>	middle frontal gyrus
<b>MNI</b>	Montreal Neurological Institute
<b>MUA</b>	multi-unit cell activity
<b>N-PLS</b>	multiway partial least squares
<b>PARAFAC</b>	parallel factor analysis
<b>PCA</b>	principle component analysis
<b>PFC</b>	prefrontal cortex
<b>pICA</b>	parallel independent component analysis
<b>PCG</b>	precentral gyrus
<b>PSI</b>	proactive behavioral shift index
<b>RT</b>	reaction time
<b>SMC</b>	supplementary motor cortex
<b>sMRI</b>	structural magnetic resonance imaging
<b>SVD</b>	singular value decomposition
<b>TR</b>	repetition time
<b>WAIS-IV</b>	Wechsler Intelligence Scale for Adults fourth edition
<b>WM</b>	working memory

## 1. Theoretical Background and Aims

### 1.1 Promoting psychological research with simultaneous EEG-fMRI

#### 1.1.1 The benefits of combining EEG and fMRI

Neuronal activity of cognitive or affective processes can be studied from a large variety of measures, thereby revealing unique perspectives on brain activation. Electroencephalography (EEG) mainly reflects the summation of postsynaptic potentials in pyramid cells with a similar orientation at a cortical level (Luck, 2005). Through sufficient coverage of the head surface with electrodes, synchronized activity of these cells can be recorded at a high temporal resolution. Being able to observe changes of electrical potentials on a scale of milliseconds, is the reason EEG is often chosen as a direct link to cortical activity. However, EEG is recorded at a relatively large distance from cells and considerable portions of the original activity spikes fall off outside a 50  $\mu\text{m}$  radius (Henze, Borhegyi, & Csicsvari, 2000). In addition, shorter spike durations with high-frequency oscillations far above 200 Hz decrease the odds of spike summation. The measurement on the skull surface prevents higher frequency signals from affecting the EEG and the recorded signal predominantly consists of slower Local Field Potentials (LFP).

Unlike in measuring of action potentials of single cells and multi-unit activity (MUA), LFP are dependent on temporal and spatial summation of potentials. For this reason, EEG only represents the summation of surface potentials. Furthermore, despite advances in signal source estimation (e.g., Lei et al., 2011), its spatial resolution is severely limited. The difficulty to pinpoint neuronal sources and to reconstruct the original flow of current of a given potential on the head surface is referred to as the inverse problem (Koles, 1998; Christophe Phillips, Rugg, & Friston, 2002). Source estimation analyses, as a tool of uncovering dipoles and brain areas most likely responsible for event-related electric voltage fluctuation at the surface, rely on several assumptions. Among others these include largely homogenous electric conductivity and resistance throughout brain tissues, a linear mixing process of electric signals, a mathematical approximation of the orientation and fluctuation of the current as well as a fixed template for the anatomical brain structure underlying these approximations (Cuffin, 1998; Koles, 1998; Sanei, Chambers, Sanei, & Chambers, 2013; Xu, Xu, & He, 2004). Whereas the lack of knowledge on individual test subjects' brain can be compensated by letting structural magnetic resonance imaging (sMRI) inform source estimations (Christophe Phillips, Rugg, & Friston,

2002; Whittingstall, Bartels, Singh, Kwon, & Logothetis, 2010), other assumptions remain improbable to be met.

While the electromagnetic fields measured in the EEG directly relate to neuronal activity, MRI is taking advantage of differing magnetic properties of nuclei within tissues of the human brain to produce images of different spatial resolutions (Huettel, Song, & McCarthy, 2004). Functional magnetic resonance imaging (fMRI) for instance is based on blood oxygenation. Due to a powerful static magnetic field ( $B_0$ ), the magnetic moment of the atoms in the observed tissue adapts an orientation parallel or anti-parallel to the magnetic field. Through a high frequency coil placed above the subject, a controlled manipulation of the nuclei's magnetic moments via radiofrequency pulses causes the nuclei's spins to change their orientation. Superposed on the  $B_0$ -field, magnetic gradients fields form a new magnetic field and enable the successive acquisition of slices, which taken together form a 3D volume of the subject's head. Relating the signal to a certain spatial point within a probe is a basic principle of most MRI techniques. In fMRI specifically the repeated assessment of hemoglobin in the brain and its location in the brain is used as an indicator of brain activation. The hemodynamics assessed by fMRI is linked to the oxygen consumption of neuron populations. Thus, fMRI results show the flow of oxygenated blood in accordance to the metabolic demands of brain regions (Logothetis & Wandell, 2004). For this reason, the signal used in fMRI is referred to as blood oxygenation level dependent (BOLD). With the idea in mind that brain regions supporting a cognitive process consume more oxygen, the BOLD is thought to vary in correspondence to increased synaptic current flow, shifted by a delay in form of the hemodynamic response function (HRF). Instead of an instantaneous increase in accordance to cognitive processes, the BOLD reacts with an initial dip, followed by a peak and a decline after multiple seconds. The exact shape of the HRF depends on many factors, such as measurement parameters and brain regions. In order to differentiate consecutive peaks in the continuous BOLD signal, thus, requires a well-designed experiment with enough time between modeled events.

Since the BOLD signal is a correlate of neuronal activity (Rosen, Buckner, & Dale, 1998), it is regarded as a rather indirect measure. Plus, it is confined to a low temporal resolution on a timescale of seconds and is less flexible in terms of modeling complicated, quick stimulus sequences. In return, functional BOLD signals offer a higher spatial resolution compared to other imaging methods, while still operating entirely non-invasively. As such, MRI is a powerful method for studying the spatial dynamics of brain activation and for gaining anatomical information without harming patients or test subjects.

Comparing the two methods, it becomes apparent that EEG and MRI complement each other well. Together they combine next to ideal temporal and spatial resolution (Debener, Ullsperger, Siegel, & Engel, 2006). Both measures require an in depth understanding about their signals' physiological properties, in order to draw reasonable conclusions from experimental results. This is because their respective limitations often decrease the conclusions' validity (Turner, Rodriguez, Norcia, McClure, & Steyvers, 2016). Instead of relying on a selective view with a single method, simultaneous or separate recordings provide multifaceted insights into brain activation. In principle, a setup for parallel EEG-fMRI experiments entails that subjects are tested at least twice using one test for each method separately (Herrmann & Debener, 2008). This type of experiment is easier to perform compared to concurrent recordings. More importantly, it ensures higher data quality, since EEG and MRI, in their basic configurations, inflict severe measurement artefacts on each other when combined (Allen, Josephs, & Turner, 2000; Bénar et al., 2003; Iannotti, Pittau, Michel, Vulliemoz, & Grouiller, 2014; Ihalainen et al., 2015). The two most impactful artefacts for the EEG are caused by the magnetic gradients during volume acquisition (i.e., gradient artefacts; Yan, Mullinger, Brookes, & Bowtell, 2009) and electromotive forces that are active as a result of moving electric charges within the magnetic field (i.e., ballistocardiac artefacts; Iannotti et al., 2014; Mullinger, Havenhand, & Bowtell, 2013).

Gradient artefacts (GA) are largely stationary and periodic changes in the EEG signal. They are most striking due to their high amplitude. Moreover, their characteristic shape and occurrence at a rate parallel to the repetition time (TR) set in the echo-planar imaging (EPI) sequence make them easy to spot. By contrast, ballistocardiogram (BCG) artefacts arise from small movements of electric charges within the magnetic field (Mullinger, Havenhand, et al., 2013; Yan, Mullinger, Geirsdottir, & Bowtell, 2010). Most notable in terms of severity of EEG signal distortion are vibrations resulting from the MRI's helium pump (Rothlübbers et al., 2015). These are handily prevented by temporarily turning off the helium pump during simultaneous data acquisition. Yet, smaller motions, such as subject movement, also account for BCG artefacts. Displacements of electrodes due to cerebral blood flow, head motion and muscle contraction pose a serious problem to the data quality. Due to its electrically conductive properties, even pulsatile blood flow in intracranial and large cranial arteries can account for this non-stationary, aperiodic and unobtrusive artefact group in the EEG.

Conversely, EEG-related artefacts in the MRI data can be prevented by a sensible experimental setup. To preserve the magnetic fields' homogeneity within the scanner room, the utilized EEG system has to be made from exclusively para- or diamagnetic materials. Generally,

appropriately shielding electrode leads and other materials as well as choosing MRI-compatible equipment is essential to the data quality, but even more important to the subject's safety (Lemieux, Allen, Franconi, Symms, & Fish, 1997). Attaching electrodes to a subject in the scanner environment creates risks, such as electrodes heating up and causing severe burn injuries depending on the EPI sequence and the strength of the magnetic field (Yeung, Susil, & Atalar, 2002).

In spite of these artefacts and safety requirements, simultaneous compared to separate EEG-fMRI recordings yield the greater potential. While free from artefacts, separate recordings do not represent identical psychological processes in test subjects. No brain activation at a given time point in a given experiment can be perfectly replicated. Using human subjects implies that the dependent variable (i.e., physiological signal variation) is influenced by several individual processes, which experimenters are unable to account for. Even when performing identical experiments with the same experimental protocol, the timelines of signal changes in the two experiments eventually diverge. As a consequence, matching time series data from these recordings might work on a level of matching trial succession, but not on a level of neuronal activity. Thus, in separate EEG-fMRI it is ill-advised to relate for instance single-trial EEG and fMRI signals, because they were acquired successively instead of concurrently. Other problems, such as training effects, habituation or fatigue, further add to the limitations of separate recordings.

Perhaps even more notable than the complementing spatial and temporal resolutions in combined EEG and fMRI is the benefit stemming from their physiological relation. Variation in LFP often bears more similarity to changes in BOLD than to recordings of single cell activity or MUA (Logothetis, Pauls, Augath, Trinath, & Oeltermann, 2001). At the same time, it is irrefutable that EEG and fMRI represent brain activity from two very different perspectives. Considering their physiological basis, it seems plausible that modulations across experimental conditions of BOLD and EEG activity do not align all the time (Im, Jung, & Fujimaki, 2005; Nunez & Silberstein, 2000). Whereas EEG signals only show the result of multiple, non-linear activity summations across cortical layers, changes in the BOLD signal reflect variations of oxygen concentration in different brain regions over time.

The fact that the two signals do not vary identically can be regarded as an upside and a downside to concurrent EEG and fMRI recordings. For one, non-coinciding variation of neuronal activity and cerebral blood flow, also referred to as neurovascular decoupling, could be seen as impeding to the validation of a result. If the multimodal results do not correspond, this might shed doubt on a significant finding, which is discovered in one method but not the

other, although the one significant finding might still be meaningful. However, when relating, for instance, event-related potentials (ERP) to functional contrasts, both neurovascular coupling itself and changes in this coupling would yield the entirety of results to be more meaningful. In addition, information from both sides aid the interpretation and integration of results into the greater theoretical background. Here, neurovascular decoupling might provide information as relevant as neurovascular coupling (Rosa, Daunizeau, & Friston, 2010). Decoupling could be merely the result of failed signal detection or it could be unrelated to experimental conditions. However, it could also be attributed to pathological characteristics (Schridde et al., 2008).

Lastly, finding discrete variances in EEG and fMRI data can be regarded as a great advantage to single recordings, since it supports statistical predictions. Capitalizing on a larger variety of physiological signals aids predictive modeling by, for instance, either constraining or enriching a single signal's prediction with the other (Turner et al., 2013; Turner et al., 2016; Turner, Sederberg, Brown, & Steyvers, 2013). Multiple investigations from Turner et al. (e.g., Turner, Forstmann, et al., 2013; Turner et al., 2016; Turner, Sederberg, et al., 2013) revealed a significant advantage of multimodal predictors as compared to single EEG or MRI regressors. Hence, integrating the two signals holds the potential to achieve a better understanding of how brain activity relates to behavior. This advantage can hardly be undervalued, because the weak correlations of functional or electrophysiological findings to a subject's behavior have often been puzzling as to how otherwise promising experimental results can be interpreted. Paying tribute to the fact that the measures used in these predictions only make up a limited part of brain activity, a joint approach opens up the possibility of testing the predictive value of multiple regressors.

As a result, approaches for combined EEG-fMRI recordings allow analyzing shared and discrete signal variation (see **Figure 1**) in the respective data sets (Herrmann & Debener, 2008). Highlighting neurovascular coupling and decoupling promises new insights for the study of physiological foundations of EEG and fMRI as well as opportunities for testing hypotheses in the experimental investigations of cognitive processes. For example, in decision-making research combined EEG-fMRI has already been applied in a framework for outlining how spatio-temporal measures derived from both methods can change as a function of increasing task complexity and how they can predict performance in a delay discounting task (Kyathanahally, Franco-Watkins, Zhang, Calhoun, & Deshpande, 2016). Albares et al. (2014) were successful in a similar demonstration of the benefits from combined analyses for EEG and fMRI. By relating early ERPs associated with visual attention (i.e., N170) and increased alpha band power over the medial prefrontal cortex with increased BOLD responses in the

supplementary motor cortex, they have provided evidence for the neural circuitry coupled with precise temporal dynamics underlying flexible behavioral correction to unforeseen changes of environmental demands for goal-achievement.

Consequently, enriched neuronal correlates enabled a more sophisticated discussion and interpretation of experimental results. These improvements might be rendered less appealing by considering the increased effort necessary for both experimental setups and analyses. Yet, they have major relevance to all fields studying brain functions, which justifies their expenses.

Generally in biological psychiatry and psychology, neuroscientific methods like EEG and fMRI are applied to study mental processing. For a psychological phenomenon, which is not yet fully understood, researchers struggle to identify physiological correlates, which they do not fully understand either. This basic dilemma can also be found in clinical studies of biomarkers. In order to separate groups of patients and healthy controls or to improve the accuracy of prognoses for patients, clinical researchers strive to detect reliable biomarkers of a specific pathology (Fu & Costafreda, 2013; McGorry et al., 2014). Still, in clinical research these biomarkers, be it in EEG, sMRI, fMRI or in-vitro studies, of either pathological symptoms or higher cognitive functions, tend to be unprecise (Venkatasubramanian & Keshavan, 2016). This can be attributed to small sample sizes, symptom overlap in patient groups, a focus on purely symptom-correlated markers, poor methodology, fundamentally insufficient

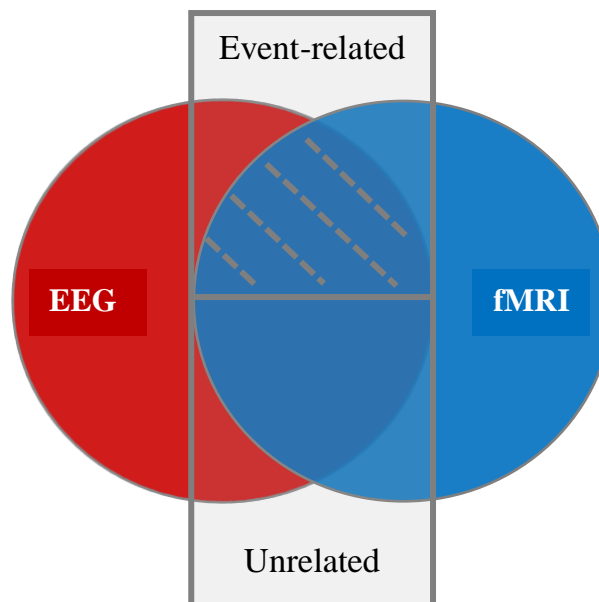


**Figure 1** Illustration of variance proportions in EEG and fMRI signal attributed uniquely to EEG (red) or fMRI (blue) and event-related neurovascular coupling (striped) or event-unrelated coupling (not striped shared area) adapted from Herrmann and Debener (2007).

understanding of the involved cognitive processes or any number of additional flaws (Sprooten et al., 2017).

A reliable way to combat these issues is to refine methodologies by either perfecting existing procedures, such as pre-processing or higher statistical analyses, taking advantage of emerging approaches for handling vast amounts of data (i.e., machine learning) or by enriching study designs with multiple methods (Fu & Costafreda, 2013). Through these innovations the consistency of clinical and non-clinical, neuronal correlates can be assessed and evaluated. Hence, combining methods is not only a promising scientific paradigm shift for basic research, but also for clinical applications. Better characterizing the sensitivity and discriminatory power for specific pathologies or their development might allow for more precise prognoses (Nouretdinov et al., 2010), predicting treatment responsiveness (Ances et al., 2005; Robinson et al., 1999) or even more effective screening methods (Johnstone, Ebmeier, Miller, Owens, & Lawrie, 2005) in psychiatry.

### 1.1.2 Cognitive efforts of proactive control and optimal performance

In the aforementioned study of neuronal processes underlying the delay discounting task by Kyathanahally et al. (2016) multimodal research has been effectively utilized to characterize cognitive control as employed in this particular experiment. Cognitive control can be beheld as the ability to adaptively recruit cognitive resources and subordinate executive functions in a manner that is beneficial and compatible to a person's goals (Braver, 2012; Gray, 2004). In delaying an expected reward, the gain can be maximized, which might be momentarily dissatisfying, but more remunerating in the long run. To suspend the need for reward, prepotent reactions need to be inhibited, while keeping in mind context information about how behavior and rewards can be optimized. In their theoretical framework Dual Mechanisms of Cognitive Control (DMC) Braver, Gray and Burgess (2007) postulated two distinct modes, in which cognitive control operates, to explain inter- as well as intra-individual variability of working memory (WM) performance: 1) proactive control (i.e., anticipatory planning, early information selection, context-driven) and 2) reactive control (i.e., flexible behavioral adaptation, late correction, stimulus-driven).

There is substantial evidence that proactive control, as the mode that optimizes behavior, is the more resource demanding and puts a larger load on WM (Braver, 2012; Braver, Cole, & Yarkoni, 2010; Braver, Reynolds, & Donaldson, 2003). Past research points to the DLPFC to be the core structure of both main control strategies. In particular, proactive control as opposed to reactive control tendencies are thought to be supported by increased activation of the DLPFC

(Barbey, Koenigs, & Grafman, 2013; Lopez-Garcia et al., 2016). While also involved in reactive control through information updating, the more prominent region in this case should be the anterior cingulate cortex (ACC) rather than the DLPFC. Unlike proactive control, reactive control is meant to integrate unexpected events and react to conflict detection. By modulating the DLPFC's control resource recruitment it is postulated to trigger updating and thus motor response adaptation. These are prime tasks of the ACC (Barch et al., 1997; Carter, Braver, Barch, & Botvinick, 1998; MacDonald, Cohen, Stenger, & Carter, 2000). In the DMC account the authors point to dopaminergic pathways ascending from midbrain dopamine cells to cingulate and dorsolateral parts of the prefrontal cortex. Phasic dopaminergic activity is often assumed to support reinforcement learning (Montague, Dayan, & Sejnowski, 1996). As such, it is also thought to enable reward predictions (Roesch, Calu, & Schoenbaum, 2007) and to have a potency for modulating goal or reward related behavioral responses. Triggered by unexpected events, a phasic burst of dopamine might activate information updating in the ACC and DLPFC, as involved in many cognitive control paradigms (D'Ardenne et al., 2012). Therefore, the DMC describes a balance of tonic and phasic dopaminergic activity driving its control strategies (Braver, 2012; Braver et al., 2007). Initial phasic bursts trigger updating in WM after the presentation of a goal-relevant stimulus. These bursts are thought to be particularly important to reactive control. In the case of proactive control, weak tonic activation is supposed to follow the initial bursts, since context maintenance is more essential to this control strategy.

The DLPFC is linked to an abundance of functions all similar in the cognitive effort they require, be it attentional control or WM (Arnsten & Rubia, 2012; Barbey et al., 2013). According to the DMC account, it is responsible for a gating mechanism, first taking in new information imperative to behavior and then protecting it against interference or temporal decay before goal attainment. Proactive control, being based entirely upon early predictions, would therefore be more reliant of the DLPFC's maintenance of context information. This is further expanded in the DMC by postulating a biasing path from the prefrontal cortex over the supplementary motor cortex (SMC) and primary motor cortex (i.e., precentral gyrus) connecting it to the associative parietal cortex. Here, response tendencies can be primed in order to facilitate behavioral optimization (Braver, 2012; Braver et al., 2007).

However, conceptually, proactive control is intended to rely on context information with a high predictive value and goal relevance. Therefore, decisions can be made at an early point and outcomes are maximized (Braver, 2012). Further, as classic theories of motor control hypothesized (e.g., Feldman, 1986), optimal behavior in relation to cognitive resources is

achieved through automatization and reduction of conscious effort. According to a theory of optimal motor control (Emanuel Todorov & Jordan, 2002; Emmanuel Todorov & Jordan, 1889) and equilibrium point control (Bizzi, Hogan, Mussa-Ivaldi, & Giszter, 1992; Feldman, 1986), adding prefrontal control to a routine task execution in a highly predictable environment is detrimental to the performance. The involvement of the prefrontal cortex disrupts automatic control loops, which would act faster on their own account. Still, considering proactive behavior that requires remembering a complex plan or information sequence necessary for task performance, it becomes apparent that proactive control cannot be a unitary construct. Instead, it might constitute an underlying pattern of how predictions form our behavior in the long-term, but can be executed in a resource demanding or automatized fashion.

Investigating this hypothesis is a challenging research undertaking, since a wealth of information is needed. To test the involvement of prefrontal structures associated with cognitive control, such as the DLPFC and ACC, spatial data are needed. Furthermore, the exact time course and identification of goal-relevant information is best highlighted in ERPs and changes in oscillatory synchronization. To test if a subject forms a decision at an early point of task performance, visual potentials of information selection as the N1 or P2 (Chen et al., 2014; Kirmizi-Alsan et al., 2006) as well as later positive potentials connected to WM updating (Barcel & Cooper, 2017; Mento, Tarantino, Vallesi, & Bisiacchi, 2015; Polich & Criado, 2006) in response to context information could be analyzed. Proactive control, which is exerted by first taking in information into WM and then maintaining it via a dopaminergic gating mechanism (Braver et al., 2007), can likely be studied through observing these correlates of maintenance and updating information processing in WM (Polich, 2007; Polich & Criado, 2006).

In addition to these ERPs, event-related spectral perturbation (ERSP) in the alpha (i.e., 8-12 Hz) as well as theta (i.e., 4-7 Hz) spectrum lend insight into synchronization of cognitive resources to support behavioral planning and correction (Griesmayr et al., 2014; Hwang, Ghuman, Manoach, Jones, & Luna, 2016; Murias, Swanson, & Srinivasan, 2007). Their exact function can further be assessed by, for instance, adding spatial data coupled to the onset of oscillatory synchronization (Gonçalves et al., 2005; Jann et al., 2009). To be more precise, increased occurrence of the theta frequency band over the middle section of the prefrontal and posterior parietal cortex is supposed to aid the maintenance of information and early behavioral planning (Bickel, Dias, Epstein, & Javitt, 2012; Voytek et al., 2015). Hence, theta power might support the intake and maintenance of an imperative context that has a high potency for triggering decision-making through synchronizing activity in the aforementioned network

(Cavanagh & Frank, 2014; Cavanagh & Shackman, 2015). At the same time, alpha suppression should be observed, as frontal alpha is also involved in cognitive control, but rather in a tonic modulation of neuronal excitability (Griesmayr et al., 2014; Hwang et al., 2016; Sadaghiani & Kleinschmidt, 2016). Plus, alpha suppression is often associated with response preparation and anticipation of a stimulus (Bickel et al., 2012).

Concluding from these theoretical considerations, clarifying how cognitive control, in particular proactive control, governs behavior represents a promising research opportunity for joining EEG and fMRI data. It is perfectly suited to provide more precise neuronal correlates of cognitive processing. What remains to be determined is the choice of analysis. Enriching available data most likely entails increased computational effort, complicating the search for the best suited statistical modeling.

## 1.2 Multivariate and asymmetric EEG and fMRI data integration

Despite the short time combined EEG and fMRI has been developing as a major research field, there is already a wealth of literature for statistical analyses (Laufs, 2012). Next to the isolated types of analyses, which can be performed with one modality alone (i.e., ERP, time-frequency analysis, fMRI contrasts, connectivity analysis), there is asymmetric types of data analysis, such as EEG-informed fMRI and fMRI-informed EEG. In both cases one of the two methods takes precedence over or excludes the other (Huster, Debener, & Eichele, 2012). Further, each of these analyses only uses part of the data.

As noted in section 1.1.1, EEG data suffers from poor spatial resolution and the so-called inverse as well as forward problem. Both in principle label a similar problem, but from different perspectives. A missing inverse solution denotes the lack of certainty about a neuronal source for a given electric potential in the EEG, whereas a forward solution would give insight into electric potentials created at the head surface from a given dipole in the brain. One problem with the former, for instance, is that both skull and brain shapes deviating from normalized head templates can distort the analysis (Ollikainen, Vauhkonen, Karjalainen, & Kaipio, 1999). Here, combined EEG-fMRI recordings present a useful tool for improving the creation of inverse and forward solutions. By informing the analysis procedure about anatomical idiosyncrasies of a subject via individual sMRI data, estimating the source of a potential becomes more reliable (Dale & Sereno, 1993).

Another way of enhancing the EEG analysis with MRI data is to perform connectivity analyses within the source space. As opposed to the sensor space, which represents the outer

head model with EEG electrodes on top, the source space is a statistically created space where estimated neuronal sources for EEG potentials are located. In assuming there is a common space shared between EEG sources, dipole estimations require a template. Moreover, physiologically it is reasonable to assume that the successive or concurrent emergence of dipoles has interdependent effects on neuronal sources, as in MRI it is widely accepted that brain activity can be analyzed in its connectivity patterns between different brain regions. Brought to the EEG source space, the strength of connectivity (i.e., correlations between brain activities) can be assessed between EEG sources (Barzegaran & Knyazeva, 2017; Schoffelen & Gross, 2009). This, however, is predicated on a precise definition of brain areas as can be provided by sMRI data. Such connectivity analyses are often carried out using surface data (Nunez et al., 1997; Nunez & Srinivasan, 2006; Srinivasan, Winter, Ding, & Nunez, 2007). Yet, these models are difficult to interpret and often criticized for being unreliable. This is due to the lack of information on neuronal sources and due to the results being vulnerable to artefacts caused by conductance heterogeneity of brain layers.

Parallel to the enhancement of EEG analyses, entering MRI data into higher statistical models can also be improved by adding EEG data. One of the most widely spread and straightforward approaches in this research is to compute single-trial EEG parameters from continuous data. For instance, if there is significant ERSP in the theta band (i.e., 4-7 Hz), single-trial theta power can be extracted from the EEG data, convolved with an estimation of the HRF from the respective subject and fed as a parametrized EEG measure into the General Linear Model (GLM) of first level fMRI analysis (Debener, Ullsperger, Siegel, & Engel, 2006; Scheibe, Ullsperger, Sommer, & Heekeren, 2010). A basic schematic of the pre-processing and creation of the parametric regressors can be seen in **Figure 2**.

This approach has multiple advantages compared to the aforementioned MRI-informed EEG analyses. Firstly, it enables an estimation of the contribution of an EEG-derived parameter. Therefore, it allows insight into voxel activation presumably coupled to increased EEG activity, which could also be labelled as a measure for neurovascular coupling. Secondly and perhaps more notably, the estimation is not only performed on a single-subject level, but on a single-trial level. An important drawback to asymmetric data integration is that multimodal data are not fully synchronized. Instead, a small portion of one original data set is allowed to limit or inform the other data set. This, for example, accounts for source estimations in the EEG when only the sMRI data are utilized in the analysis. Depending on the research goal, this might be sufficient. However, if the aim is to link as much of the EEG and the MRI as possible, namely on a single trial level, entering parametric EEG-regressors into the MRI's GLM makes more

sense. However, with explaining more variability in voxel activation patterns as the primary goal of this analysis, it can hardly be argued that it reveals any information about the EEG. Thus, it remains an EEG-informed fMRI analysis and an asymmetric way of thinking about multimodal results.

In order to adequately test a hypothesis, such as joint increased theta, late positive potentials and decreased prefrontal BOLD responses being associated with proactive control, it seems implausible to have one data source taking precedence. Demonstrating that EEG-derived parametric regressors can add explanatory value in predicting significant voxel activation is merely ample evidence supporting the hypothesis. The calculated results speak for additional variance explanation in functional contrasts. Therefore, a small fraction of the EEG data is related to a small fraction of the fMRI data. It is hard to argue that minimizing the utilized data is a valid representation of the supposedly underlying cognitive processes. The same would account for taking an MRI-informed source estimation and comparing it with EEG results – it would simply represent a fraction of data that has been integrated asymmetrically. More variance in both data sets can be tapped into when joining them. While still being meaningful, these results of asymmetric integration, for example, do not allow for the previously discussed improved validity or the inclusion of single trial variance from two multimodal data sets.

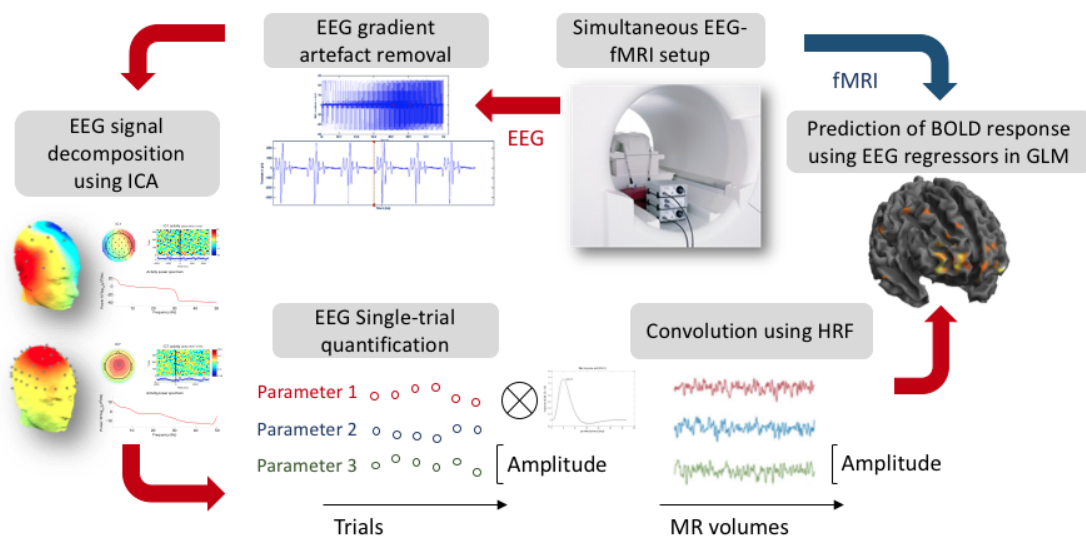


**Figure 2** Schematic procedure of pre-processing of EEG data (red arrows) as well as the computation of the EEG regressor for EEG-informed prediction of fMRI voxel activation (blue arrow), adapted from Debener et al. (2006).

### 1.3 Approaches for multimodal data fusion

The main advantage of data fusion is that it represents a multivariate approach which attempts to take into account almost all available information (Huster et al., 2012; Sui, Adali, Yu, Chen, & Calhoun, 2012). As in supervised machine learning (Besserve et al., 2007; Pereira, Mitchell, & Botvinick, 2009), data fusion can be informed by categorical variables about the experiment (i.e., distinction between conditions) and can identify common signal sources in data sets associated with levels of the categorical variable (e.g., Haynes, 2009). Again, as in machine learning, the extent of informing data limiting the analysis can be varied. To multimodal data fusion as well there is blind, semi-blind or informed approaches (Sui et al., 2012). In addition to the data entered and prior information limiting analyses, fusion approaches can be distinguished by prerequisite statistical or physiological assumptions about one data modality, both or the relation between modalities.

#### 1.3.1 Joint and Parallel Independent Component Analysis

A popular method for fusing different kinds of medical imaging and EEG data is joint independent component analysis (jICA; Calhoun, Adali, & Liu, 2006; Calhoun, Liu, & Adali, 2009; Eichele et al., 2008; Kyathanahally, Franco-Watkins, Zhang, Calhoun, & Deshpande, 2016). As with ICA in single modalities, a generative model with an unknown, linear mixing process of signal components is assumed to underlie the observed data. The basic idea of ICA is dimension or data reduction. At first, this might seem counter-intuitive, since the goal in data fusion is maximal data usage, but analyzing EEG and fMRI poses a severe problem to any type of signal decomposition, which is high dimensionality. With usual ICA in EEG, a two-dimensional data structure is explored (i.e., electrodes by time), which can be very conveniently displayed in an unmixing matrix. In a combined feature matrix with voxels from fMRI data, there is a large quantity of variables depicting a three-dimensional space being observed over time. This is a far more complex, multidimensional data structure, which, in order to be interpretable, has to be decomposed.

jICA aims at identifying maximally independent components from multiple sources contributing to the signal by unmixing signal parameters. However, a spatiotemporal decomposition, instead of a purely temporal or spatial one, is performed on at least two different data modalities to extract new features. In the context of multimodal data fusion, a feature refers to a data set, representing a relevant part of each data modality, which contributes to a data

matrix as an input vector. In other words, it is a simpler data space displaying links between modalities.

In terms of ERP and fMRI data, a spatio-temporal decomposition from jICA refers to the ERP time course and voxel intensity. However, the jICA adds a strong constraint by assuming that neuronal sources associated with the two data modalities vary the same way across subjects. Therefore, only features with identical linear covariation across data sets are extracted from the unmixed data matrix. Correspondingly, beta weights are assigned to pairs of components from both data modalities (see **Figure 3**). When extracting complementary components from ERP time courses and fMRI contrasts, each time point in the extracted ERP time course is assigned a combination of the associated fMRI voxels, adding spatial to the temporal data. Here it should be noted that an assignment of voxel clusters to ERP time courses is not to be interpreted as increased temporal resolution in the fMRI data, since the amount of observations (i.e., volumes) per variable (i.e., voxels) has not changed. Averaged voxel clusters coupled to time points in the ERP represent spatial variation in the fMRI, which are correlated with temporal variation in the EEG time course.

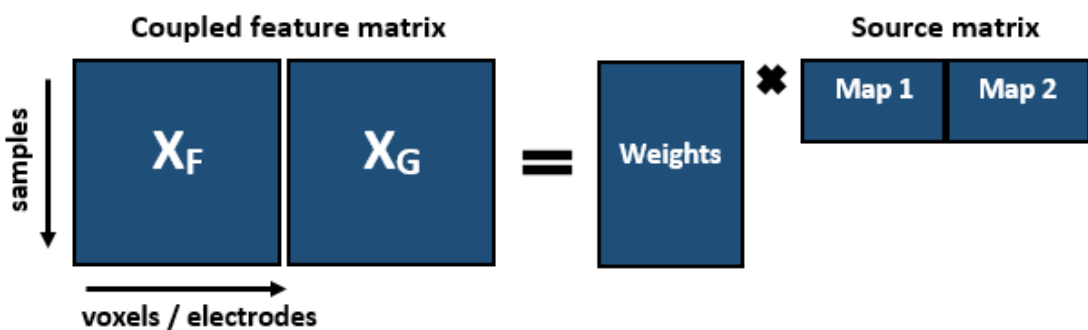


**Figure 3** Diagram of jICA with coupled feature matrix of multimodal datasets  $X_F$  and  $X_G$  in a shared data matrix (left) and in an umixed matrix with shared beta weights (right) adapted from Calhoun and Adali (2009).

The likelihood function used in the jICA is similar to common ICA, as well. The joint unmixing data matrix  $W$  of two datasets  $X_F$  and  $X_G$  from the same sample of test subjects  $N$  is estimated so that the likelihood  $L(W)$  is maximal. In the estimated unmixing matrix each dataset has the dimensions  $N$  and voxels ( $V_1$ ) or ERP time course ( $V_2$ ). The basic estimation of  $L(W)$  follows **Equation (1)**:

$$L(W) = \prod_{n=1}^N \left( \prod_{v=1}^{V_1} p_{F,n}(u_{F,v}) \prod_{v=1}^{V_2} p_{G,n}(u_{G,v}) \right) \quad (1),$$

where the vectors  $u_F$  and  $u_G$  represent observations for sample  $n = 1, \dots, N$  in the matrices  $U_F$  and  $U_G$  (Calhoun & Adali, 2009).

As mentioned in section 1.1.2, with this method for multimodal data fusion Kyathanahally et al. (2016) were able to detect decision-making components underlying simple to more complex delay discounting task. Joint components identified in simpler tasks with certain rewards could predict parts of activation patterns found in more complex tasks with reward and punishment uncertainty, indicating that decision-making processes might occur in an additive fashion.

Although data fusion attempts to use all the available information, the jICA framework puts limitations to this principle. First of all, the constraint of identical modulation of features restricts the amount of data affecting the extraction of signal components. This constraint is necessary to focus on shared data sources. It can be relaxed by either choosing different datatypes or by switching to a semi-blind form of ICA-based signal separation. By assuming correlated instead of identical modulation of the datatypes, parallel ICA (pICA) performs a mostly identical signal decomposition as jICA. The most important difference lies in the relaxed, physiologically more accurate assumption about the relation of multimodal signals. On top of that, while the authors advise to use the jICA as a second level analysis on single subject data (e.g., Calhoun & Adali, 2009), other approaches have gone farther by performing data fusion on single trials (Debener et al., 2006; Huster et al., 2011; Murta, Hu, Tierney, Chaudhary, & Walker, 2016).

Lastly, until now only amplitude measures and functional contrasts derived from GLM parameter estimates were considered for data fusion. However, the current state of literature suggests that amplitudes of ERPs actually have less in common with BOLD variation than oscillatory activity, such as ERSPs (Magri, Schridde, Murayama, Panzeri, & Logothetis, 2012; Murayama et al., 2010; Murta, Chaudhary, Tierney, Dias, & Leite, 2016). For instance, Murta et al. (2016, 2015) were able to demonstrate that when entered into multiple GLM models, predictors either representing frequency band power or phase-amplitude coupling strength could better explain variance in amplitude fluctuation of the BOLD. As to replicate this finding and to benefit from potentially better correlation of signals, in the final data fusion approach oscillatory measures from the EEG shall be included.

Of course, when discussing single trial measures, one would be amiss not to pay attention to properties of single trial estimates in the fMRI. In fMRI these crucially depend on the type of experiment. A high frequency of modeled trials entails a high autocorrelation and inflated inter-trial similarity. Furthermore, in designs relying on a high amount of trials or a poor signal

to noise ratio, results like functional contrasts drawn for each trial can be highly unstable (Mumford, Davis, & Poldrack, 2014; Mumford, Turner, Ashby, & Poldrack, 2012).

### 1.3.2 Multiway Partial Least Squares for EEG and fMRI

Multiway Partial Least Squares (N-PLS, Bro, 1996; Martínez-Montes et al., 2004; McIntosh, Bookstein, Haxby, & Grady, 1996), like jICA, is a blind source separation method that lends itself ideally to explaining spatio-temporal, linear relationships between data sets. Depending on the subtype (for an overview see Krishnan, Williams, McIntosh, & Abdi, 2010), applications vary from finding spatio-temporal activity patterns differentiating between experimental conditions (task PLS) to identifying seed voxel activations that optimally vary with behavioral or other measures (seed PLS).

Unlike ICA-based approaches or similar dimension reduction methods, like principal component analysis, N-PLS and other PLS methods utilize Singular Value Decomposition (SVD; e.g., Harshman, 1970) of a matrix with values X over time points S in accordance to the values in vector Y containing time series data. SVD has been established as a handy tool for creating a decomposition of a matrix without forcing independence constraints to the components as in ICA. Therefore, there are less a priori restrictions on data decompositions.

As is common for multiple time series vectors, each value over S time points for both X and Y is highly correlated to the adjacent points. This results in the problem of collinearity. In PLS, the difficulty of estimating parameters for regressors with highly correlated time points is solved by resampling data into new time blocks, which do not or suffer less from collinearity (i.e., bootstrapping; Davison & Hinkley, 1997).

By fitting multilinear models to nested data sets, specifically N-PLS aims at finding optimal covariations between more complex, multidimensional data sets like EEG and fMRI. Here, nested refers to grouping related classes, such as n participants and q experimental conditions, for example, into rows listing values of n within q for p variables (i.e., voxels and electrodes). Thereby, in this example a matrix with n rows nested in q by p columns (McIntosh & Mišić, 2013) is formed.

When extracting features from multiple sets, N-PLS identifies those signal components from EEG data that exhibit maximal temporal covariance with certain BOLD profiles. Therein, the fMRI data are conceptualized as a matrix of voxels by time. From this matrix, the linear voxel combinations displaying maximal temporal covariance with components extracted from a second three-dimensional matrix (i.e., electrodes by frequencies by time) are chosen. Next, a final covariance matrix of the relations between the original matrices is build and decomposed

with SVD (McIntosh et al., 1996). To account for the multidimensionality problem of combined data and for the abundance of variables in the fMRI, EEG data are reduced to a sum of so-called atoms each with specific spatial, temporal, and spectral traces. At the same time, fMRI voxel activation is decomposed to the same amount of atoms with a spatial and temporal dimension, so that each atom will have maximal covariance with its counterpart in the EEG (Martínez-Montes et al., 2004; McIntosh & Mišić, 2013).

Extracting data features from raw or single trial data this way bears some pitfalls regardless of modality. For one, there is larger variability and noise levels to be expected. More than that, modeling data sets on such a precise level implies proneness to overfitting, since statistical models are adjusted until the empirical data can be estimated to the best extent (McIntosh & Mišić, 2013). As a result, N-PLS might fit noise in either data set to explain signal modulations. Finally, since no physiological assumptions before source separation are set, there is no guarantee that the resulting unmixing process represents the optimal or even a sensible model of the original neuronal processes in the subjects.

### 1.3.3 Mixed-effects modeling with multimodal regressors

Lastly, since N-PLS and ICA serve the purposes of dimension reduction and relating different data sets, the last task remaining is connecting improved processing of neuronal data to behavioral measures. In the end, the criterion of predictive validity is often treated as a minor concern. Admittedly, not all brain data can be related to a suitable correlate, since there are large gaps between the original brain activation and a behavioral equivalent. Still, the pursuit of explaining behavior is important. The idea behind understanding brain mechanisms is to make reliable predictions about people at some point, be it in a clinical or non-clinical context. Thus, even a negative test result from correlating an activation with a behavior can hold value.

One of the initial claims in section 1.1.1 and one that was put forward by Turner et al. (2016) is that enriching statistical predictors and methodology leads to enhanced prediction. If there is merit to the claim, EEG- or fMRI-based parameters should provide incremental contributions to explaining variance in reaction times (RT). However, it stands to reason if blindly entering variables into a predictive model serves any real purpose. Without assumptions about the relation of predictor and criteria, significant explanatory value might be coincidental.

For testing the hypothesis of cumulative explanatory values in single and joint EEG-fMRI parameters, a mixed-effects model for a nested data set with an exploratory model sequence (Hox, 2010; Hox, Moerbeek, & van de Schoot, 2017; Hox & Kreft, 1994) was performed. The basic idea of nested data or multilevel models is that a hierarchical data structures causes

dependent values to be more similar within naturally occurring subgroups. This applies, for instance, for a subject's performance levels, which are more similar within blocks or within conditions of an experiment than between blocks or measurement runs.

As in this example, mixed-effects regression is a regressional model that allows for both fixed and random linear effects from multiple levels. Since this regression is performed on nested data, these are organized in a manner that shows all observations collected from a subject ordered as repeated measurements within ascending categorical levels. As an example, an ERP measure would be entered as single-trial voltage values within a trialtype within a block or run within a subject. Consequently, a multilevel modeling approach ensures that there is less distortion of results due to false assumptions about homogenous or even unrelated distributions of dependent values or their residuals. In general, multilevel modeling benefits from being more robust (Maas & Hox, 2004), as they are less heavy on distributional assumptions than conventional inferential statistical models for comparing levels of multivariate designs (i.e., analysis of variance or covariance).

Furthermore, a mixed-effects approach lends itself to multimodal data fusion and prediction, since it allows for a sequential modeling of different types of effects. First, both slopes and intercepts of pre-defined experimental manipulations can be entered separately as random (i.e., residuals) or fixed effects. While the former represent the fixed, or systematic, part of the model equation, the later stands for unexplained deviation of predicted intercepts or slopes from the observed. Second, these can be added as effects on different levels or as so-called cross-level-interactions, indicating the contribution of interactional effects between varying levels of multiple hierarchical predictors.

In summation, the approach eases to assess the specific contributions of each step in an iterative specification of the most complex model (Hox, 2010). In an exploratory model sequence, each iteration can be tested by assessing the improved explanation of variance with each added fixed or random model parameter. This is done by either observing changes in a model's failure to account for variance (i.e., deviance) or by indexing a model's fit on empirical data (i.e., Akaike Information Criterion, Pseudo-R<sup>2</sup>).

## 1.4 Aims of this study

### 1.4.1 Investigating mechanisms of cognitive control with EEG-fMRI

The main goal of this study is to present a framework of measures for both optimizing the processing and statistical modeling of combined EEG-fMRI data. Further, this framework shall

be demonstrated on a specific example that benefits from having enriched data foundations and analysis. After all, next to the methodological concerns, the ideas collected in this framework were meant to serve researchers in neuroscience, psychology, medicine or other fields as tools for answering questions about mental processes.

Cognitive control, as the ability to flexibly regulate and control cognitive resources in a goal-oriented manner, has great value to clinical research. Populations suffering from deficits in this ability range from eating disorders (Tchanturia et al., 2012; Volkow, Wang, & Baler, 2011) and schizophrenia (Berger et al., 2016; Lesh, Niendam, Minzenberg, & Carter, 2011; Poppe et al., 2016) to drug addiction (Tang, Posner, Rothbart, & Volkow, 2015; Wiers, Gladwin, Hofmann, Salemink, & Ridderinkhof, 2013). Particularly the latter display reduced proactive control capacity to perform adequate behavioral perseverance or adaptation to long-term goals when stimuli, which are relevant for the addiction, are present (e.g. Brevers et al., 2017). Therefore, understanding cognitive control mechanisms might lead to a more refined knowledge of the associated disorders. As stated at the end of section 1.1.1, precise neuronal correlates can aid clinical predictions concerning treatment responsiveness or the development of the disorder.

In adapting a continuous performance task, originally designed for measuring cognitive control functions in schizophrenic patients (Henderson et al., 2012), for simultaneous recordings, this study aims at comparing the outlined approaches. The neuronal correlates of cognitive control in WM, as assessed in the Dot Pattern Expectancy (DPX) task or AX Continuous Performance task (AX-CPT), in both EEG and fMRI have already been studied extensively (e.g., D'Ardenne et al., 2012; Lopez-Garcia, Lesh, Salo, & Barch, 2016; MacDonald et al., 2005). For this reason, the DPX task adequately matches the purposes of this study. The existing literature on the task and proves its compatibility with both EEG and fMRI.

In this task, long-term goal maintenance optimizes behavior. Subjects learn how to process predictive information, which is imperative to their task performance. If they are successful, they should learn to identify the reliable context, reduce cognitive effort and simply maintain the goal-relevant behavioral strategy. Therefore, proactive cue maintenance should be less demanding than information updating and behavioral correction in terms of prefrontal cortex resources as compared to ambiguous context cues. In turn, it should involve larger activations in the medial PFC (i.e., dorsal and anterior cingulate) as well as the SMC and adjacent areas in the primary motor cortex, such as the precentral gyrus (PCG) for response preparation. Concerning late behavioral correction, as applied in situations with uncertain contingencies, the

ACC should be activated. Similar differences in neural activity should be found in ERPs and oscillatory measures.

In particular, late frontoparietal positivity associated with WM updating and maintenance (i.e., P3, late sustained positivity) and midline theta activity should relate to the processing of predictive context cues, due to the evaluation of an essential information for goal-pursuit at a later stage of cognitive decision-making. As compared to components found at prior stages of the information processing stream (i.e., N1, P2), sustained positivity has been demonstrated to correlate with early selection in decision-making as well as evidence accumulation (Barcel & Cooper, 2017; Pisauro, Fouragnan, Retzler, & Philiastides, 2017). Consequently, we assume that this positivity should yield a significant covariation with reduced activity in the DLPFC including the bilateral middle frontal gyrus (MFG) and its connections to the triangular inferior frontal gyrus (IFG). As to theta and alpha frequencies, we hypothesize increased synchronization for theta over the medial prefrontal cortex as well as the associative parietal cortex, due to its link to the biasing path supporting motor preparation along these regions. As opposed to theta, alpha activity should decline for proactive control across the discussed regions, but increase along with ACC activation in less certain contexts.

To our knowledge there have been no attempts at investigating these correlates in simultaneous EEG and fMRI recordings. Therefore, another secondary goal of this study is to replicate results from past, isolated EEG and fMRI studies on cognitive control in the DPX task.

#### 1.4.2 The practicability of multimodal data fusion

Finally, since the primary goal of this study is to evaluate the practicability of multimodal data fusion, special focus shall be put on results unique or common to one or multiple analyses compared to unimodal data analyses (i.e., isolated EEG or fMRI). By testing the psychological hypotheses on cognitive control in section 1.4.1, each analysis' value can be assessed in terms of how convincingly it finds answers to the hypotheses.

Taken together, jICA and pICA, N-PLS and multilevel modeling of EEG-fMRI data represent different approaches to data fusion. Each vary in how much information they utilize, which specific measures of fMRI or EEG are entered and in the physiological or statistical assumptions they make. Hence, they form a promising collection of analyses for evaluating benefits and drawbacks of multimodal data fusion.

By highlighting differences and similarities between approaches, the framework put forth shall be an indication as to how specific research questions can be more accurately addressed

by corresponding analyses. This methodological focus promises to improve the glaring flaw of lackluster validity and interpretational issues in neuroscientific research. As such, each approach shall be discussed in regards to its contribution in explaining results on cognitive control mechanisms involved in the DPX task.

## 2. Methods

### 2.1 Data and code availability statement

All behavioral data, log files as well as electrophysiological and neuroimaging data are available upon request. Future publication projects based on this study can be found on Open Science Framework under the project designation ‘The lame, the blind and the ugly – multimodal data fusion for simultaneous EEG-fMRI’ (<https://osf.io/z3tx9/>).

Annotated analysis scripts in Python and R, Jupyter Notebooks for exemplary analyses, plots, conference contributions regarding this study, the original ethics proposal submitted to the Department of Psychology of the University of Marburg, open lab notebooks documenting the progress of this study as well as additional code scripts in Matlab, Python and R for supplementary analyses are publicly available in the linked repository on GitHub (<https://github.com/MalteGueth/MSc thesis MalteGueth>).

### 2.2 Participants

For the experiment thirteen healthy, right-handed medicine students from the University of Marburg (7 males and 6 females) were recruited. Each of them took part in an MRI introduction course to familiarize themselves with the method and to experience having an MRI scan performed on themselves. During the course, subjects were offered to participate in an EEG-fMRI experiment. In exchange, they were provided an anatomical scan of their brain. Before subjects decided, they were ensured that participation in the study had no impact on grades for the course. Subjects were excluded from the experiment if they were not between 18 and 35 years old, reported impaired vision, left-handedness, prior experience with the task, current use of prescription drugs and acute or a history of neurological or psychiatric disorders. All subjects ranged between the ages of 18 and 32 years ( $M = 23.23$ ,  $SD = 4.28$ ). Participants provided informed consent after they were given a summary of the risks and requirements involved as well as a rough outlet of the experimental procedure. A summary of all subject information can be found in **Table 1**. This study was approved by the local ethics committee at the Department of Psychology.

**Table 1**  
*Participant characteristics*

	Participants M (SD) (N = 13)
Sex	7 M 6 F
Age (in years)	23.23 ( $\pm$ 4.28)
Education	6 A-levels ('Abitur'), 3 finished apprenticeship, 4 university degree
Average Grade (of last degree)	1.8 ( $\pm$ 0.47)
Digit Symbol Coding Test Score (correct items)	84.15 ( $\pm$ 11.15)
Task performance (1-10)	7.08 ( $\pm$ 1.44)
Alertness (1-10)	7 ( $\pm$ 1.41)

*Note.* SD = standard deviation, M = male, F = female.

## 2.3 Experimental Design and Setup

### 2.3.1 General Procedure

All experiments were performed on the premises of the section for Brainimaging located at the clinic for psychiatry and psychotherapy at the Department of Medicine in Marburg. Before the day of the experiment, all participants of the MRI course had received notification about the chance to take part. This way they had enough time to read through the informed consent and to familiarize themselves with the study's basic ramifications.

When subjects arrived at the clinic, they were greeted and asked to take a seat in front of a desk in a comfortable office chair in a well-lit room. The desk was empty, except for a few sheets of paper, a stop watch and a pen. At this point, the conditions for participation as well as risks were repeated, before subjects were handed the written version of the informed consent and a metal anamnesis to assess risk factors for fMRI (see Appendix A). The latter was used to ensure that there were no pieces of metal or electrical devices permanently attached to the subject's body. On request subjects could receive a written report, describing the study's background, risks and conditions of participation in detail. Starting from here, all experimental procedures were documented on the standardized protocol (see Appendix B).

Next, subjects were provided an oral overview of the following proceedings (i.e., pre-tests, questionnaires, EEG preparation etc.). If the subject had filled out all forms and had no further questions, the interviewer conducted pre-experimental interview (see Appendix B), in order to assess demographic and personal data (i.e., age, highest academic degree). Further, to control for the influence of stable capacities for informational load, the Digit Symbol Coding Test from the German version of the Wechsler Intelligence Scale for Adults (WAIS-IV, fourth edition; Petermann, 2012) was administered as a pretest (see Appendix B). A collection of combined scatter and distributional bar plots for cross-correlations of demographic, pretest and interview data is provided in Appendix C.

Afterwards, subjects were brought into the MRI control room, where they could change into a hospital gown. This was offered to prevent soiling the participants' private clothing with gel from the EEG and ECG electrodes at the head and upper back. While subjects sat in a chair in front of the computer running the EEG and ECG recording software, the experimenter could check the signal quality (i.e., electrical impedance, voltage at each electrode). Two sizes of EEG caps were available (size 56 cm and 58 cm) with mounts for 31 ring electrodes plus one grounding (AFz) and one reference channel (FCz) on the fronto-anterior and fronto-central scalp positions, respectively.

Before the EEG cap was put on, skin portions that would be covered were cleaned with Isopropanol (70%), followed by measuring the subject's head circumference. By assessing the distances between the left and right preauricular points as well as between the nasion below the forehead and the inion at the back of the head, the central vertex point (Cz) was marked as the intersection of the two axes (Klem, Lüders, Jasper, & Elger, 1999). The EEG cap was then put on at this central position. An elastic chin band prevented the cap from sliding.

Electrical impedances were reduced with a conductive electrolyte gel, containing pumice, as this gel component aids roughening the skin and removes detrimental elements to the electrical conductance, such as callus skin or fat. The gel was distributed across the electrode sites, starting with the reference and grounding electrodes. For this purpose, blunt plastic syringes were used, after slightly roughening the skin with cotton swabs. These were also applied for pushing away hair blocking the contact of the electrodes to the scalp. All impedances were kept at or below 5 kΩ. At last, the ECG electrode integrated in the EEG system was placed on the upper back. Before the electrode was attached and the impedance was optimized, subjects were asked if they preferred a person of the same sex to perform this step.

When the EEG and ECG signal were optimal, subjects were lead into the scanning room to the MRI bore. Here, several measures, as can be read in protocols from Ritter and Villringer

(2006) or Mullinger, Castellone, & Bowtell (2013), were met to achieve optimal data quality. For a detailed description on these measures specific for simultaneous recordings, see section 2.4.2. During the entire time in the scanner, subjects were able to communicate with the experimenter via a two-way intercom system connecting the two adjacent rooms.

Following an anatomical T1-weighted scan, subjects were introduced to the DPX (see section 2.3.2) on ten slides with written instructions. When they felt confident, they could start with 18 practice trials. As opposed to the subsequent four experimental blocks, subjects received feedback on their performance ('correct', 'incorrect', 'too slow', 'too early, please wait for the probe'). The feedback was initially given to make sure subjects had properly understood the task. Before the experiment and the functional data acquisition was started, subjects were asked one last time if they were well and ready to begin. From that point on, not counting practice trials and instructions, the experiment lasted approximately 32 minutes.

Finally, when the task was over, subjects were moved out of the scanner, freed of all EEG equipment and provided the opportunity to wash their hair and back in a bathroom of the clinic. When they had cleaned themselves, all subjects participated in a post-experimental interview (see Appendix B). Among other questions, they were asked how they rated their task performance on a scale of one to ten and which ideas they had on the purpose of the task. Concluding the experiment, subjects were informed about the background of the task and the complete purposes of the study. In case they were interested, subjects could indicate if they wanted to be notified of the results of the study and provide an e-mail address.

### 2.3.2 DPX Paradigm

The DPX paradigm is a continuous performance task with four different trialtypes (AX, BX, AY, BY) repeated across four experimental blocks. Each block consisted of 52 trials. Blocks were separated by fixed one minute breaks and preceded by 18 practice trials. A counter reminded subjects of how much time was left during breaks. Every trial entailed the successive presentation of two stimulus types: a cue, which provided predictive information about which of two possible goal responses would be required, and a probe, signaling when to show a goal response. Therefore, the DPX task allows for the assessment of early predictions based on goal-related information locked to the cue as well as updating behavioral responses with the onset of the probe.

All stimuli were made of dot patterns highlighted within a square of nine equidistant blue dots. The first dot pattern (i.e., the cue) was presented in light blue for 100 ms on a white background, followed by a jittered interstimulus interval of 3 to 5 seconds. The second dot

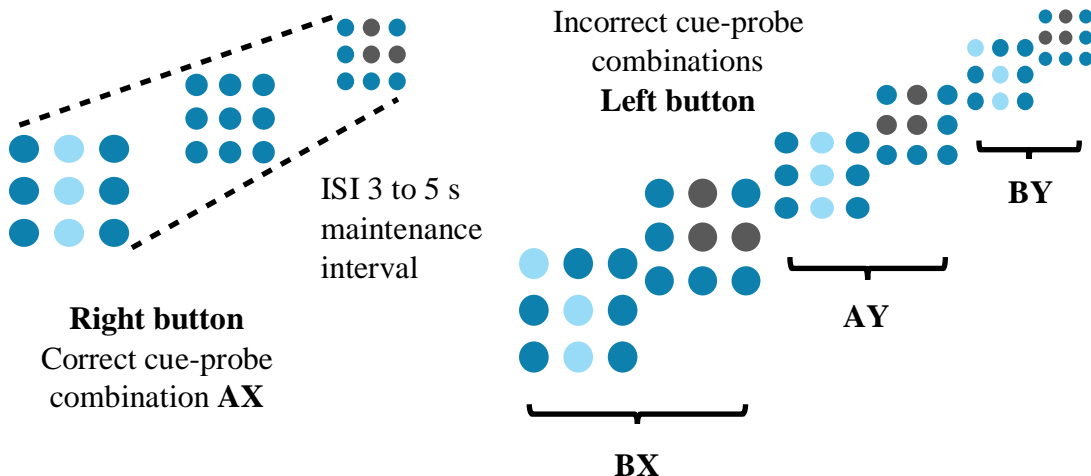


**Figure 4** Illustration of the DPX task adapted for simultaneous EEG-fMRI recordings. One trial consists of a cue lighting up within in the square, followed by a mask and then the probe appearing in grey (left side of the figure). A correct combination is presented on the left and all incorrect combinations on the right side.

pattern (i.e., the probe) was presented in grey. As soon as the probe appeared, subjects had a time window of 800 ms to respond. After 300 ms the probe disappeared. A jittered intertrialinterval of 2.5 to 4.5 seconds separated the probe from the next cue. Thus, the minimum duration of each trial was 6.4 s and the maximum duration 10.4 s. These parameters were based on prior implementations of the AX-CPT and DPX task (D'Ardenne et al., 2012; Lopez-Garcia et al., 2016) as well as our own analysis of fMRI design efficiency.

Subjects were instructed to respond with a right button push after a correct cue-probe combination and with a left button push after an incorrect combination. In the correct combination (AX) in the vertical midline three blue dots lit up as a cue. During the maintenance interval subjects fixated the square of nine dark blue dots as a mask. The corresponding probe had the two upper dots of the vertical midline and one on the right in the middle in grey. Any deviation in the cue, probe or in both patterns was considered incorrect. All patterns were constructed starting with nine equidistant dots arranged in a square. Moreover, all colors were checked for equiluminance to control for contrast effects. They were each tested in the configurations they were pesented in during the experiment.

Across the four blocks 208 trials were presented with 136 AX (65%) and 24 trials (11.6%) for BX, AY and BY respectively. However, due to a programming error in the pseudo-randomized stimulus list, the fourth block contained 33 AX and 8 BX trials. Therefore, the actual amount is 135 AX, 25 BX, 24 AY and 24 BY trials. An overview of the paradigm is given in **Figure 4**.

As often found in EEG paradigms, this design was intentionally unbalanced. For the paradigm to work, the correct trialtypes AX had to have the highest frequency of occurrence. Of the 52 trials per block, 33 were AX (65%) and 8 trials were each of the remaining trialtypes (11.6%). Thus, subjects developed a dominant response tendency towards AX to push the right button. However, in a small amount of trials (i.e., AY trials) the expectation to see a correct probe after a correct cue was violated. An AY trial required subjects to correct their behavioral planning by updating WM in a reactive control style. They had to integrate the unexpected information, since the last stimulus and not the context was relevant to their behavior.

By contrast, when subjects saw a wrong cue (B), a strong proactivity was triggered. Regardless of the probe, in a trial starting with a wrong cue there is only one possible response, since both cue and probe have to be correct in order for the trial to be correct. The wrong cue had to be maintained in WM, because in this case it was the imperative stimulus. As soon as subjects saw the correct probe, they had to inhibit the dominant response tendency to push the right button by having the context direct their behaviour. The last combination BY was a control condition and presumably did not require noteworthy cognitive control efforts.

## 2.4 Data acquisition

### 2.4.1 Materials and software

For electrophysiological recordings inside the MRI scanner, the BrainAmp MR (Brain Products GmbH, Gilching, Germany), an fMRI compatible 32-channel EEG system including an integrated ECG channel, was used. This system amplifies the recorded electrical signal with a shielded amplifier connected via a fiber optic cable to the USB interface in the control room. As a result, there are no artefacts caused by data transmission and the amount of electrical wiring inside the MRI room is minimized. All EEG and ECG channels were recorded using silver/silver chloride (Ag/AgCl) ring electrodes. Imaging data were collected in a 3 Tesla MRI scanner (Trio Tim System, Siemens, Erlangen, Germany) with a 12-channel receive coil.

Unlike in common EEG systems, short cables connect the electrode cap to the amplifier. This quality reduces safety risks for the subject and potential sources of artefacts due to free moving wires inside the MRI. Another characteristic of the BrainAmp MR system is that it is clocked by the USB interface at the other end of the fiber optic cable. In other more sophisticated setups, for instance involving more than 32 channels, using an external system for temporal alignment can safe electric connections in the MRI. On top of that, implementing an external clock serves another essential purpose. There is virtually no approach for the correction

of artefacts from simultaneous recordings in the EEG that does not rely on temporal synchronization. This task is very demanding, since the EEG has to be acquired with a much higher sampling rate than technically feasible for any MRI scanner and both have to be precisely aligned. Achieving this feat on a data level after the recording is more than likely insufficient for optimal data quality. Hence, a SyncBox (Brain Products GmbH, Gilching, Germany) is used as an intermediary between the MRI and the EEG. The scanner clock is connected to the SyncBox Scanner Interface, which in turn is coupled to the SyncBox main unit. The latter contains all the circuitry necessary for detecting inputs from the clock and for downsampling the input. Lastly, the SyncBox puts out a clock signal to the USB interface, thereby enabling markers for events timed by the scanner clock (i.e., volume acquisition) to be set in the EEG. A schematic illustration of this setup can be seen in **Figure 5**.

During the experiment EEG data were recorded and observed with BrainVision Recorder (Version 1.21, Brain Products GmbH, Gilching, Germany). The DPX task, as described above, was programmed and presented using Presentation (Neurobehavioral Systems, Albany, USA) on a screen behind the MRI scanner. Subjects were able to view the stimuli through a mirror above them, which reflected the images on the screen.

For subsequent pre-processing and analysis of the EEG data, the MNE-python software (Gramfort et al., 2013), the Bergen plug-in for EEGLAB (A Delorme & Makeig, 2004), provided by the fMRI group of the University of Bergen, Norway, as well as the Fusion ICA Toolbox<sup>1</sup>, provided by the Medical Image Analysis Lab of the University of New Mexico, USA, for Matlab (Release 2014b, The MathWorks, Inc., Natick, Massachusetts, United States), were used. The latter was chosen to perform jICA and pICA. Pre-processing of the fMRI data was performed with processing pipelines build in Nipype (Gorgolewski et al., 2011). For this purpose, software packages containing functions from FSL (Smith et al., 2004), FreeSurfer (Reuter, Schmansky, Rosas, & Fischl, 2012) and SPM (Friston et al., 1995) were integrated in the pipeline.

Basic descriptive analyses, GLM and mixed-effects regression on behavioral, electrophysiological and imaging data were carried out in python utilizing the SciPy (Jones, Oliphant, & Peterson, 2014), NumPy (van der Walt, Colbert, & Varoquaux, 2011) as well as the lme4 package (Bates, Machler, Bolker, & Walker, 2015) in the R Programming Environment (R Development Core Team, 2016). Plots were created with the Pandas (McKinney, 2010), Matplotlib (Hunter, 2007), and Seaborn (Waskom et al., 2014) libraries in python and the ggplot2 package in R (Wickham, 2009). Further, results of BOLD predictions

---

<sup>1</sup> <http://mialab.mrn.org/software/fit/#>

using parametric EEG regressors and N-PLS atom weights on fMRI spatial data were plotted using the nilearn library for python, as demonstrated by Abraham et al. (2014).

As in unimodal fMRI analysis, asymmetric data integrations by predicting BOLD response with EEG parameters were performed in FSL. sMRI-informed dipole estimation was carried out using EEGLAB's DIPFIT2 plugin (Delorme & Makeig, 2004). Mixed-effects, the comparative model sequence as well as the N-PLS decomposition were all written and performed with the R Programming Environment also using the lme4 (Bates et al., 2015) and the sNPLS packages (Hervas, 2018).

#### 2.4.2 Experimental protocol for simultaneous recordings

Besides the aforesaid aspects of the experimental setup, a number of additional measures were taken to follow a sensible protocol for the concurrent assessment of electrophysiological and imaging data.

Even with MRI-compatible materials, performing an EEG recording inside the MRI scanner causes the electrodes and other materials to heat up, posing a potential safety risk to the

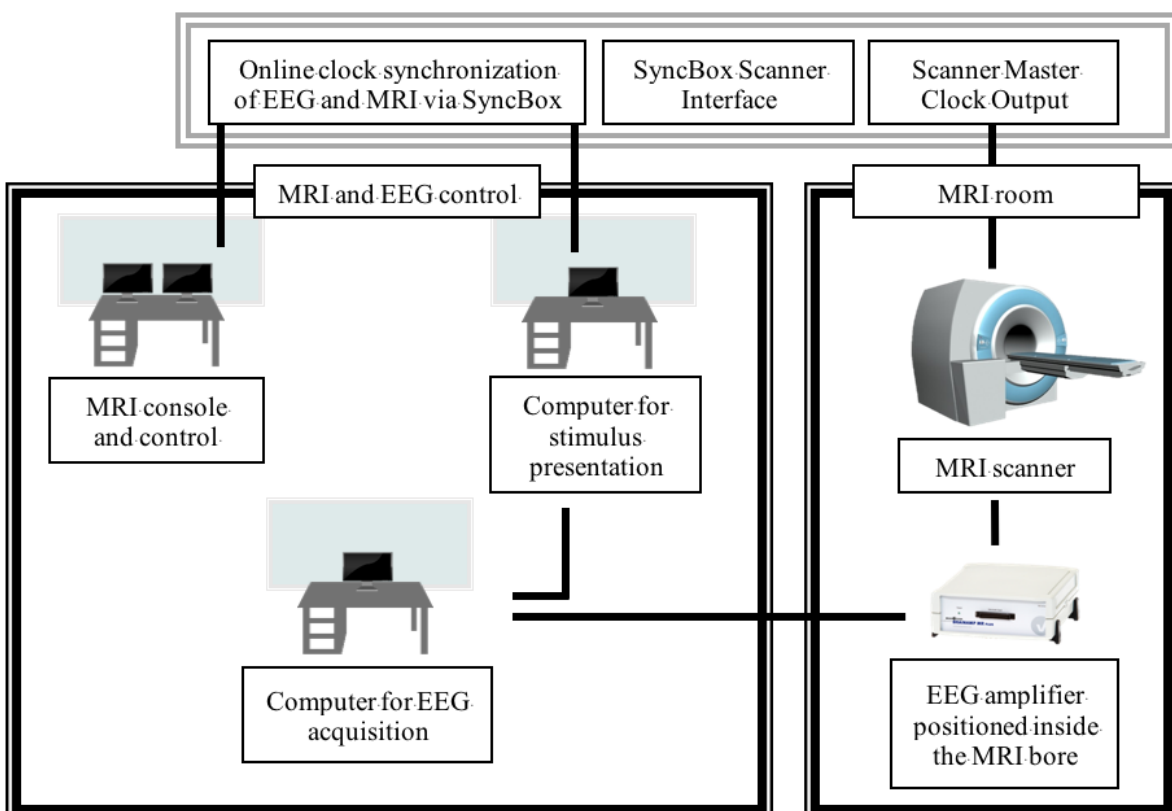


**Figure 5** Schematic illustration of the experimental setup for simultaneous EEG-fMRI recordings adapted from Ullsperger & Debener (2010). EEG and fMRI acquisition is performed with a SyncBox synchronizing data acquisition of the two methods to ensure that TR markers are set precisely in the EEG data.

subject (Yeung et al., 2002). As a preventive step, it is necessary to assess how intensively materials of the EEG system heat while using the planned EPI sequence. During the test run over the entire experiment all electrodes showed temperatures equal to or below 27 °C. As a result, it was concluded that the materials were safe for usage on subjects.

An important precaution taken before running an experiment, was to switch off the helium pump. With subtle vibrations (Rothlübbers et al., 2014) cables and other materials are moved inside the magnetic field. This causes artefacts that are hard to correct, degrading the quality of the EEG data.

During the experiment, when subjects first entered the MRI room, they were once more instructed about how to behave during the experiment. They were asked to abstain from any unnecessary movements of the head, torso or shoulders and to avoid crossing their limbs, as this would cause severe artefacts for both the EEG and fMRI. Furthermore, they were given a brief oral explanation of the experimental task. The participant's head was then placed on a pressure-insensitive cushion and further stabilized with foam pads to minimize head movements.

Electrode leads were passed through the head coil above the subject. Before moving the subject into the scanner bore, they were given an emergency control button to be able to abort the experiment at any time when they felt in danger. Inside the bore electrode leads were connected to the amplifier positioned behind the subject's head. All cables between the electrodes and the amplifier were fastened firmly with adhesive tape to avert movement. For additional stabilization, sandbag weights were put on electrode leads.

#### 2.4.3 Recording parameters for EEG and fMRI

Before the experiment, a T1-weighted structural image was acquired for all subjects. Functional data were recorded with EPI parameters (TR = 1800 ms, TE = 30 ms, 75° flip angle, FOV 240 mm, voxel size 3 x 3 x 4.6 mm, matrix 64x64) based on previous adaptations of the DPX task for fMRI studies (D'Ardenne et al., 2012; Lopez-Garcia et al., 2016). For each volume data from 32 axial slices (slice thickness 3.6 mm) were collected oriented to the AC-PC line in ascending order using a 12-channel head matrix receive coil.

EEG data for all 32 channels were collected with a sampling rate of 5 kHz. An online band-pass filter excluded data above 100 Hz and below 0.001 Hz. During the recording data were online referenced to FCz. As mentioned in section 2.3.1, all impedances were kept below 5 kΩ.

## 2.5 Unimodal data analysis

Before joining data features, behavioral, EEG and MRI data were first pre-processed and then analyzed independently from one another. This was done to achieve a baseline level of informational value and to compare unimodal results with existing literature. Pre-processing started with behavioral data, followed by fMRI and at last EEG data. For both EEG and fMRI it was necessary to note which trials had correct responses. Furthermore, optimal EEG pre-processing required the movement parameters resulting from realigning the raw functional data to the structural image of a subject. Thus, EEG pre-processing was performed last.

### 2.5.1 Behavioral Data

RT were assessed starting with the onset of the probe until the subject showed its first response. Button presses applied before, less than 100 ms after or 800 ms after the onset of the probe were categorized as invalid or miss, respectively. For all analyses performed with RT only valid, correct responses were included. The ER, as a measure of accuracy, was specified as the relative amount of incorrect button presses to the total amount of trials.

To test main effects and interactions for statistical inference, single trial RT measures were modeled in a mixed-effects regression. Dependencies of measurements were modeled by entering performance values for different trialtypes as observations within blocks within subjects. To this end, trialtypes and blocks were dummy coded ranging from 0 to 3 as factor levels. For final model equations a random effects term was included to model grouping variables for nesting and to fit varying slopes and varying intercepts trialtypes within blocks. Due to the authors of the lme4 package not allowing for p-value estimation, Wald tests for the fixed effects of each model were performed. In case of PSI values and ER, values were averaged over blocks before entered into the regression.

Since cognitive control strategies presumably balance each other, it is often more appropriate to index their balance rather than single trialtypes. Therefore, a proactive behavioral shift index (PSI) was computed (Braver, Paxton, & Locke, 2009) based on **Equation 1**:

$$PSI = \frac{AY-BX}{AY+BX} \quad (1).$$

**Equation 1** can be used for both RT, total errors and ER. However, in case values equaling zero would have to be entered, ER were corrected in accordance to **Equation 2**:

$$Corrected\ ER = \frac{error\ (0)+0.5}{Frequency\ of\ trialtype+1} \quad (2).$$

The PSI indicates increasing or decreasing proactive control tendencies. A higher difference in performance for AY and BX trials was interpreted as a shift towards proactive control, as could be observed in case of improved BX and/or diminished AY performance. A higher numerator, resulting in higher PSI values, hinted at elevated proactive control levels. Vice versa, a low PSI for RT or ER was interpreted as a stronger reactive control tendency.

Across four blocks on average subjects responded correctly to 196 out of 208 trials. In respect to the four trialtypes, they achieved 129 (AX, SD = 8.26), 23 (BX, SD = 9.2), 20 (AY, SD = 7.02) and 23 (BY, SD = 9.95) correct responses throughout the experiment. An overview of descriptive behavioral data is given in **Table 2**.

**Table 2**

Descriptive behavioral results from the DPX task

DPX Measure	Participants M (SD) (N = 13)	DPX Measure	Participants M (SD) (N = 13)
Speed (RT in milliseconds)		Inaccuracy (ER, errors divided by trialtype frequency)	
AX	400.71 ( $\pm$ 107.37)	AX	.02 ( $\pm$ .03)
BX	367.4 ( $\pm$ 122.14)	BX	.06 ( $\pm$ .08)
AY	523.62 ( $\pm$ 91.29)	AY	.12 ( $\pm$ .14)
BY	393.14 ( $\pm$ 130.64)	BY	.02 ( $\pm$ .03)
PSI	.18 ( $\pm$ .08)	PSI	.26 ( $\pm$ .62)

*Note. SD = standard deviation.*

### 2.5.2 fMRI pre-processing

Before the pre-processing of fMRI data, structural images were entered into the BET brain extraction module from FSL to remove skull and other tissue besides the brain (Smith, 2006). All outputs were manually checked before this step was added as a node to the analysis pipeline. If the brain extraction produced erroneous results by either removing too little or too much tissue, extractions were repeated and iterated or the fractional intensity threshold was varied accordingly (Popescu et al., 2012).

With the aforementioned pre-processing pipelines written in Nipype, fMRI data were motion corrected and co-registered to anatomical images with FSL's MCFLIRT and FEAT modules. Spatial smoothing of the co-registered images was carried out using a 5mm FWHM Gaussian kernel. Finally, single subject voxel time courses were filtered with a high-pass filter cut-off of 120 seconds to attenuate slow frequency drift and checked for further artefacts by identifying outlier volumes.

On single subject level BOLD responses were predicted with regressors for the cue and probe onsets modeling a duration of 1.5 s after the event onset. For this purpose, SPM's design specification and model estimation were used. Event regressors included event names, their onsets and durations. Trials followed by invalid responses were not entered in the model, as they most likely reflected distinct cognitive processes or failed execution of cognitive control compared to valid responses. Besides the event regressors, movement parameters were entered as covariates into the GLM. Single subject contrasts included comparisons of modeled events to baseline activity. Moreover, cue A and B as well as trialtypes AY and AX and BX and BY were contrasted.

Also for group level analysis SPM's design specification, estimation and contrast estimation modules were utilized. For results on group level, identical contrasts between cues and probes were specified. Results were calculated for both whole brain contrasts and for regions of interest. These were centered around structures specified in the hypotheses (i.e., IFG, MFG, ACC, SMC, PCG). Regions were defined in accordance to DPX and AX-CPT results from Lopez-García et al. (2016) and D'Ardenne et al. (2012).

### 2.5.3 EEG pre-processing

As alluded to previously, the EEG requires larger changes to conventional pre-processing compared to fMRI, since most artefacts resulting from combined recordings are inflicted to the EEG. Thus, the first step in cleaning the EEG data was to subtract GAs caused by the periodically changing magnetic fields during fMRI acquisition. For this purpose, a realignment parameter informed average artefact correction (Moosmann et al., 2009), as implemented in the Bergen plug-in for EEGLAB, was performed. By selecting the markers set through the TR clock synchronization as onsets for volume acquisitions and by specifying the TR as well as silent gaps between volumes, acquisition periods with relatively stable GA could be identified. In case the synchronization of the EEG and fMRI acquisition was successful, the distance between markers should align to the TR timing of the fMRI experiment. Given a sampling rate of 5 kHz a variability of 0.2 ms can result from failed synchronization (Gutberlet, 2009).

The average artefact subtraction, as presented by Allen et al. (2000), intends for an artefact template, which is based on a time window made up of a pre-selected amount of artefacts. This template is subtracted from the continuous EEG signal by sliding over the portion of the signal the TR markers are distributed over. For example, if a time window of 25 artefacts is required, artefact n is corrected by the mean resulting from the artefacts averaged from n-12 to n+12. However, in applying this procedure it is assumed that GAs are invariant across the experiment, which is unlikely due to influences like head movements. To tackle this issue, realignment parameters are brought into the picture. Significant movements are indicated by parameters resulting from single subject co-registration. By informing the correction analysis of when a subject's movements exceeded a set threshold (i.e., 0.5 mm in any direction), the correction window is reset at the respective artefact. In principle, the flexible correction window serves to avoid averaging over discontinuities of the artefact properties, thereby improving the correction procedure's accuracy (Moosmann et al., 2009; Yan et al., 2009).

Data from co-registration about movement in a three-dimensional space were transformed to a single movement value by Euclidian metric. This motion parameter indicates millimeter per data point and, thereby, rather shows movement speed instead of position coordinates. To avoid slow head drifts biasing the correction procedure, the motion parameter is set to a threshold. As a result, supposedly only critical abrupt movements are accounted for. The threshold is usually determined in relation to the scanner's field strength (i.e., 0.5 mm for 1.5 T, 0.3 mm for 3 T). In this experiment 25 artefacts were chosen as length of the artefact window and 0.3 mm as threshold for a window reset. Each artefact volume was baseline corrected. In continuous fMRI recordings without silent gap the artefact period itself can be used as baseline epoch (i.e., 0 ms to 1800 ms).

After all data were GA corrected, they were cut. Sections representing task practice were removed, since these trials were not valid for analysis. Breaks remained in the data to feed more data into ICA and improve identification of BCG artefacts. Further, EEG data were filtered with 0.5 Hz high-pass and a 30 Hz low-pass finite impulse response filters. For the ECG data these cut-offs were set to 1 Hz as high-pass and 20 Hz as low-pass limits. As offline-reference for all channels, the mean of the bilateral mastoids TP9 and TP10 at the lower rear of the ears was used.

To account for BCG artefacts, all EEG and ECG channels were entered into ICA utilizing the Infomax algorithm implemented in MNE-python at the original sampling rate. As stated in section 1.1.1, BCG artefacts are caused by movement of electrodes and cardiac-related activities (Allen, Polizzi, Krakow, Fish, & Lemieux, 1998). The magnitude of these artefacts is

impacted by among other factors the  $B_0$  field strength. At 3 T, as in this experiment, their amplitude can range up to 400  $\mu$ V at frequencies from 1 to 50 Hz (Allen et al., 2000a; Debener, Mullinger, Niazy, & Bowtell, 2008). Their shape and size can vary over time and between subjects. In addition to spectral composition and amplitude, BCG artefacts can be recognized by their characteristic topographies. It has been demonstrated that BCG artefacts occur as a progression of topographies marked by reversed polarities over the left and right hemisphere and higher amplitudes at temporal electrodes (Yan et al., 2010). Finally, a reliable indicator of BCG artefacts is their temporal correlation to R peaks, and more broadly the QRS complex, in the ECG, which mark a rapid depolarization of the right and left heart ventricles (Debener et al., 2008; Shams, Alain, & Strother, 2015; Wu, Wu, Zhan, Yao, & Wen, 2016).

In unmixing the EEG signal, 25 ICA components were extracted for each subject. Distorting data portions exceeding a threshold of  $+/-$  100  $\mu$ V were excluded from the component extraction. To identify artefact components the ECG signal was epoched around the QRS complex. These epochs were then correlated to all ICA component's source signal time course, in order to compute artefact scores and identify components likely representing BCG artefacts. An example of artefact scores can be seen in **Figure 6**, depicting almost linear dependencies of ICA components and ECG epochs from subject 10. For an ideal selection of artefact components, they were all inspected in terms of their artefact score and their properties, such as topography, amplitude and spectral power. In order to validate the selection two further steps were taken: 1) ECG epochs for the QRS complex were averaged and compared to a

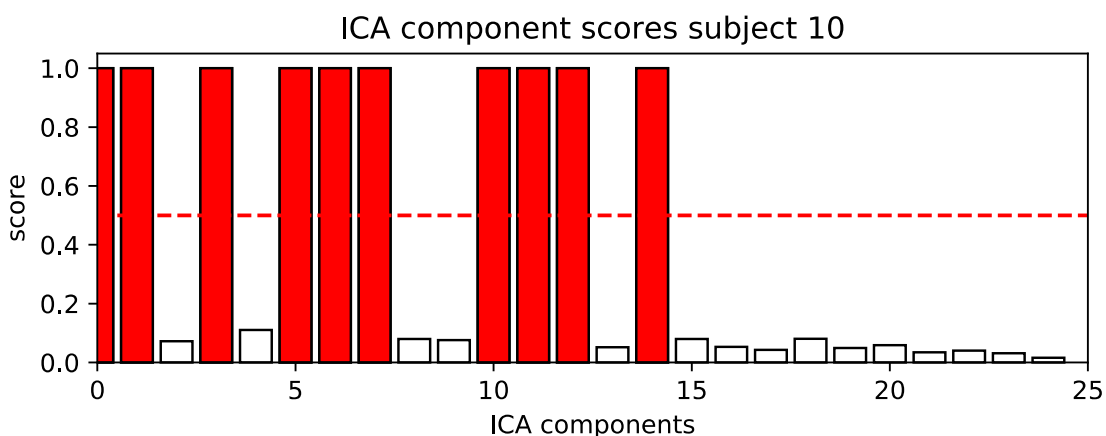


**Figure 6** Artefact scores of ICA components from subject 10. The artefact scores represent correlations of ECG epochs with ICA components' source signal time courses. The red, dotted line indicates an artefact score of 0.5. Any component exceeding this threshold with the characteristic topography and spectral power was considered an artefact.

component's signal time course. 2) All ICA components of all subjects but subject 10 were correlated to a tuple of model BCG artefact components. The ICA decomposition of subject 10 was chosen as a reference ICA, since it contained typical components with high artefact scores. This procedure was based on an ICA tutorial for ocular artefact removal<sup>2</sup> in MNE-python provided by the MNE Developers. In addition to BCG artefacts, components reflecting eye or muscle movement were also rejected before back-projecting the components to the continuous EEG signal. Again, components were classified based on their topography, amplitude and spectral power.

Before epoching, continuous data were downsampled from 5 kHz to 250 Hz. Epochs for all events were extracted -2000 ms prior and 2500 ms after the event to provide an appropriate baseline window for time-frequency analyses. When aligning EEG and fMRI segments, EEG epochs were cut to an upper limit of 1500 ms to ensure EEG epochs and modeled BOLD responses would align. Only trials followed by a correct response were kept. Plus, RT had to be above 100 ms and below 800 ms to be considered valid for epoching. Both cue- and probe-locked epochs were analyzed. Global Field Power (GFP) was calculated as the average standard deviation of all EEG channels, indexing topographical trends of differences between electrodes.

Before trials were averaged, those likely contaminated by uncorrected movement artifacts were marked and excluded from grand averages (max. voltage gradient of 35  $\mu$ V/ms; max. amplitude of  $-/+100 \mu$ V). ERPs for cues and probes were computed separately for each subject. To ensure that observations were not distorted by edge artefacts, a baseline correction for the time window 250 ms prior to the event onset was performed.

Statistical inference was drawn by entering baseline corrected single trial amplitudes averaged for the time window from 250 ms to 800 ms into regressional models similar to the ones from behavioral analysis.

#### 2.5.4 Time-frequency and Parallel Factor analysis

For time-frequency transformations, the same epoch selection as for ERPs was used. Epochs were convolved using a Morlet wavelet for frequencies from 1 to 30 Hz. Since theta and alpha bands were of primary interest, frequencies for the wavelet were logarithmically spaced for points between 1 and 12 Hz. Temporal power for single frequencies were baseline corrected through dividing temporal power by the mean of the period of 1700 ms to 300 ms before the event onset.

---

<sup>2</sup> [https://www.martinos.org/mne/stable/auto\\_tutorials/plot\\_artifacts\\_correction\\_ica.html](https://www.martinos.org/mne/stable/auto_tutorials/plot_artifacts_correction_ica.html)

In previous time-frequency analyses of similar continuous performance tasks, results featured elevated power in the theta, alpha and also beta frequency band (Bickel et al., 2012). To focus analyses of this study on relevant frequency bands, a Parallel Factor Analysis (PARAFAC) for time-frequency results (Harshman, 1970) was computed utilizing its implementation in the multiway package (Helwig, 2017) in R. PARAFAC uses three-dimensional EEG data structures (i.e., time by frequency by electrode) for a principal component analysis of the EEG spectrum. Similar to PLS, it decomposes data into atoms, each with a temporal, spatial (i.e., electrode) and spectral signature.

Subsequent analyses were focused on frequency bands most prominent in the time-frequency analysis and PARAFAC decomposition. For the latter, the solution with the best fit to empirical data was chosen utilizing Bro's core consistency diagnostic criterion (Bro, 1998).

## 2.6 Multimodal data analysis

For the multimodal data integration and fusion, analyses were focused on cue-related activity. This was done to deal with the large amount of data and because for answering the hypotheses stated in sections 1.4.1 and 1.4.2 the cues represent the most important part of the experiment.

### 2.6.1 Asymmetric data integration

In terms of asymmetric data integration, two types of analyses were implemented: As an sMRI-informed EEG analysis, dipole source estimation and, on the fMRI side, BOLD prediction with an EEG-derived parametric regressor.

#### *Dipole source estimation using DIPFIT2*

The DIPFIT plugin decomposes the observed scalp current distribution into a set number of equivalent current dipoles. However, in estimating dipoles the question remains what part of the EEG signal is best suited to be unmixed. Raw signal is contorted by noise and multiple dipole projections can mix in identical observations, because systematic brain activity is still mixed in the continuous signal. Averaged ERPs, in turn, lose the original time course of single trial projections, as they merely represent a mean value of time series points.

For the purposes of this study, unmixed ICA components were chosen as scalp distributions, since it has been suggested that temporally independent signal sources can

resemble dipoles more than raw or averaged EEG data with single components often almost perfectly fitting a single dipole (Delorme, Palmer, Onton, Oostenveld, & Makeig, 2012). Therefore, in estimating dipoles for components, each component map is assumed to be the resulting projections of a fixed brain source. In order to enhance this estimation, a subject's sMRI data was co-registered with the subject's head shape to position the head and the sensors in a common coordinate system as a source space. 31 channels were entered for this co-registration excluding the ECG.

To this end, the Boundary Element Method (BEM) was applied, transforming output data to Montreal Neurological Institute (MNI) space. In the context of source reconstruction, this method serves to solve integral equations of the estimation by using values from boundary information (i.e., brain issues, skin, skull) to fit into the integral equation. Via DIPFIT's autofit function, electrode positions were projected to the BEM head model and dipoles were located in a rough coarse grid to ease the following more refined best-fitting localization. All 30 components from the ICA unmixing were fit to this 3D coarse grid, while disregarding sources outside the head. Rejection threshold for unexplained variance in the component fit were set to 100%, thus, only excluding dipoles virtually non-fitting to the component's time course. Next, components were fine fit by adjusting dipole orientation to reduce residual variance.

Finally, likely candidates for ERP components were chosen based on their scalp distribution, spectral composition and residual variance. Here, it is important to note that the sustained positivity investigated in this study reflects stages of ERP succession, including both an initial P3a and P3b. This succession of components has been explained in the past as several sources distributed across the medial prefrontal and parietal cortex (Debener, Makeig, Delorme, & Engel, 2004; Rogers et al., 1991). Hence, multiple components on a single subject level were selected in this study.

#### *BOLD prediction with parametric, single-trial EEG regressors*

The BOLD estimation GLM with parametric EEG regressors was implemented following the procedure described in section 1.2. Before trials were averaged to single trial amplitude and frequency power estimates, they were pre-processed as outlined in section 2.5.3 including baseline corrections. Trials marked by artefact detection were excluded, as were their counterparts in the fMRI.

For each epoched, cue-locked trial a mean amplitude was derived reflecting the averaged value from 250 ms to 800 ms after the cue's onset. Despite the P3 or sustained positivity rising

after about 250 ms and peaking after about 500 ms, a larger time window was included into averaging amplitudes to account for single trial variability of noise fluctuations (Scheibe et al., 2010). Along with movement parameters as covariates and non-parametric regressors for the cue and probe onsets, the EEG estimates were entered into single subject level GLMs.

## 2.6.2 Joint and Parallel ICA

For both the jICA and pICA, pre-processing for EEG and fMRI data was done as described in sections 2.5.2 and 2.5.3 with few alterations. To account for the hemodynamic lag between electrophysiological and BOLD responses, the canonical HRF was used to convolve EEG epochs. More precisely, since EEG activity can be thought of almost instantaneous to electric changes at the synapse, the BOLD response is delayed compared to the original neuronal activity. Thus, fluctuations in its signal curve occur later than in the EEG. In order to appropriately relate the two signals, the authors recommended a transformation of EEG epochs using the canonical HRF as an approximation of the delay (Calhoun & Adali, 2009; Sui et al., 2012). Moreover, instead of averaging EEG and fMRI data, jICA and pICA allow for statistical modeling of first level data. While both ICAs can be performed on group level, the authors have suggested use subject data. Therefore, both EEG and fMRI data were only averaged on the level of single subjects.

### *Joint Independent Component Analysis*

Using contrast images from cues to baseline and averaged evoked responses to cues, all data were entered into the Fusion ICA Toolbox for Matlab. Pz was chosen for the EEG input, because the sustained positivity was most pronounced. For both EEG and fMRI a duration of 1.5 s after the cue was modeled. The design for the conducted experiment was specified as a matrix including one group with two data modalities separated by condition or type of cue (i.e., cue A or B) resulting in two EEG and two fMRI features each. Before fusing data features, each was normalized via square root of mean of squared data for all subjects. The number of components was estimated via standard Minimum Description Length Criterion estimation (Li, Adali, & Calhoun, 2006). Each component was scaled to the original data units and masked using non-zero voxels for fMRI and original data indices for the EEG. Data were reduced using Eigen value decompositions from normalized data and extracting Eigen vectors.

The two ICAs were performed using the Infomax algorithm (classic sphering) on the previously reduced data. For each condition the six components explaining most of the spatio-

temporal variability across subjects and data features were extracted from the unmixed signal. Hence, a single component with time course ERP data and negative as well as positive weights on voxel clusters contained data from both features specific to one type of cue. To derive final ICA decompositions and components, these were averaged across three repeated runs of the ICA.

#### *Parallel Independent Component Analysis*

For pICA matrix definition, normalization, masking, data reduction and ICA specifications were adopted. Yet, since pICA represents a semi-blind source separation method, correlations between mixing coefficients of features were estimated instead of assuming identical covariation across subjects.

To assess a baseline level of correlation between EEG and fMRI, raw time series data instead of mixing coefficients were also analyzed. Here, single trial correlations of EEG amplitude, theta power, alpha power as well as time series signal for all regions of interest underwent permutations tests of time segments. However, this procedure is sensitive to the naturally occurring autocorrelation of time series data, as each point is highly correlated with the juxtaposed time points. For this reason, the *ccf* function implemented in the *stats* package in R (R Development Core Team, 2016) was applied to compute the cross-correlation of each univariate time series with one another.

### 2.6.3 Multiway Partial Least Squares

The N-PLS analysis with the goal of relating two multidimensional sets of data were performed using the sNPLS package for R and N-way toolbox for Matlab. In preparation for the calculations necessary for N-PLS each EEG and fMRI data set was pre-processed as described before. Like in the ICA-based approaches, EEG frequency data were convolved with the canonical HRF. However, as opposed to ICA, N-PLS was performed on single trial data.

In case of the EEG, the basic matrix underlying the analysis was comprised of three dimensions with trials as time points for each cue and frequencies nested within electrodes. For the fMRI intensity values for voxels over time were represented as a two-dimensional matrix.

Both decompositions were based on the same principles as established by Bro (1996) and as summarized in section 1.3.2. The very basic structural model used in this decomposition for EEG and fMRI vectors can be thought of as expressed in **Equations 3 and 4**:

$$\hat{S}_{dwt} = \sum_{k=1}^{N_k} a_{dk} b_{wk} c_{tk} + e_{dt} \quad (3),$$

$$\hat{F}_{st} = \sum_{k=1}^{N_k} u_{sk} v_{tk} + \varepsilon_{st} \quad (4).$$

The structural models for decomposition with the matrices S and F are estimated by identifying a set of normalized loading vectors, which are represented in the equations as  $a_k$ ,  $b_k$  and  $u_k$ . In an iterative procedure these vectors are calculated so that their respective least-squares score vectors  $c_k$  and  $v_k$  have maximal covariance. Vectors  $a_k$ ,  $b_k$  and  $u_k$  are modular, as in  $a_k$  holds the EEG's spatial signature or topography and  $b_k$  the spectral signature, while  $u_k$  represents the fMRI-specific voxel signature. Accordingly, d indexes electrodes and s voxels in each matrix and vector. The error terms  $\varepsilon_{st}$  and  $e_{dwt}$  both refer to elements of noise matrices. Lastly, the index k denotes components or atoms, as they are referred to in N-PLS literature, which are extracted separately. This entails that each atom k gets a rank-one model for the EEG matrix S with times by electrodes and the fMRI matrix F with times by voxels. These models are then subtracted from the original data, and a new atom of signatures is built from the residuals.

Each load of a vector for an atom can be seen as a signature which demonstrates maximal covariance with its counterpart in the other modality or matrix. For example, the vector  $b_k$  is the spectral signature from the EEG whose variation across time points shows maximal alignment with the variation in the signature  $u_k$  representing the BOLD signal. It should be noted that unlike  $a_k$ ,  $b_k$  and  $u_k$  the temporal signatures  $c_k$  and  $v_k$  are constrained while atoms are extracted.

Before N-PLS decompositions were performed, results from PARAFAC were taken into account to compare which frequencies from the spectral signature should be prominent in the analysis. When decomposing EEG and fMRI data in this manner, it is essential to choose the appropriate data format. For instance, there are several time points even in a downsampled EEG data set for each fMRI time point. Plus, entering all available fMRI voxels for each time point would entail an excess of elements in the response variable. So decomposing these variables via SVD, could easily result in a lack of data in the predictor variables, since there are not enough data in the spatial or spectral EEG signature. For this reason, EEG points were averaged for each trial and fMRI voxels were limited to the structures relevant to the hypotheses.

#### 2.6.4 Mixed-effects modeling with multimodal regressors

To assess the predictive value in mixed-effects models for the relation between behavioral and neuronal data, a succession of mixed-effects models was tested. For this purpose, data were ordered in a data frame with single trial RT nested within cue types and blocks. Predictors were continuous, as model equations included regressors reflecting single trial MRI parameters, EEG parameters or both. This type of regression was performed for the reasons outlined in 1.3.3. Cue-locked neuronal correlates from both EEG and fMRI were chosen as regressors. Processing context cues adequately, is vital to good task performance. Ideal performance levels in the DPX task are reached when subjects control themselves cue- instead of probe-oriented. Hence, activation pattern representing the success of cue processing might yield relevant relations to RT.

In mixed-effects models there is both fixed and random effects characterizing the relationship between independent and dependent variables. While fixed effects allow to test the observed variation in the dependent variable in accordance to variation in the independent variable (i.e., intercepts and slopes of experimental conditions), random effects represent the dependent variable's variance disregarding the predictors. Compared to other regressional models, this type of effect modeling has the advantage of decreasing error variance resulting from unaccounted variability in the criterion.

A predictor's value was operationalized in multiple ways. For one, the variable's fixed effect was taken into account. More than that, a model sequence was set up and tested for incremental fit to the empirical values of the dependent variable. Here, a model's deviance and fit to the empirical data in relation to the previous model's fit was assessed. By sequentially allowing for intercepts and slopes for each predictor, the contribution of a more complex model to explaining the data was tested. Fixed and random parameters were estimated using a Full Maximum Likelihood estimation, since the fixed part of the model was different between model comparisons, thus, not allowing for Restricted Maximum Likelihood estimation.

Deviance is a measure of model misfit and is calculated according to **Equation 6** (Bates et al., 2015), wherein L represents the likelihood of finding the observed values assuming the specified model parameters fitted on the sample are accurate in the population:

$$\text{Deviance} = -2 \log(L) \quad (6)$$

Another way of comparing mixed-effects models is to assess information criteria, such as Akaike Information Criterion (AIC; Akaike, 1974), which is based on classical maximum likelihood estimation. A good fit of the model on empirical data, or a high likelihood estimation, will lead to a decrease in the AIC. At the same time, the addition of model restrictions is considered in the AIC calculation and increases it.

In case of nested models a  $\chi^2$  difference measure of model misfit can also be calculated. This difference measure is described in **Equation 7**:

$$\chi^2 = Dev_{model\ a} - Dev_{model\ b} \quad df = df_{model\ a} - df_{model\ b} \quad (7)$$

As opposed to deviance, a Pseudo-R<sup>2</sup> was computed representing incremental value in terms of explained variance when comparing two successive models. The calculation of Pseudo-R<sup>2</sup> followed **Equation 8**:

$$\text{Pseudo} - R^2 = \left( \frac{\hat{\sigma}_{\varepsilon(1)}^2 - \hat{\sigma}_{\varepsilon(2)}^2}{\hat{\sigma}_{\varepsilon(1)}^2} \right) \quad (8)$$

This Pseudo-R<sup>2</sup> utilizes the error variance  $\hat{\sigma}_{\varepsilon}^2$  of a given model and given parameter. The same error variance is taken from a second model and subtracted from the first's. If the denominator is large, there is a noteworthy discrepancy between error variances with the second model having a much smaller error variance. To express this difference as a proportion, it is divided by the first model's error variance. This equation can easily be adjusted to allow for an average reduction of multiple error variances and to correct for correlations between R<sup>2</sup> statistics. This was implemented using the r2glmm package in R in accordance to the R<sup>2</sup> coefficient presented by Nakagawa and Schielzeth (Nakagawa & Schielzeth, 2013).

Lastly, for models with equivalent deviance or informational value, the model with less restrictions or parameters was considered superior, as it required less specifications for the same values. In summation, all contributions from EEG and fMRI predictors received a model fit and deviance showing their use in predicting RT performance in the experiment.

### 3. Results

#### 3.1 Unimodal results

##### 3.1.1 Behavioral results

Performance concerning RT divided by trialtypes over the four blocks as well as the corresponding PSI values can be seen in **Figure 7**. Single trial measure for RT were entered into a mixed-effects model to estimate effects for factors trialtypes and block as well as their interaction. PSIs were calculated for averaged RTs over blocks and then compared using GLM. A distribution of raw behavioral values of RT can be found in Appendix C.

As indicated by the fixed effect for block, RT performance did not change significantly across time disregarding trialtypes,  $\chi^2 (3, N = 13) = .73, p = .87$ . Also the interaction of block and trialtypes proved to be non-significant,  $\chi^2 (9, N = 13) = 2.54, p = .98$ . However, as the differences between colored bars highlight, trialtypes yielded a significant fixed effect ( $\chi^2 (3, N = 13) = 343.58, p < .001$ ) with highest RT for AY. Subsequent comparisons of factor levels showed that subjects responded significantly slower to AY ( $t(12) = 6.62, p < .001$ ) and significantly faster to BX ( $t(12) = -2.05, p < .05$ ) compared to the most frequent trialtypes AX. PSI values based on RT did not vary significantly across blocks,  $F (1, 50) = -.08, p = .9, \eta^2 = .0001$ .

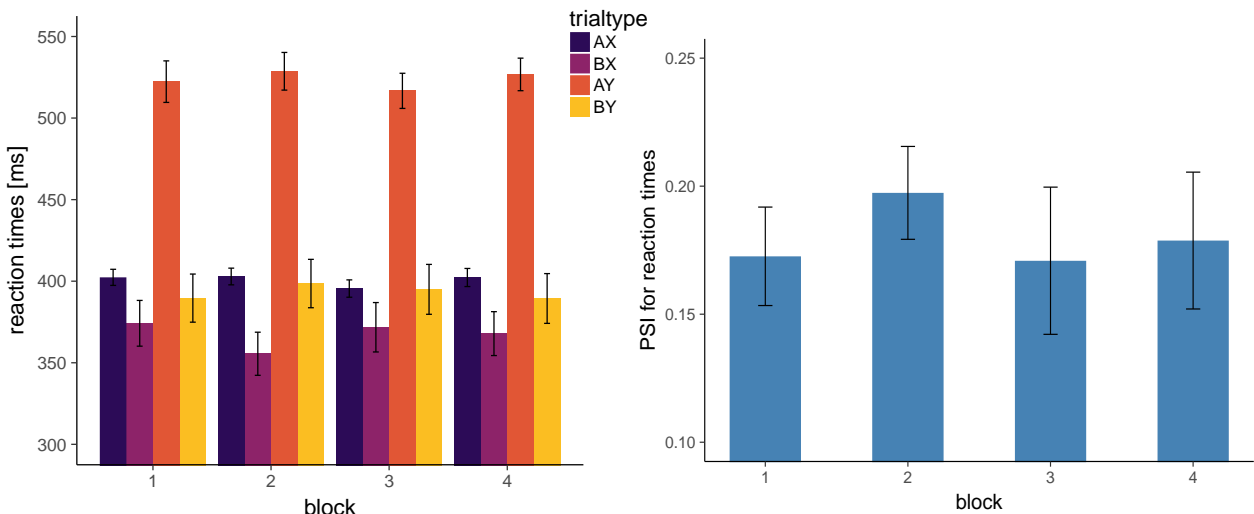


**Figure 7** The left panel displays RT in the DPX task divided by trialtypes (in ms) over four blocks. The panel on the right shows the same RT results transformed to PSI values in accordance to **Equation 1** over the four blocks. Error bars in each panel depict the range of  $\pm$  a single standard error of the mean.

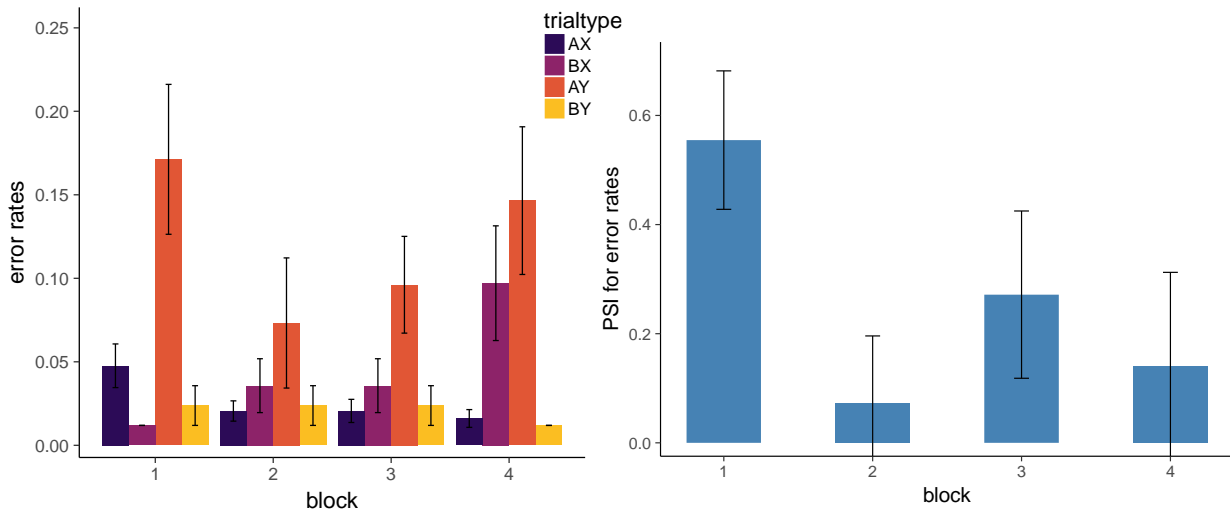


**Figure 8** The bar graph on the left shows ER from the DPX by trialtypes across all blocks. ER correspond to the amount of errors divided by the frequency of the respective trialtypes per block. The graph on the right displays ER results as PSI values over blocks. Error bars in each panel depict the range of  $\pm$  a single standard error of the mean.

Parallel to RT, **Figure 8** shows ER and PSI values based on ER over blocks. Total error scores and corresponding PSI can be seen in Appendix C. Like RT performance, ER did not change over time ( $\chi^2 (3, N = 13) = 4.99, p = .17$ ), but differed between trialtypes ( $\chi^2 (3, N = 13) = 51.95, p < .001$ ). Despite a trend of ER performance aligning for trialtypes over blocks, the interaction of trialtypes and blocks proved to be non-significant ( $\chi^2 (9, N = 13) = 16.4, p = .06$ ). Total error counts disregarding frequency were also significantly impacted by trialtypes,  $\chi^2 (3, N = 13) = 43.74, p < .001$ . In case of total error counts, the interaction of blocks and trialtypes mirrored the trend detected for ER ( $\chi^2 (9, N = 13) = 22.04, p < .01$ ) with decreasing errors overall, but especially for trialtypes AX ( $M = 0.2, SD = 1.19$ ). As with RT, PSI based on total error counts or ER scores did not change significantly over blocks,  $F (1, 50) = 2.5, p = .12$ ,  $\eta^2 = .05$ .

### 3.1.2 EEG results

Concerning EEG data, the same mixed-effects models was used for amplitude as for RT data. Single trial amplitude and averaged oscillatory measures were included.

As can be seen in **Figure 9** and **Figure 10**, there were multiple ERPs following cue onsets. In both cases, there was a negative deflection at bilateral occipital electrodes, ensued by a small positive potential peaking after approximately 300 ms at the frontal and posterior midline. This initial positivity was succeeded by an elevated sustained positivity reaching its maximum at the

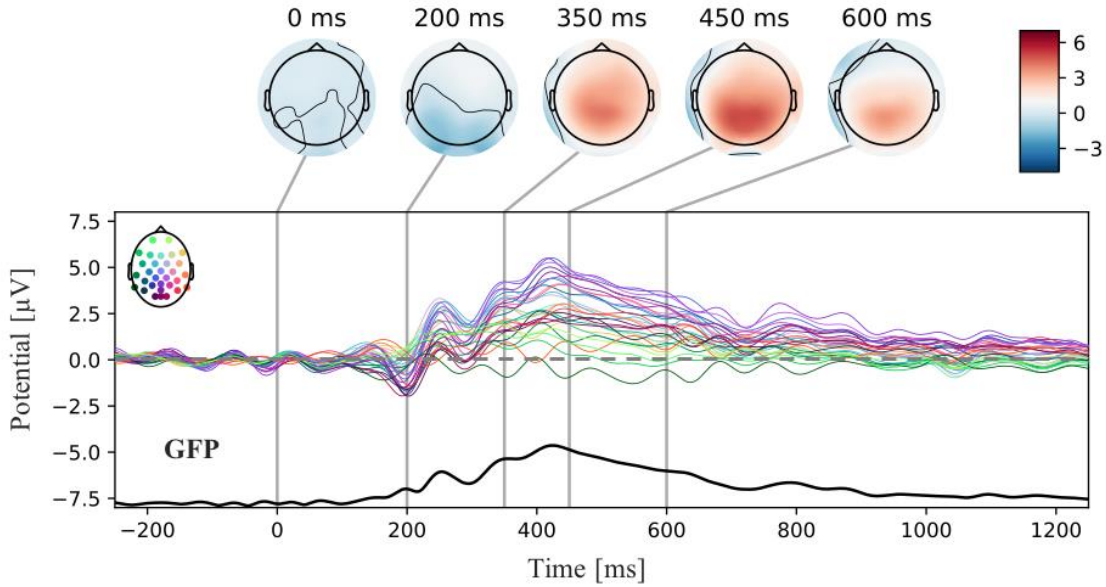


**Figure 9** ERPs following cue A, baseline corrected for the displayed time window of 250 ms before cue presentation to the cue. Graphs show the 31 EEG channels color-coded for their spatial distribution across the scalp. A legend for spatial distribution of channels is provided with the colored head figure in the upper left corner of the ERP panel. The black graph equals the Global Field Power (GFP) for all channels disregarding the ECG. Topographic maps on top show the averaged scalp distribution for an interval of 50 ms around the indicated time point.

posterior midline (Pz) around 500 ms. The averaged amplitude at Pz was significantly larger for B compared to A,  $\chi^2 (1, N = 13) = 11.11, p < .001$ .

A relatively similar succession of potentials was observable after probes. All channels probe-locked to AX, BX, AY and BY are depicted in Appendix D. **Figure 11** shows amplitudes

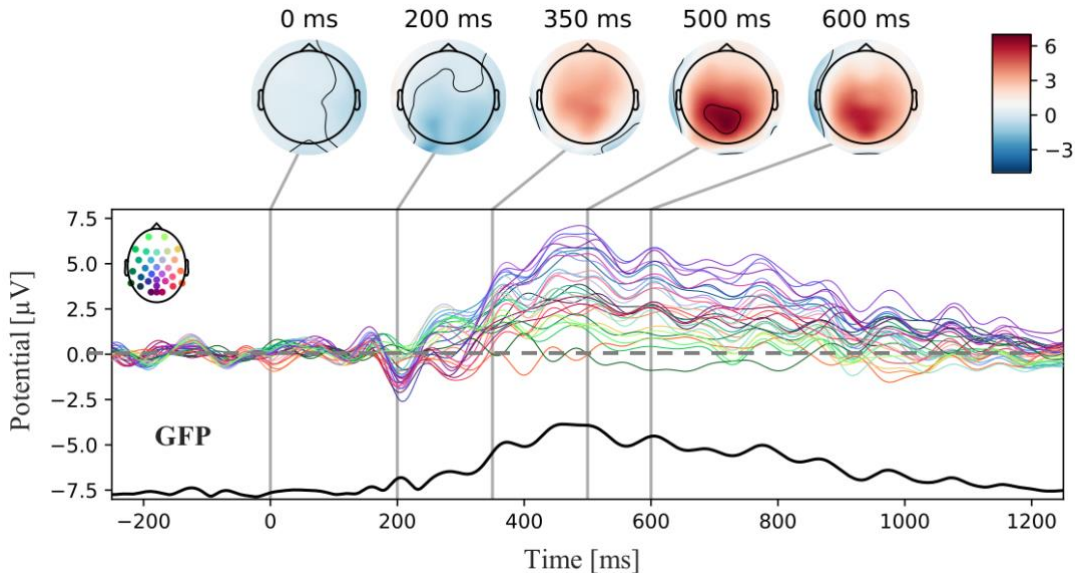


**Figure 10** ERPs following cue B, baseline corrected for the displayed time window of -250 ms before cue presentation to the cue. Graphs, spatial distribution and GFP are identically plotted to cue A in **Figure 9**. Also topographic maps and scaling are kept the same.

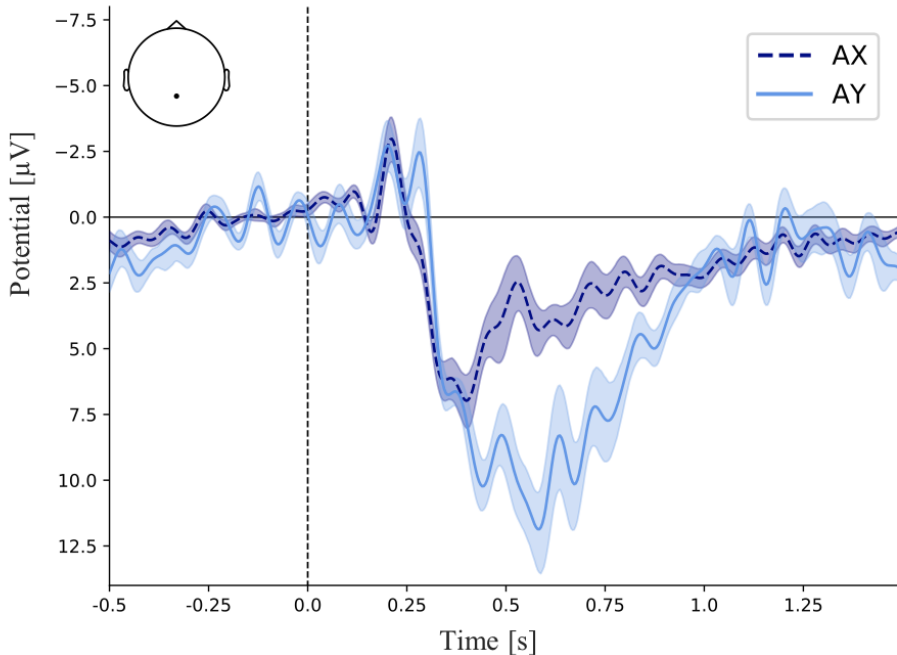


**Figure 11** Probe-locked ERPs at Pz separated for trialtypes AY (solid light blue line) and AX (dotted purple line). ERPs were baseline corrected for -250 ms to 0 ms before probe onset. The topographic map in the upper left corner displays the position of potentials on the scalp. Shaded areas depict  $\pm$  a single standard error of the mean for the respective time points.

following probes of trialtypes AX and AY, as this contrast was most prominent and relevant to this study. Averaged positive deflections at Pz for the chosen time frame of the sustained positivity were significantly attenuated in AY trials relative to AX trials,  $\chi^2 (1, N = 13) = 10.83$ ,  $p < .001$ .

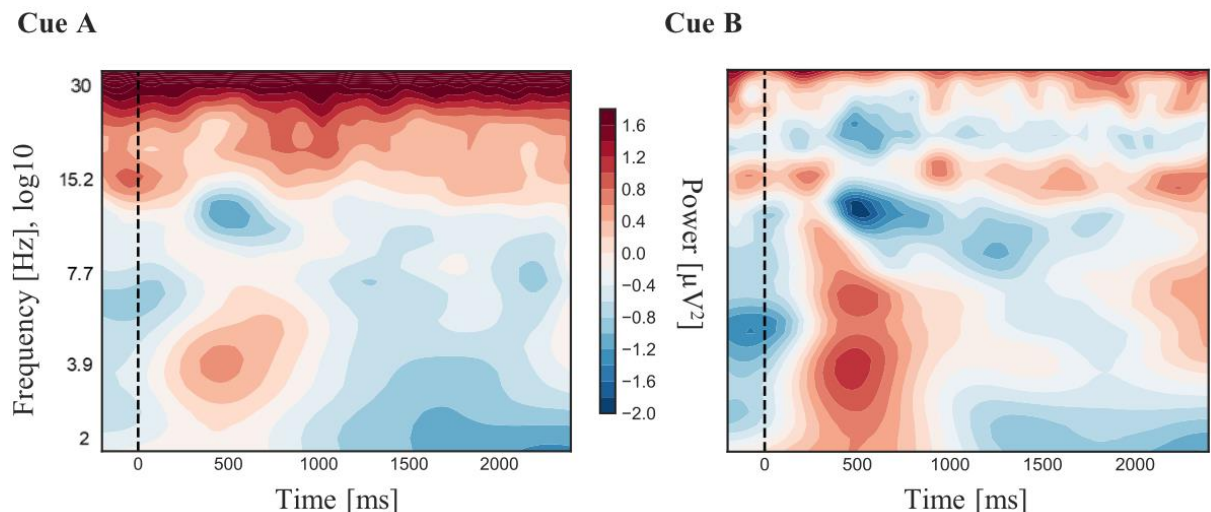


**Figure 12** ERSPs following cue A (left) and cue B (right) baseline corrected for -1700 ms to -300 ms before cue presentation at Pz. Contour plots show temporal power color coded by logarithmically scaled frequency band over time. Dotted vertical lines mark the cue presentation

Regarding time-frequency analyses, there were notable event-related power changes compared to the baseline window before cue presentation approximately 200 ms after cue presentation. Contour plots depicting these results can be seen in **Figure 12**. Increases in power were observed mostly in the alpha and theta band between 200 ms and 700 ms. However, theta perturbations extended into delta frequencies (i.e., 1-3 Hz), especially for cue B. Alpha suppression was predominantly focused on the upper alpha band with peak power decreases around 13 to 14 Hz. Both alpha decreases ( $\chi^2 (1, N = 13) = 6.57, p = .06$ ) as well as theta increases ( $\chi^2 (1, N = 13) = 8.51, p < .01$ ) were stronger for cue B relative to A.

As shown in **Figure 12**, there were perturbations compared to baseline power in the beta range, as well. Therefore, PARAFAC was performed for two models, one with two factors and one with three factors. These were then evaluated in regards to their fit to the empirical data using Bro's core consistency diagnostic criterion. An ideal score of 100% can be interpreted as multilinear fit of extracted components to the empirical data. Scores below indicate deviations from this ideal multilinear structure for the specified factor solution. While the two-factor model was able to explain 93.2% and 94.9% of the variance in cue A and B related activity, respectively, the three-factor model only accounted for 80.6% and 80.4% of the time-varying EEG spectrum. In **Figure 13** results of the two-factor model for cue A and B are displayed. For both cues there was one component with strong power loading in the theta frequency, therefore, most likely reflecting the observed theta increase following cues. In terms of alpha band power, the first component of the cue A decomposition had weak power in the alpha band, whereas for cue B both components had peaks in the upper alpha band, as was noticeable in the averaged results. Compared to this, the three-factor solution had an additional component peaking in the

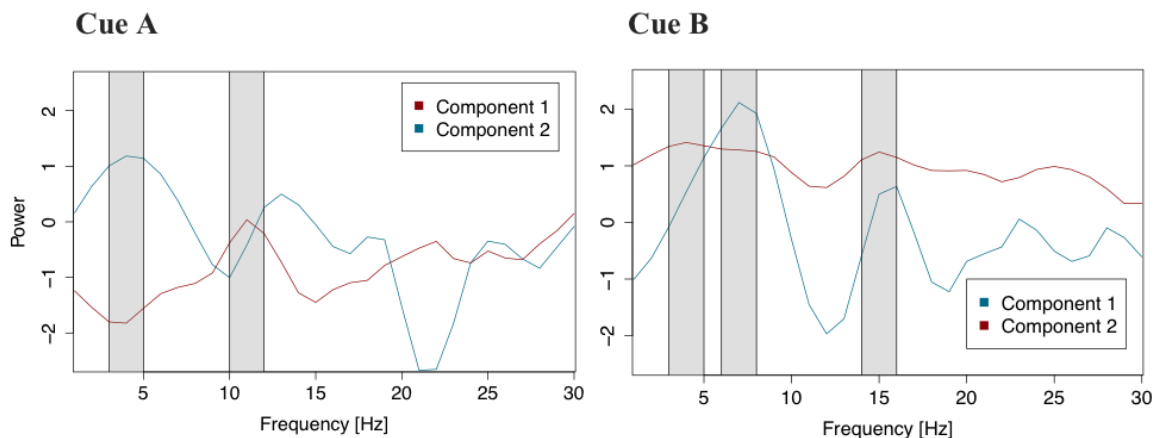


**Figure 13** Two-factor PARAFAC decomposition of time-frequency results separated by cue (A left, B right). Red and blue lines depict power loading of components across frequency bands. Peaks in the components' power values are marked with grey bars.

beta spectrum. Due to the better fit of the two-factor decompositions, multimodal analyses kept focusing on the theta and alpha spectra.

### 3.1.3 fMRI results

For the whole brain analysis, cue- and probe-related contrasts showed no significant activation clusters after correcting for multiple voxel comparisons. To test structures involved in the previously described cognitive control network focused on the prefrontal and parietal cortex, small volumes were extracted for the regions of interest.

**Figure 14** depicts contrast activations for both cues. The only significant voxel cluster for cue A that remained after familywise error (FWE) correcting p-values for multiple comparisons was found in the triangular section of the IFG,  $t(12) = 5.21, p < .05$ . No such activations were found in the left hemisphere. Regarding the ACC, a non-significant voxel cluster was detected at the intersection of the left IFG pars triangularis and ACC. With contrast weights for cues reversed, there were significant voxel cluster in the left MFG without correcting for multiple comparisons ( $t(12) = 3.05, p < .05$ ) as well as around the left ( $t(12) = 3.62, p < .05$ ) and right PCG ( $t(12) = 3.17, p < .05$ ). When applying corrections for multiple comparisons, the only significant cluster was identified at the intersection of the SFG and SMC,  $t(12) = 4.52, p < .05$ .

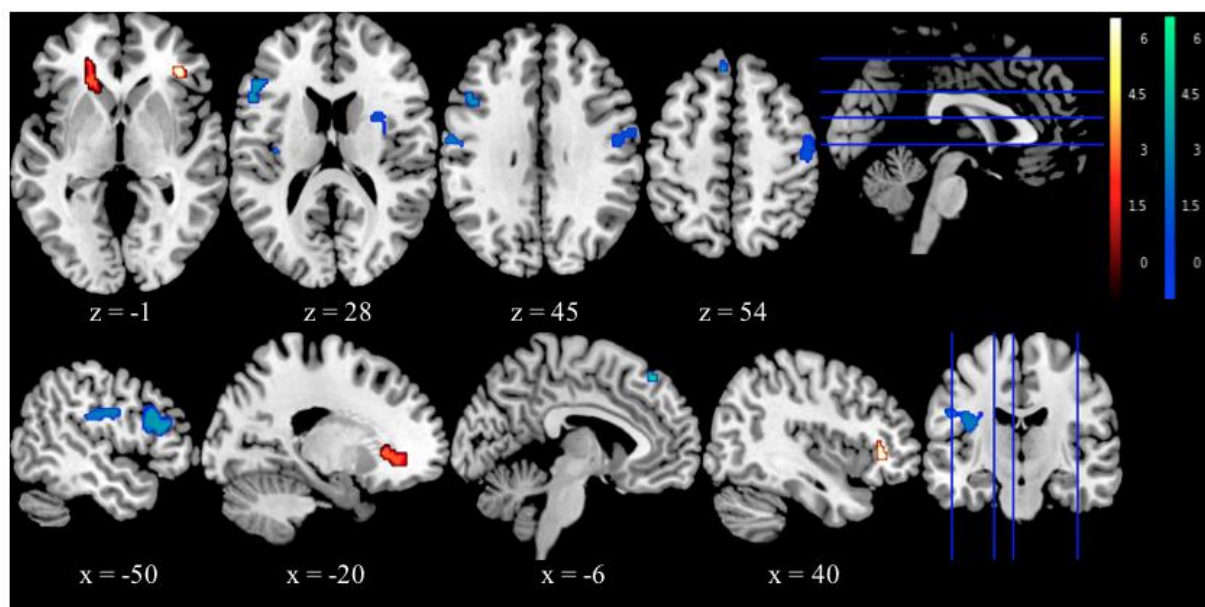


**Figure 14** fMRI group results ( $N=13$ ) for cues. Contrast images are plotted according to neurological convention with left side corresponding to the left hemisphere. Upper panels display the axial view in ascending order from left to right. Lower panels show the sagittal view moving from the left to the right hemisphere. Red and yellow signify t-values for voxel clusters with stronger activations for A, while blue and green highlight clusters that were activated stronger for cue B.

All clusters for this contrast are also shown in **Figure 14**. Statistics and anatomical descriptions for each contrast are summarized in **Table 3**.

Contrasts derived from probes were focused on the comparison of AY and AX, as proactive control is mostly locked to cues and reactive control activations are supposed manifest in the updating in WM. This predominantly occurs during the expectancy violation after an incorrect probe followed a correct cue. Therefore, AY likely reflects the most substantial effort in cognitive control.

**Table 3**

*fMRI results for contrasts of cues and probes in the DPX tasks*

Contrast	Region of interest	BA	R/L	Cluster size (voxel)	Peak t-value	MNI coordinates		
						x	y	z
A>B	ACC/IFG	32	L	78	2.33	-22	38	-1
AY>AX	ACC/IFG	32	L	49**	5.21	-28	30	14
B>A	MFG	46	L	181*	3.05	-44	28	20
A>B	IFG	45	R	32**	4.42	38	34	0
B>A	SMC/SFG	6	L	10**	3.8	-6	38	52
AY>AX	SMC	6	L	60**	4.52	-4	0	56
B>A	PCG	4	R	90*	3.17	54	-5	50
B>A	PCG	4	L	100*	3.62	-42	-12	26
AY>AX	PCG	4	L	38**	4.53	-50	0	4

*Note.* BA = Brodmann Area, R = right, L = left, MNI = Montreal Neurological Institute, \* =  $p < .05$  (uncorrected for multiple comparisons), \*\* =  $p < .05$  (FWE-corrected for multiple comparisons).

When contrasting AY and AX, stronger activations for AY were found around the same intersection of the IFG and ACC ( $t(12) = 5.21, p < .05$ ) as for cues, which sustained its significance after FWE-correction of p-values. In addition, there were enhanced activations for AY at the SMC ( $t(12) = 4.52, p < .05$ ) and left PCG ( $t(12) = 4.53, p < .05$ ). These reached significance after p-value correction, as well. For the opposite contrast, no significant voxel

clusters stronger for AX compared to AY were detected. Probe-locked contrasts are displayed in **Figure 15**.

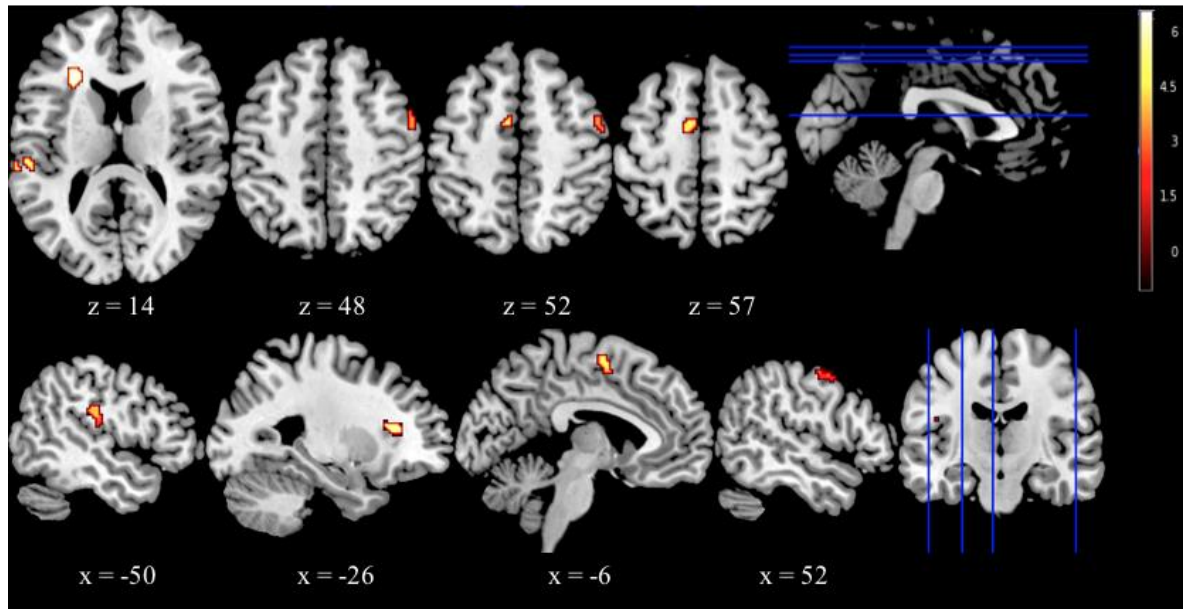


**Figure 15** fMRI group results (N=13) for probes. Red and yellow areas represent t-values for significant voxel clusters (all FWE-corrected,  $p < .05$ ) that had larger activations for AY than for AX.

### 3.2 Multimodal results

#### 3.2.1 Asymmetric integration

##### *Dipole source estimation using DIPFIT2*

From 13 subjects, subject 12 was chosen as an exemplary subject, because the ICA components reflecting ERPs in the unmixed signal were remarkably distinct. Four component clusters were similar to the scalp distribution of the ERPs involved in the sustained positivity. Peak positive deflections in these ranged from the right and central frontal electrodes to central parietal-occipital positions.

The resulting fitted dipoles are presented in **Figure 16** along with residual variances, dipole coordinates and the original ICA components. Source positions varied from medial prefrontal cortex to the parietal cortex. Components 18 and 21 most likely contributed to peak activations seen in the EEG and were located in the left posterior cingulate cortex (BA 23 and 31). These components had maximal spectral power in the range of 3 to 7 Hz and strongest positive amplitudes above the central parietal cortex. Additional dipoles were located in the right

Hippocampus (component 12, BA 54) and right pars opercularis of the inferior frontal gyrus (component 26, BA44).

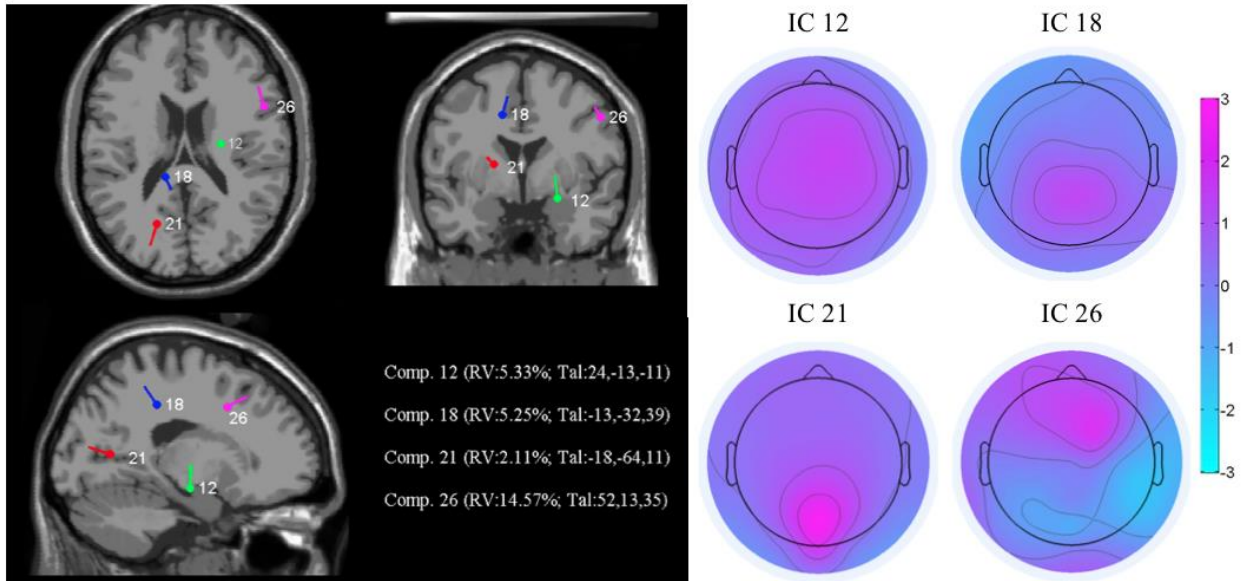


**Figure 16** Independent component (IC) dipoles for components 12, 18, 21 and 26 from subject 12. Left panels show the locations of single equivalent current dipoles for each component from axial, sagittal and coronal view. Residual variance (RV) and Talairach (Tal.) coordinates for dipole positons are plotted in the lower left corner for each component. Right panels display scalp projections for components and dipoles. Color-coded values signify amplitude in

#### *BOLD prediction with parametric, single-trial EEG regressors*

Group results for single-trial BOLD prediction based on parametric amplitude regressors are shown in **Figure 17**. As in section 3.1.3, results and plots were separated by cue. An overview of statistical contrasts is provided in **Table 4**.

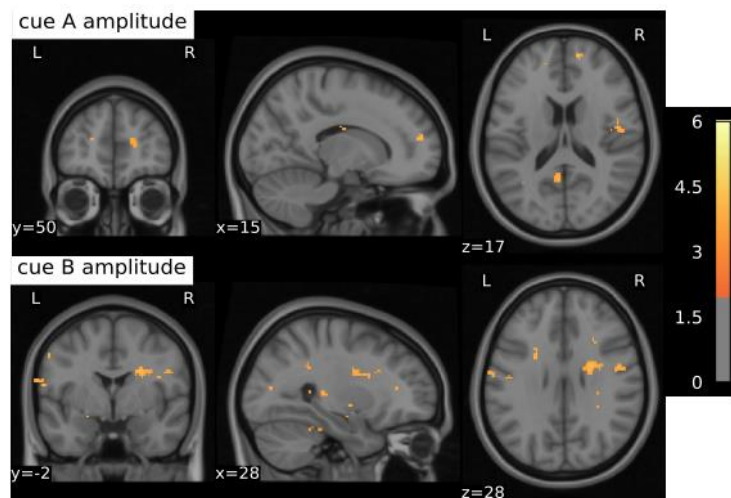


**Figure 17** fMRI group results for single-trial BOLD prediction using amplitude regressors for cues A (upper panels) and B (lower panels).

When contrasting activations on whole brain level, no significant voxel clusters remained. However, when only looking at the pre-defined regions of interest, such as the right IFG (BA 44) and the right rostral cingulate cortex (BA 10), small significant voxel cluster activations that co-varied with amplitudes of the sustained positivity were found for cue A. As for cue B, activations in the right SMC showed higher t-values. None of these activation patterns was significant after correcting for multiple comparisons.

**Table 4**

*Results for group contrasts derived from parametric EEG regressors for cues*

Contrast	Region of interest	BA	R/L	Cluster size (voxel)	Peak t-value	MNI coordinates		
						x	y	z
A>B	Rostral ACC	10	R	13*	3.53	19	57	17
A>B	IFG	44	R	22*	3.05	50	15	17
B>A	SMC	6	R	32*	4.6	28	-2	28

*Note.* BA = Brodmann Area, R = right, L = left, MNI = Montreal Neurological Institute, \* =  $p < .05$  (uncorrected for multiple comparisons).

### 3.2.2 Joint and parallel ICA

#### *Time Series correlation*

**Figure 18** depicts univariate time series correlations between different EEG and fMRI measures for both cues. On the EEG side, based on prior results theta power, alpha power and amplitude were used for correlations. Concerning the fMRI, **Figure 18** shows Z-transformed scores for the IFG, MFG, PCG and the middle cingulate. Pearson coefficients are summarized in a table of cross-correlations in

#### Appendix E.

Generally, correlations between fMRI activation and frequency band power were slightly stronger than for amplitudes. Averaged over all subjects, amplitudes did not significantly correlate with any fMRI measures. Significant correlations were found between theta power and all specified regions, including the IFG ( $r(11) = .48, p < .01$ ), MFG ( $r(11) = .42, p < .05$ ), PCG ( $r(11) = .4, p < .05$ ) and the cingulate ( $r(11) = .43, p < .05$ ). These correlations were only

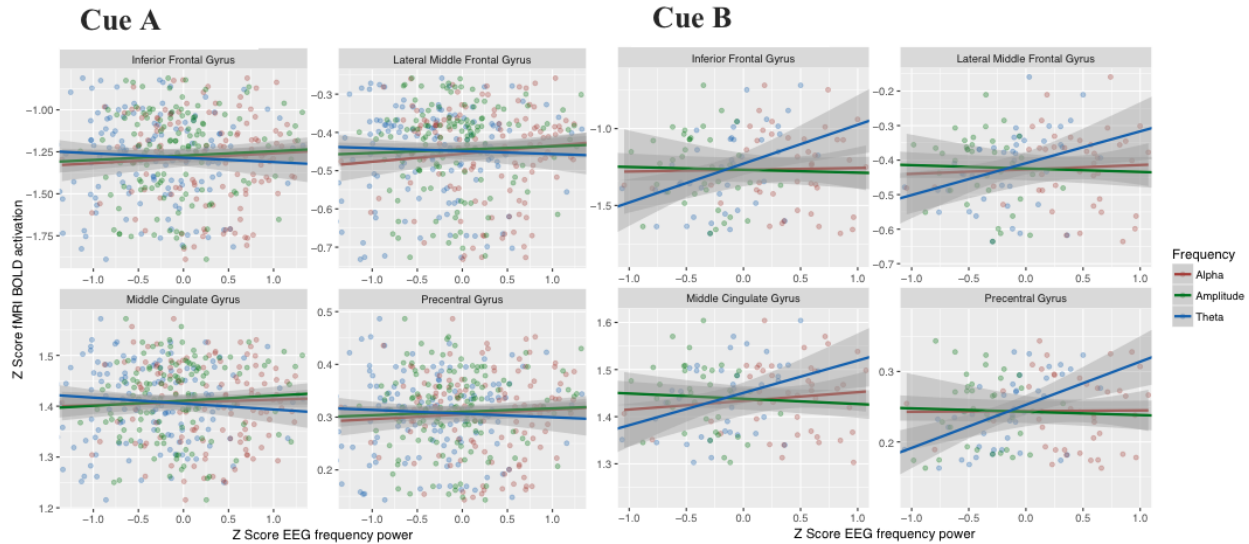


**Figure 18** Univariate time series correlations separated by cue (A on the left, B on the right). All times series data were Z-transformed. Single panels show predictions of time series data from regions of interest based on single trial theta, alpha and amplitude measures. Shaded areas correspond to  $\pm$  a single standard error.

identified for cue B. For cue A, there were only few instances of smaller significant relationships between both theta and alpha band power and fMRI signal.

#### *Joint ICA*

Results of the jICA are plotted in **Figure 19** with both EEG and fMRI features. The figure represents two components found for cue A and B that explain most of the variability in their respective EEG time course. Each EEG part of the component shows a strong positive amplitude peaking between 350 ms and 500 ms after the cue onset. The averaged ERP is also plotted in the respective EEG panels, highlighting the similarity between component signal and averaged signal. On the right of the EEG features, fMRI panels present standardized Z-scores of voxel clusters with identical variation compared to the EEG across subjects. Rising voxel cluster activations co-varying with positive amplitude increases for cue A were detected in the DLPFC and IFG. In turn, activations of the medial prefrontal cortex posterior parietal cortex decreased. As opposed to cue A, the EEG feature explaining most of the sustained positivity following cue B was closely related to a decrease in the DLPFC and an increase in the motor and posterior parietal cortex.

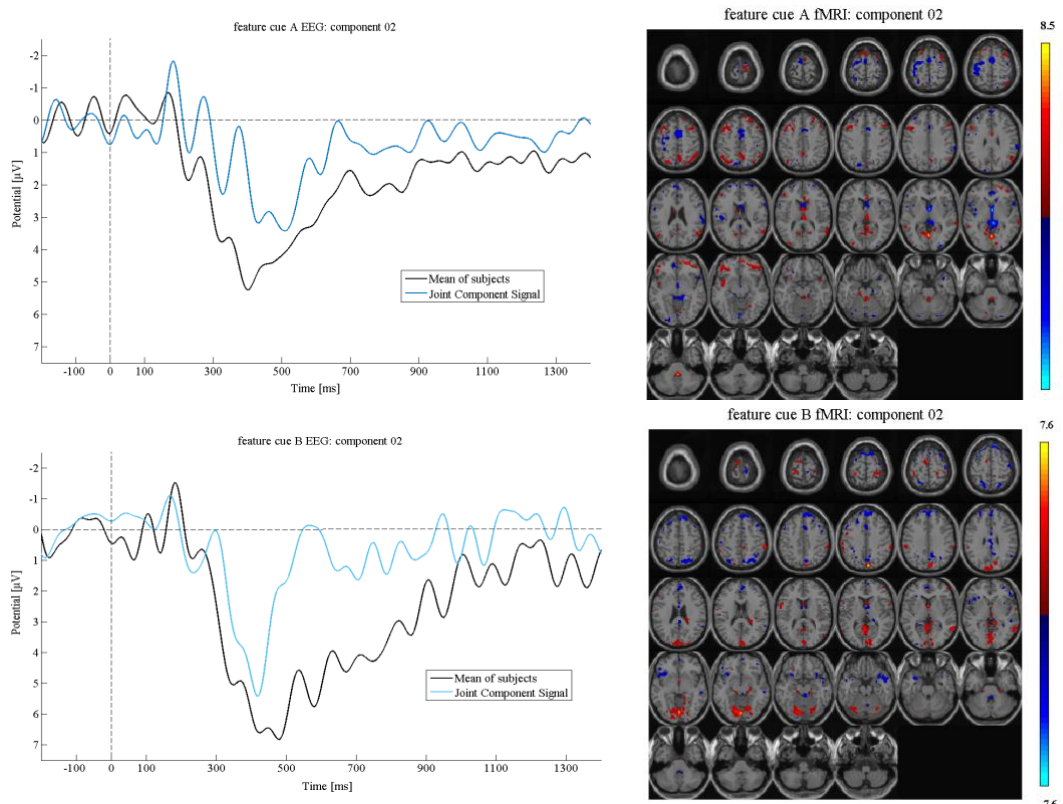


**Figure 19** Joint components with EEG (left panels) and fMRI (right panels, axial view in descending order from top to bottom) cue A (upper panels) and B (lower panels) features. Thresholded positive and negative voxel activations ( $Z$ -score  $> 2$ ) in the fMRI signify clusters that show identical variation with the EEG over subjects. The light blue line in the EEG is the unmixed joint component signal and the dark blue line the averaged amplitude over subjects.

#### Parallel ICA

As for the jICA, results of the pICA represent two components explaining most of the variability observed in the averaged ERP of cue A and B. These can be seen in **Figure 20**. In the case of cue A, these were coupled to strong increases of a cluster in the Thalamus, the motor, posterior parietal and cingulate cortex. In addition, slight increases in the medial prefrontal cortex were picked up in the component. Regarding cue B, a similar posterior cluster was extracted, but along with decreasing voxel activations in the medial PFC and the adjacent parts of the left lateral PFC.

Next to spatio-temporal decompositions, mixing coefficients of the pICA were analyzed. Across all subjects, mixing coefficients of the EEG and fMRI features for both cue A ( $r(11) = -.15, p = .88$ ) and B ( $r(11) = -.23, p = .44$ ) were only marginally correlated. An overview of mixing coefficients for all subjects can be found in

#### Appendix E.

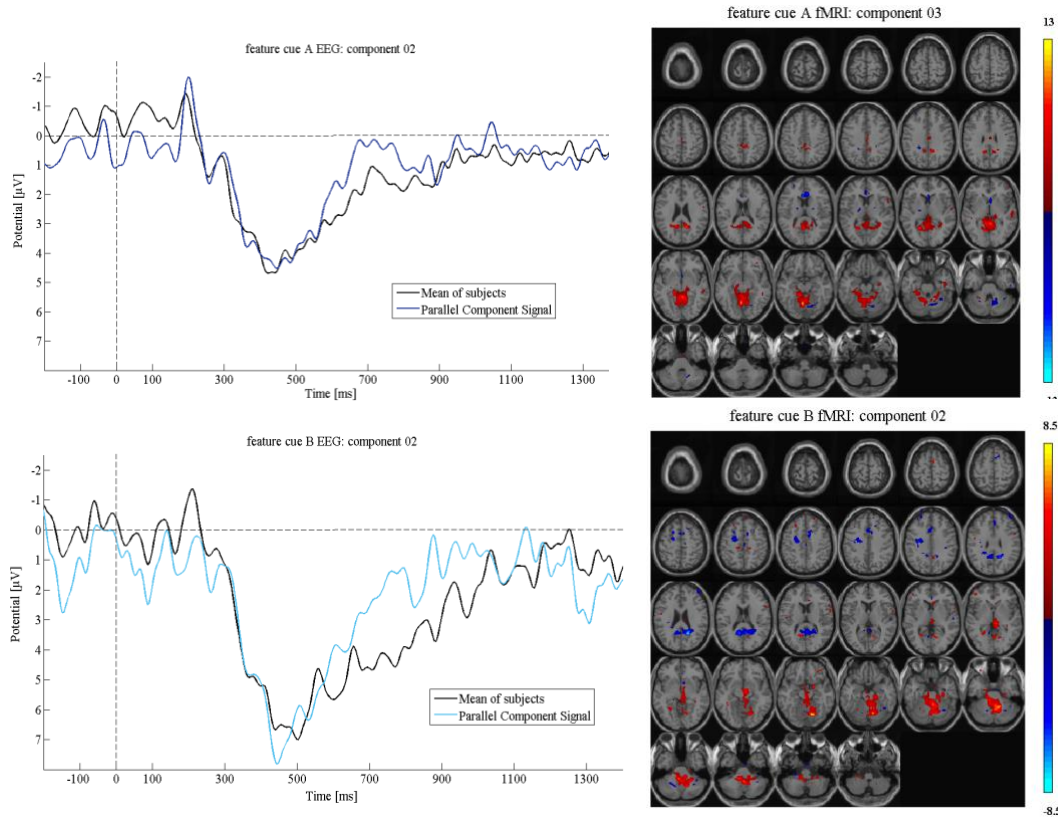


**Figure 20** Parallel components with EEG (left panels) and fMRI (right panels, axial view in descending order from top to bottom) cue A (upper panels) and B (lower panels) features. As with jICA, positive and negative voxel activations were thresholded to a Z-score  $> 2$ . These can be interpreted as variation that is strongly correlated with the EEG over subjects.

### 3.2.3 Multiway Partial Least Squares

Two atoms of the N-PLS decomposition of single trial EEG frequency power and fMRI voxel activation are displayed in **Figure 21**. While theta and alpha atoms for cue A are plotted on top, those for cue B are at the bottom. Marked clusters represent atom weights of the spectral signature on the fMRI's spatial signature. Thus, these loading can be seen as voxel signatures that have maximal covariation with the spectral signatures.

Concerning the theta atoms, there were little loadings on voxels for cue A. Only two major positive clusters were identified in the rostral part of the ACC and the Thalamus. Additionally, a small negative cluster was found in the left and right caudate. For cue B there were several clusters demonstrating strong loading on the theta atom. Most notably both medial and dorsolateral regions of the PFC showed large positive weights. This includes the bilateral MFG, IFG and SMC. Furthermore, the posterior cingulate and bilateral motor cortex had positive loadings. Finally, there were positive loadings of the bilateral associative parietal cortex and negative ones on the Thalamus.

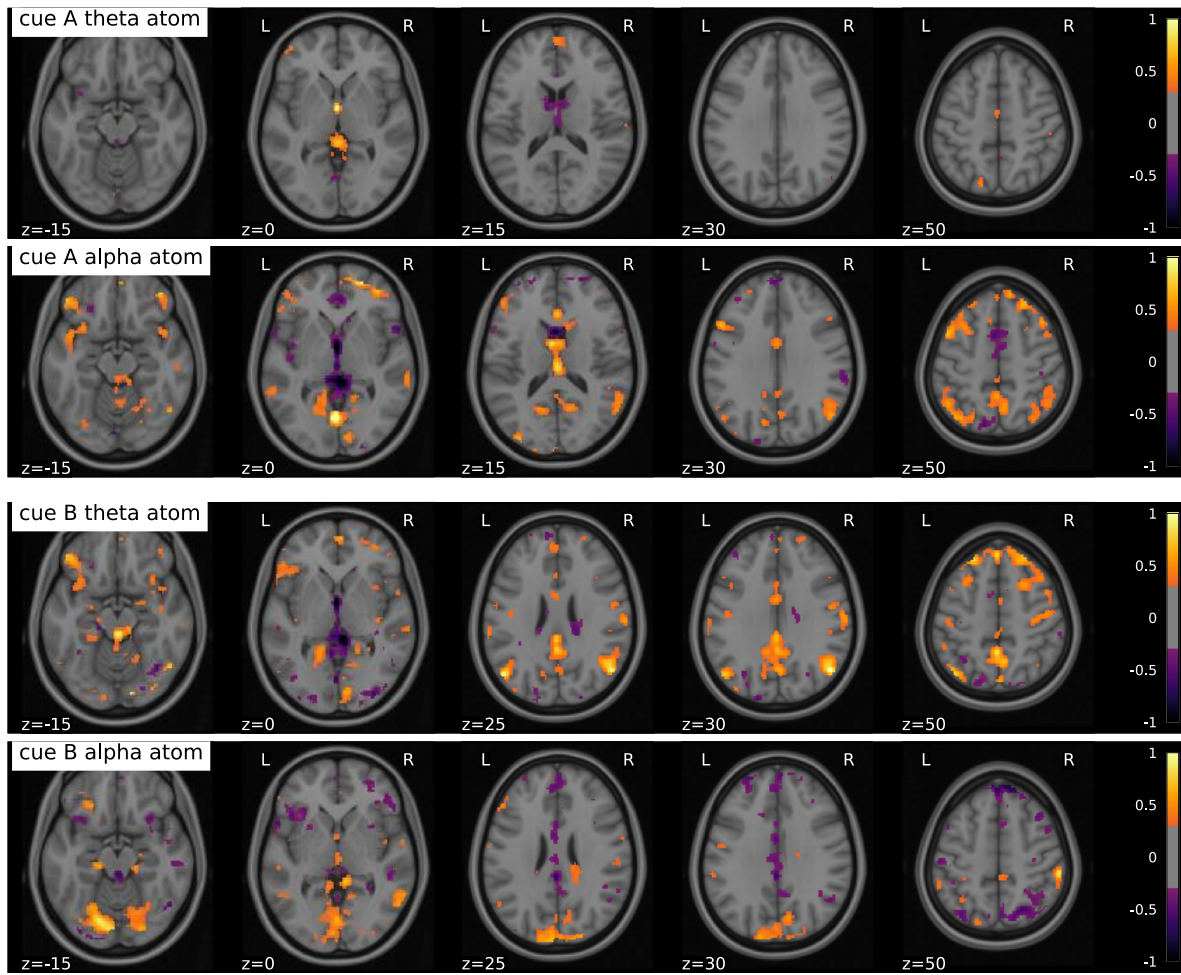


**Figure 21** Axial view on spatial fMRI signatures found in the N-PLS decomposition for the theta (4-7 Hz) and alpha (8-12 Hz) EEG atoms separated by cue (A upper two panels, B lower two panels). Colored clusters represent positive (yellow-orange) and negative (purple-black) atom weights on fMRI voxels. Weights were thresholded to 0.3 and plotted in MNI space.

As for alpha, cue A had positive cluster loadings similar to the ones of the theta atom for cue B, except that most positive clusters in the posterior parietal cortex were a little smaller cue A's alpha atom and it had negative loadings on the superior part of the medial PFC. In contrast to cue A, cue B's alpha atom had larger negative loadings on both anterior and posterior sections of the cingulate as well as the bilateral IFG. Positive clusters for this atom were found at the transition of the posterior associative regions of the parietal cortex and the occipital lobe. The superior parts of these associative cortex regions however had negative loadings.

### 3.2.4 Multimodal mixed-effects modeling

An overview of results from the final analysis of this study is provided in **Table 5**. The three most important models from the exploratory sequence of linear mixed-effects regressions was divided in its fixed and random parts. Both are listed as model parameters in **Table 5**. Next

to parameter estimates for each successive model, changes in deviance and Pseudo-R<sup>2</sup> are given at the bottom of the table. The first model only consisted of intercepts. These were allowed for each cue divided by block. For the first addition of a model parameter, a fixed slope for the EEG predictor was added and proved a slight improvement in terms of unaccounted error variance, as expressed by the increase in Pseudo-R<sup>2</sup>. Further improving the explanatory value, the last model with a fixed slope for the fMRI regressor yielded a significant increase in Pseudo-R<sup>2</sup> compared to the previous model. The AIC and deviance decreased slightly with each model, as well.

**Table 5**

*Results for exploratory model sequence of three successive linear mixed-effects regressions*

Model	Intercept block/type	Fixed EEG predictor	Fixed fMRI predictor
<b>Fixed Part</b>			
Intercept block/type	414.9	424.92	312.5
Fixed EEG		3.26	3.26
Fixed fMRI			0.63
<b>Random Part</b>			
$\sigma^2_\varepsilon$ Intercept block/type	1.29	1.72	1.67
$\sigma^2_\varepsilon$ EEG		1.81	1.81
$\sigma^2_\varepsilon$ fMRI			1.18
deviance	29824.6	29795.9	29643.3
$\chi^2$		28.7	152.6
AIC	29832.6	29806	29655.3
Pseudo-R <sup>2</sup> (CI)		.013 (.005-.023)	.015 (.007-.027)
$\Delta$ Pseudo-R <sup>2</sup> (CI)			.002** (.0019-.0036)

*Note.*  $\sigma^2_\varepsilon$  = error variance of a given model parameter,  $\chi^2$  = reduction of model deviance, CI = lower and upper bounds of confidence interval, \*\* =  $p < .001$

## 4. Discussion

### 4.1 General findings

The primary goal of this study was to compare different methods for multimodal data fusion and integration for simultaneous EEG-fMRI. For this purpose, hypotheses on neuronal correlates of cognitive control in WM were postulated and tested using unimodal and multimodal analyses.

Starting with behavioral data and judging from ER as well as RT, the adaptation of the DPX task for simultaneous recordings could be considered successful. Subjects showed worse performance for AY compared all other trialtypes, which is in line with the existing literature and theoretical assumptions about reactive control according to the DMC account. With significantly increased error counts and ER for AY, the notion of corrective behavioral control being the prominent feature in this trialttype is further supported. Unlike in previous experiments utilizing the DPX task, subjects only marginally improved over time and did not become significantly more proactive over time. The absence of this trend was represented in the mostly unchanging PSI scores for both RT, ER and error counts.

Judging from qualitative data gathered in post-experimental interviews, all subjects had understood the task and many had come up with the correct idea as to how the task was best fulfilled. By controlling behavior predominantly based on cues instead of probes and preparing responses early on, behavioral performance could be optimized in almost all trials. In addition, on average subjects indicated to have stayed adequately alert during the task and rated their overall performance positively (i.e., Alertness and Task performance, see **Table 1**). Still, the majority of subjects also reported increasing levels of fatigue due to the lighting, scanner noise, prolonged preparation time and their efforts not to move, as they had been insistently reminded by the experimenter that movement would be severely detrimental to data quality. Three subjects admitted to have dozed off momentarily in the final block of the experiment. These observations could explain why subjects could not spare the focus or cognitive resources to improve during the task. Yet, if they had automatized their response behavior, they would have expended less cognitive resources. In conclusion, on a behavioral level the task was implemented to a satisfactory degree based on the overall effects of trialttype. Yet, it is highly doubtful that subjects were able to reach the same performance levels or adapted the same in favor of a proactive control style as, for instance, in an isolated EEG experiment.

Moving to the EEG data, the resemblance of ERPs and ERSPs for different trialtypes and cues highlights the utility of the applied pre-processing framework for raw data heavily

impacted by MRI-related artefacts. With the sustained positivity moving on the central midline from anterior to posterior (see component succession in **Figure 16**) and slight detriments to otherwise recognizable visual potentials at the early progression of the evoked responses intact, the assessment of cognitive control correlates in the EEG was successful. Also prominent theta increases and alpha suppression after a cue onset support the integrity of the EEG. This is especially encouraging when looking at the overall results, because more serious deviations from the expected EEG results would have sabotaged data fusion analyses. There would have been no merit in relating activations of voxel clusters to entirely distorted or overcorrected EEG amplitudes, even if promising signal components would be detected. Besides the quality of descriptive single subject or group results, inferential statistics indicated effects in line with the hypotheses presented. Cue B with its higher predictive value for early decision-making was followed by a significantly stronger positive amplitude as well as higher theta synchronization over the central parietal cortex. Thus, cue B was associated with neuronal correlates of WM maintenance and early response preparation (Berger et al., 2016; Griesmayr et al., 2014). Relating these findings to the existing literature on the AX-CPT (Bickel et al., 2012; Voytek et al., 2015) and fastest RT performance for trialtypes BX and BY, it can be concluded that subjects correctly identified cue B as an imperative context for their behavior.

As for probes, there was a significant effect of trialtypes in regards to a large positive potential peaking after approximately 500 ms in response to probe presentation. This positivity was less prolonged, had a larger peak compared to cues and was most prominent after AY. Due to this trialtypes being closest to an oddball and representing the biggest challenge to the updating function of WM, this deflection could best be labelled as a P3b (Polich & Criado, 2006), indicating the strain reactive control puts on WM.

Concerning fMRI results, it should be noted that none of the contrasts derived for cues had prominent results when looking at them at a whole brain level. This might entail that either the task might have been adequately but not optimally designed for the fMRI. The most distinct finding when looking at specific regions of interest, which was also central to the main hypothesis on cognitive control, was a significant activation of the IFG linked to the presentation of cue A compared to B. This could be attributed to stronger uncertainty when confronted with the less predictive cue and the necessity to stay alert what the next probe turns out to be. It could also mean that as predicted in the aforementioned hypothesis on proactive control, optimal performance is best achieved when conscious effort is reduced in favor of automatization. Yet, as reported by Lopez Garcia et al. (2016), there was a voxel cluster significantly stronger for cue B in the right DLPFC when p-values were uncorrected for

multiple comparisons. This contrast was weaker and, thus, less convincing than the contrast found for cue A. In addition to these results, contrasts showed that cue B was also associated with larger activations in structures related to motor control, such as a cluster between the superior frontal gyrus and the SMC as well as one in bilateral the PCG. In both instances, the SMC (Chen, Scangos, & Stuphorn, 2010; Swann et al., 2012) and the PCG (Porro et al., 1996), this can be interpreted as increased motor preparation after the more predictive cue. However, these contrasts were not significant after p-value correction. Concerning the ACC, a voxel cluster stronger for cue A between the ACC and left IFG was found. This contrast was neither significant on whole brain level nor when focusing on regions of interest.

As in the EEG, probe-locked activations were most striking for AY compared to its baseline condition AX. When expectations were met there and A was followed by X, there were no significant voxel clusters stronger than for AY. Expectancy violations and the need for behavioral adaptation were accompanied by larger activations of the IFG, dorsal ACC, the SMC and the left PCG. All of which underline the outlined properties of the AY trialtype and reactive control. When repeatedly trained environmental contingencies (AX) are suddenly disproven, subjects detected a conflict and had to invest more effort into adjusting behavioral plans, as indicated by the dorsal ACC and motor areas.

With the first multimodal integration analysis, dipole localization for an exemplary subject informed by sMRI data showed dipoles of the ERP succession underlying the sustained positivity to be located in the posterior cingulate cortex, the right Hippocampus and the right IFG. Therefore, the dipole positions represent the first association of EEG and fMRI results, as they connect the positive potentials, which are mostly comprised of theta power, to aforementioned regions in the parietal and prefrontal cortex. Still, it can be argued that this connection is rather difficult to interpret. In the end, dipole localizations are meant to give a spatial dimension to EEG data and do not account for variability in functional activation patterns. Only variance in the EEG drives the analysis, while sMRI data restricts the estimation of dipoles. The result does not necessarily imply that there is co-variation between the located area and the oscillations in the EEG. It merely says that a given scalp distribution should have its origin at certain spatial coordinates. If this point of origin was always activated at the same time, if other areas were also contributors to neuronal processes taking place when oscillations synchronized and if this spatial dimension shares variability with the EEG cannot be adequately answered with this analysis.

With EEG-informed BOLD prediction results were mixed. While significant voxel activations were found for regions of interest, none remained significant on whole brain level

or after correcting p-values. t estimates derived from inferential tests, cluster size and voxel positions were overall scattered. Still, weak activations of the SMC, rostral cingulate cortex and IFG fit previous results, be it to an unconvincing extend.

By contrast, time series correlations as well as jICA and pICA yielded more clear-cut results. First of all, as a baseline level of relation between data modalities and different measures, cross-correlations of univariate time series revealed stronger correlations for single trial oscillatory measures as compared to amplitudes. This finding has been well documented by existing research (Chang, Liu, Chen, Liu, & Duyn, 2013; Murta et al., 2016). Especially theta frequency power showcased a strong relation to variation in the BOLD signal. However, a significant positive correlation of theta power and different regions in both the prefrontal and parietal cortex was only present for cue B. For cue A, theta power was negatively correlated to these activations, while alpha seemed to be more positively associated with prefrontal structures. Yet, these couplings were weaker than for theta during the presentation of cue B.

The presented jICA components revealed a set of EEG points with a positive peak similar to the one found in unimodal results, which were extracted along with a set of positively associated fMRI voxels in the DLPFC and negatively associated voxels in the medial PFC for cue A. Looking at cue B positive activations were mostly found in posterior cingulate and parietal cortex, while negative activations were found in prefrontal structures. With these components, jICA provided the first reliable indication, as to whether there is a shared signal source in EEG and fMRI that relates unique activation patterns to proactive control conditions. In this case, the sustained positivity accompanying proactive control was simultaneously extracted from the unmixed signal with the fMRI and negatively associated with prefrontal regions. A comparable component accounting for the sustained positivity after cue A had no positive activations in the DLPFC instead, further supporting the notion of increased cognitive effort when being unable to perform early response selection. Yet, it has to be noted that the negative voxel clusters for cue B were not exclusive to the DLPFC, but were more dispersed across the PFC. Judging from this result it cannot be argued that the sustained positivity was coupled to a decrease in the DLPF specifically. On top of that, analyses focused on identifying one component that best explained characteristics of proactive control (i.e., the sustained positivity). Whether distinct activation patterns of cue A can be seen while using a potential that is more prominent for its counterpart cue B, is uncertain. Additional components extracted that explained less variance could still be meaningful to underlying cognitive processes.

Spatio-temporal decompositions of the signal derived from jICA were then compared pICA as the less restrictive analysis. pICA results appeared noticeably different. For example, negative voxel clusters for cue B were found in the medial PFC, whereas variation in the EEG for cue A was not linked to the PFC at all. Instead both conditions had positive activation patterns in more posterior regions. The averaged ERPs for the EEG part appeared different from what was computed for the jICA, as well. At this point, it is hard to find a convincing explanation for this divergence in results. Supposedly, the major difference between the two analyses lies in their assumptions for source separation. Another noteworthy hint for results might be the weak correlation for mixing coefficient in both cues.

N-PLS decomposition, as the last source separation method, paid tribute to the finding of increased correlations between oscillatory measures and the BOLD signal. Here, atoms with spectral signatures showing loadings in the two most pronounced frequency bands, theta and alpha, were extracted. These atoms' spatial signatures from the fMRI part revealed distinct couplings of theta and alpha for both cues. While theta oscillations had high weights on the DLPFC, medial PFC including the SMC and posterior cingulate as well as bilateral motor cortex, these were unique for cue B, not cue A. Unexpectedly, cue B was related to activation of the DLPFC when using theta power instead of amplitude, but even more so to more posterior regions. The result indicates that synchronized theta power has a spatial pattern leading from medial PFC to parietal motor control areas and the associative cortex when a highly predictive cue is presented. In turn, theta has less of an impact for cue A, but, as hinted at by time series correlations, alpha power yielded positive weights on most of the regions previously assigned to theta for cue B. Concluding from this, alpha synchronization that has been triggered by ambiguous context information appears to increase instead of decline as it does for cue B. For the latter this seems plausible, since alpha suppression is often linked to anticipation and response preparation, as noted in section 1.1.2. For cue A an increase of alpha synchronization over the same regions vital to cue B could represent uncertainty and the inhibition of a dominate response tendency. After all, subjects may not connect the correct cue to one response as strongly as for cue B, but cue A is most often paired with a correct probe, making it more indicative of one response than the other. Since the probability of a correct probe after a correct cue is high but not 100%, subjects might have a tendency but inhibit the early selection that they perform for cue B.

Finally, behavioral predictions using cue-locked neuronal correlates were reported. When successively restricting the model by first entering a fixed slope for a theta regressor and then one for the DLPFC, the explanatory value of the model increased slightly. With each model

Pseudo- $R^2$  rose, while the AIC and deviance declined. For the comparison of the second to the third model, a significant decrease Pseudo- $R^2$  was found. Since the third model added an fMRI regressor, this can be interpreted as incremental value of an fMRI regressor to one based on the EEG. This would lead to the conclusion that multimodal regressors in fact improve behavioral predictions. However, the increment was small and a significant increase does not imply a practical difference, especially considering the limited extent of the increase in explanatory value.

#### 4.2 A multimodal perspective on the DPX task and proactive control

This study was devised to draw conclusions about analysis methods by judging how convincingly analyses can find answers to psychological research questions. For this purpose, it was investigated how proactive control maps out over different methods and analysis approaches. In particular, proactive control been associated with increased activations of the DLPFC (D'Ardenne et al., 2012; P Lopez-Garcia et al., 2016), linking it to maintenance of important contexts in WM. However, proactive control should lead to optimal performance and is characterized by acting on contexts with clear contingencies, thereby allowing for clear predictions about what behaviors will be profitable to goal attainment. Saving cognitive resources and improving performance can both be achieved by automatizing behavior and reducing conscious effort.

The present study shows supporting evidence for this hypothesis. In jICA and N-PLS components from time-varying EEG and fMRI data could be extracted that were maximally correlated across time. jICA successfully related sustained positivity associated with early decision-making and long-term planning to decreased activations of the medial and dorsolateral PFC. N-PLS extended this to spectral measures that have previously been connected to maintenance in WM, response selection and motor preparation (Chen et al., 2010; Helfrich & Knight, 2016; Hwang et al., 2016). Particularly the N-PLS decomposition revealed specificity of spatial signatures from alpha and theta atoms for the two cues. Here, cue B, which triggers proactive control, was associated with prefrontal theta and posterior parietal activations in both motor and associative cortex areas. This finding is in support of past research identifying synchronized theta power over the medial PFC as mechanism for behavioral adaptation (Cavanagh & Shackman, 2015). At the same time, alpha power was related to a decrease in these structures.

The wide-spread relation of synchronization of theta power could represent the intake and maintenance, mostly supported by the DLPFC, as has been often shown in the literature. Yet, this maintenance might not be demanding, but just imperative to early response selection, in that while the information is shielded against interferences, conscious effort is already subsiding, because dominant response tendencies are being developed. The rise of response tendencies would also explain the suppression of alpha power that is correlated to activations of motor areas. If proactive control conditions mapped out in this fashion across the brain, this could also help resolving the question about conscious effort for proactive control. After all, for long-term behavioral control outside the DPX paradigm in everyday life, proactive control can definitely be demanding. In this specific experiment, long-term planning only requires minimal effort that is optimized by reducing as subjects learn the contingencies of cues and probes. Thus, cue A leads to more alertness and perhaps cognitive effort compared to cue B, as indicated by unimodal fMRI contrasts. For the particular function of taking in imperative context information, however, the DLPFC might be more relevant to cue B.

#### 4.3 Insights from data integration and fusion

All in all, results represent a wide range of neuronal correlates and associations that are partially in line with our hypotheses. Starting with the asymmetric integration approaches, it has already been discussed that these results were less convincing and robust. Concerning the amplitude-based BOLD prediction, weak inter-trial consistency in the EEG due to remaining artefacts could have caused a lessened relation on a single trial basis with the BOLD signal. Also, as time series correlations showed, amplitude measures might have been the wrong parametric regressor for this experiment, as spectral measures proved to produce stronger correlations. sMRI-informed dipole localization has already been criticized in terms of its explanatory value for interpreting results and best relating EEG and fMRI variance shares. However, given the appropriate hypothesis that focuses on the EEG part and on relating scalp distributions to dipole positions that have to be as precise as possible, this analysis has its limited but valid application.

When comparing source separation methods, jICA and pICA come to mind first. Each of them was performed successfully and delivered easily interpretable results. The lack of correlation between mixing coefficient when using the pICA, however, was concerning. Furthermore, when extracting components, pICA only identified few components with sufficient correlations to meet to specified threshold. Considering that pICA loosens restrictions

on component selection, this observation is especially peculiar. Also the deviation of averaged ERPs in pICA from what was seen in jICA and unimodal analyses is reason for doubt. Yet, it is not a central part of the source separation and might be attributed to an error in data matrices. The basic idea in pICA of including non-identical covariation of modalities across subjects is plausible. Judging from results, it seems advisable to test how likely the covariation of signal sources actually is. This might shed new light on the a priori assumption of identical variation.

When addressing the idea of a more exploratory, blind source separation, the comparison of results from jICA and N-PLS appears most relevant. First of all, joint signal components for the sustained positivity as well as theta power and increased activation patterns mostly in the medial PFC, the adjacent motor cortex and posterior cingulate could be found. Both jICA and N-PLS were capable of identifying such signal sources. While the two results resembled each other, N-PLS did so based on spectral signatures. These signatures were validated by running PARAFAC on the spectral data. Two major frequency bands could be extracted and yielded the best model fit. Moreover, time series correlations demonstrated that spectral measures were superior compared to amplitudes in predicting BOLD changes in different relevant regions for both cues. This showed in the distinct spatial patterns revealed for alpha and theta atoms in each cue.

On the other hand, data selection and parameter estimation proved to be a lot less complicated for jICA than for N-PLS. How much data can be entered into N-PLS is a valid point of discussion. With an entirely blind source separation procedure the inclusion of all voxels might lead to results that are hard to interpret, because spatial data unrelated to the hypotheses receive atom weights. In the end, relating data sets on especially fine-grained level always bears the risk of overfitting and modeling every last variance share even if it is irrelevant or just noise. In addition, the grave discrepancy in observations and variables between EEG and fMRI poses a problem to decomposing the EEG in dependence of the fMRI. Another criticism of N-PLS lies in the choice of parameters. While N-PLS enables relating multidimensional data sets like spectral EEG data, this advantage comes along with the drawback of choosing appropriate measures. Particularly on the fMRI side, it is difficult to argue why single trial beta estimates, contrasts or any other measure is most appropriate and the choice is best informed by intent than arbitrariness. Single trial measures in both EEG and fMRI increase the influence of noise on the analysis, whereas averaged means for particular time windows, trials or subjects cancel out a large part of the noise.

Still, it is hard to argue that N-PLS has reasonable statistical foundations, puts less restrictions on data and allows for decompositions of complex, multidimensional data sets by

preserving temporal maximal covariation while estimating normalized loading vectors. Taken together with the promising insights from having loadings for different atoms carrying weights for different frequency bands, N-PLS can be the method of choice if an informed choice of parameters and matrix dimensions is possible. Then, the ends justify the demanding implementation.

As for the behavioral prediction, incremental values for multimodal predictors were found. On top of that, building model equations and implementing the sequence with the utilized R package can be done with reasonable effort. Still, the increments found for the model successions were not substantial. According to **Equation 8**, changes in Pseudo-R<sup>2</sup> of, for instance, 0.013 stand for a decrease of roughly 1.3% of the previous model's error variances. So even with a significant increase in Pseudo-R<sup>2</sup>, as was the case for the comparison of the second and third model, the proportional reduction of average error variance of 0.2% was inconsequential. It could be argued that cue-locked correlates were too limited, but trying different fixed effect regressors until one with greater contributions is found is an improper method of designing models for behavioral predictions. After all, any predictor variable in a given regressional model can by accident have significant relations to criterion variables and thereby increase the model fit. Another explanation for the lacking model improvement could be that cue processing is essential to behavioral performance, but still too isolated and distant from the complete process that enables quick reactions.

In rating the practicability of the utilized methods, not only statistical ideas or investment of effort should be considered. Even more importantly than these concerns, especially jICA and N-PLS were capably of adequately addressing the research questions stated at the beginning. The addition of time series correlations, PARAFAC and the knowledge of an informational baseline in the unimodal results certainly aided interpretations. Hence, a combination of a more exploratory method like N-PLS in conjunction with unimodal results or time series analysis is closest to a universally applicable approach, which of course is just a theoretical notion.

#### 4.4 Limitations

Starting at the utilized design, it has to be noted that task produced more robust effects for the EEG than for the fMRI. A re-analysis of the design efficiency and subsequent adjustment of task parameters could improve the task's fit to fMRI recordings. Additionally, parameter adjustments could improve the overall task. For example, the jitter of maintenance intervals could be shortened and presentation times extended. The former would also serve better

capturing activity related to response preparation, as subjects can build a firmer grasp on how they have to wait until the probe. Extending stimulus durations might help subjects encode stimuli. However, it might also reduce focus due to ease of stimulus processing.

In terms of utilized parameters it has already been mentioned that the selection of adequate parameters and their statistical transformation is an intricate issue. Especially regarding the EEG parameters it is questionable that the convolution of single trial measures with a fixed HRF is a suitable procedure. The HRF is highly variable. Taking a canonical HRF as a template for all subjects is a heavy generalization. Yet, the basic idea is to just approximately fit the hemodynamic lag between EEG and fMRI. A template might not be exact but sufficient to roughly align peaks in the signals. Plus, in some cases only a peak value instead of a time frame is of importance, rendering the convolution less relevant.

Despite advantages and disadvantages of a broad variety of data fusion methods could be compared in this study, this has only been done in regards to practical concerns and insights into the utilized paradigm. A more objective way of demonstrating the utility of these analyses would be to design a simulation study and establishing a ground truth every analysis could be judged by. By specifying a quantitative criterion, a statistical decision concerning whether one method is superior to other could be made. The criterion could be a proportion of identified alpha power when subjects close their eyes or motor cortex activation during finger tapping (Murta et al., 2016). Based on these one could compare how well analyses find the respective signal components or how sensitive they are to signal distortions. This study is limited to qualitative comparisons in regards to an exemplary application with the DPX task. Still, the DPX task represents a more relevant paradigm to current cognitive control research compared to a finger tapping task. Therefore, the implementation and results of the fusion approaches of this study might carry greater meaning relative to more robust, sensorimotor paradigms.

In addition to methodological concerns, psychological research questions might be more appropriately addressed by looking at activations following cues in a different way. Perhaps group contrasts and source decompositions in the fMRI turn out the way they do, because the extent of activations especially in the DLPFC change over time. For example, at the beginning of the experiment when subjects are least proactive they might utilize the DLPFC more intensively, because they actively focus on maintaining the cue. This activation might scale down over time with rising proactivity and automatization. A counterpoint against this idea is provided by the lack of change in PSI scores over time. Yet, the PSI might be insensitive to more nuanced changes in neuronal correlates, as it only represents an average score on the

behavioral level. In order to test the outlined hypothesis, data would have to be split up or blocked differently to detect trends that are unique to specific parts of the experiment.

Besides different approaches to analysis, future research might also tackle to problem of asymmetry between EEG and fMRI by choosing an different or additional method. For instance, functional Near-Infrared Spectroscopy has become a popular neuroimaging technique that is more flexible than fMRI, can assess cortical hemodynamic responses at a higher sampling rate, puts less of strain on subjects, is more cost-effective and is easily combined with EEG. Since this method is based on measuring a balance of oxygenated and deoxygenated hemoglobin via the reflection of light with different wave lengths, it has limited reach into the brain. More precisely, it can only penetrate the upper surface of the neocortex depending on the thickness of the skull. Nevertheless, provided a well-specified hypothesis concerning spatial data, the limited spatial resolution compared to the fMRI is entirely sufficient. When testing activations and deactivations of the PFC or the DLPFC, a rough indicator of hemodynamic signal changes averaged over multiple gyri of the PFC could already be enough to answer research questions. Furthermore, in the absence of a strong magnetic field EEG data could be simultaneously recorded at identical quality compared to isolated EEG recordings. Analyzing the time series data or performing source separation at more similar sampling rates, could also prove promising.

#### 4.5 Conclusions

The bottom line of this study has been that multimodal data fusion and combined EEG-fMRI was successfully applied to refine our understanding of cognitive control dynamics in the DPX task. Each analysis improved upon flaws of the previous and could be assessed in terms of its utility to answering the posed research question.

Depending on amplitudes and spectral signatures, cues associated with proactive control and those leading to more alertness due to uncertainty demonstrated different spatial distributions across the brain. A proactive control framework mostly depending on synchronized theta oscillation accompanied by activations in medial PFC, posterior parietal cortex as well as alpha suppression over the PFC and parietal cortex was put forth.

Simultaneous EEG-fMRI experiments are predicated on increased temporal and financial efforts for experimenters. As demonstrated in this study, the effort can significantly promote informational value gained from data. In this context, the result is more than the sum of its parts, as variance shares in the EEG revealed new insights into fMRI and the other way around. While

by far not every experiment will profit from adapting multimodal data fusion or combined EEG-fMRI recordings, the outlined results show that categorically limiting research questions to unimodal assessments merely for convenience, deprives researchers of the chance to profit from enriched perspectives on neuronal data.

## 5. References

- Abraham, A., Pedregosa, F., Eickenberg, M., Gervais, P., Mueller, A., Kossaifi, J., ... Varoquaux, G. (2014). Machine learning for neuroimaging with scikit-learn. *Frontiers in Neuroinformatics*, 8, 14. <https://doi.org/10.3389/fninf.2014.00014>
- Akaike, H. (1974). A new look at the statistical model identification. *IEEE Transactions on Automatic Control*, 19(6), 716–723. <https://doi.org/10.1109/TAC.1974.1100705>
- Albares, M., Lio, G., Criaud, M., Anton, J. L., Desmurget, M., & Boulinguez, P. (2014). The dorsal medial frontal cortex mediates automatic motor inhibition in uncertain contexts: Evidence from combined fMRI and EEG studies. *Human Brain Mapping*, 35(11), 5517–5531. <https://doi.org/10.1002/hbm.22567>
- Allen, P. J., Josephs, O., & Turner, R. (2000). A method for removing imaging artifact from continuous EEG recorded during functional MRI. *NeuroImage*, 12(2), 230–239. <https://doi.org/10.1006/nimg.2000.0599>
- Allen, P. J., Polizzi, G., Krakow, K., Fish, D. R., & Lemieux, L. (1998). Identification of EEG events in the MR scanner: The problem of pulse artifact and a method for its subtraction. *NeuroImage*, 8(3), 229–239. <https://doi.org/10.1006/nimg.1998.0361>
- Ances, B. M., Vitaliani, R., Taylor, R. A., Liebeskind, D. S., Voloschin, A., Houghton, D. J., ... Dalmau, J. (2005). Treatment-responsive limbic encephalitis identified by neuropil antibodies: MRI and PET correlates. *Brain*, 128(8), 1764–1777. <https://doi.org/10.1093/brain/awh526>
- Arnsten, A. F. T., & Rubia, K. (2012). Neurobiological circuits regulating attention, cognitive control, motivation, and emotion: disruptions in neurodevelopmental psychiatric disorders. *Journal of the American Academy of Child and Adolescent Psychiatry*, 51(4), 356–67. <https://doi.org/10.1016/j.jaac.2012.01.008>
- Barbey, A. K., Koenigs, M., & Grafman, J. (2013). Dorsolateral prefrontal contributions to human working memory. *Cortex; a Journal Devoted to the Study of the Nervous System and Behavior*, 49(5), 1195–205. <https://doi.org/10.1016/j.cortex.2012.05.022>
- Barcel, F., & Cooper, P. S. (2017). An information theory account of late frontoparietal ERP positivities in cognitive control. *Psychophysiology*. <https://doi.org/10.1111/psyp.12814>
- Barch, D. M., Braver, T. S., Nystrom, L. E., Forman, S. D., Noll, D. C., & Cohen, J. D. (1997). Dissociating working memory from task difficulty in human prefrontal cortex. *Neuropsychologia*, 35(10), 1373–80. [https://doi.org/S0028393297000729 \[pii\]](https://doi.org/S0028393297000729 [pii])
- Barzegaran, E., & Knyazeva, M. G. (2017). Functional connectivity analysis in EEG source space: The choice of method. *PLOS ONE*, 12(7), e0181105. <https://doi.org/10.1371/journal.pone.0181105>
- Bates, D., Machler, M., Bolker, B. M., & Walker, S. C. (2015). Fitting Linear Mixed-Effects Models using lme4. *Journal of Statistical Software*, 67(1), 1–48. <https://doi.org/10.18637/jss.v067.i01>
- Bénar, C. G., Aghakhani, Y., Wang, Y., Izenberg, A., Al-Asmi, A., Dubeau, F., & Gotman, J. (2003). Quality of EEG in simultaneous EEG-fMRI for epilepsy. *Clinical Neurophysiology*, 114(3), 569–580. [https://doi.org/10.1016/S1388-2457\(02\)00383-8](https://doi.org/10.1016/S1388-2457(02)00383-8)
- Berger, B., Minarik, T., Griesmayr, B., Stelzig-Schoeler, R., Aichhorn, W., & Sauseng, P. (2016). Brain oscillatory correlates of altered executive functioning in positive and negative symptomatic schizophrenia patients and healthy controls. *Frontiers in Psychology*, 7(MAY), 1–14. <https://doi.org/10.3389/fpsyg.2016.00705>

- Besserve, M., Jerbi, K., Laurent, F., Baillet, S., Martinerie, J., & Garnero, L. (2007). Classification methods for ongoing EEG and MEG signals. In *Biological Research* (Vol. 40, pp. 415–437). Sociedad de Biología de Chile. <https://doi.org/10.4067/S0716-97602007000500005>
- Bickel, S., Dias, E. C., Epstein, M. L., & Javitt, D. C. (2012). Expectancy-related modulations of neural oscillations in continuous performance tasks. *NeuroImage*, 62(3), 1867–76. <https://doi.org/10.1016/j.neuroimage.2012.06.009>
- Bizzi, E., Hogan, N., Mussa-Ivaldi, F. A., & Giszter, S. (1992). Does the nervous system use equilibrium-point control to guide single and multiple joint movements. *Behavioral and Brain Sciences*. <https://doi.org/10.1017/S0140525X00072538>
- Braver, T., Paxton, J., & Locke, H. (2009). Flexible neural mechanisms of cognitive control within human prefrontal cortex. *Proceedings of The*. Retrieved from <http://www.pnas.org/content/106/18/7351.short>
- Braver, T. S. (2012). The variable nature of cognitive control: A dual mechanisms framework. *Trends in Cognitive Sciences*. <https://doi.org/10.1016/j.tics.2011.12.010>
- Braver, T. S., Cole, M. W., & Yarkoni, T. (2010). Vive les differences! Individual variation in neural mechanisms of executive control. *Current Opinion in Neurobiology*. <https://doi.org/10.1016/j.conb.2010.03.002>
- Braver, T. S., Gray, J. R., & Burgess, G. C. (2007). *Explaining the many varieties of working memory*. In: *Variation in working memory*. Oxford University Press.
- Braver, T. S., Reynolds, J. R., & Donaldson, D. I. (2003). Neural Mechanisms of Transient and Sustained Cognitive Control during Task Switching. *Neuron*, 39(4), 713–726. [https://doi.org/10.1016/S0896-6273\(03\)00466-5](https://doi.org/10.1016/S0896-6273(03)00466-5)
- Brevers, D., Bechara, A., Kilts, C. D., Antoniali, V., Bruylants, A., Verbanck, P., ... Noël, X. (2017). Competing Motivations: Proactive Response Inhibition Toward Addiction-Related Stimuli in Quitting-Motivated Individuals. *Journal of Gambling Studies*, 1–22. <https://doi.org/10.1007/s10899-017-9722-2>
- Bro, R. (1996). Multiway calibration. Multilinear PLS. *Journal of Chemometrics*, 10(1), 47–61. [https://doi.org/10.1002/\(SICI\)1099-128X\(199601\)10:1<47::AID-CEM400>3.0.CO;2-C](https://doi.org/10.1002/(SICI)1099-128X(199601)10:1<47::AID-CEM400>3.0.CO;2-C)
- Bro, R. (1998). *Multi-way analysis in the food industry: Models, Algorithms & Applications*. Retrieved from <http://citeseerx.ist.psu.edu/viewdoc/download?doi=10.1.1.719.6062&rep=rep1&type=pdf>
- Calhoun, V., Adah, T., & Liu, J. (2006). A feature-based approach to combine functional MRI, structural MRI and EEG brain imaging data. In *Annual International Conference of the IEEE Engineering in Medicine and Biology - Proceedings* (pp. 3672–3675). <https://doi.org/10.1109/IEMBS.2006.259810>
- Calhoun, V. D., & Adali, T. (2009). Feature-based fusion of medical imaging data. *IEEE Transactions on Information Technology in Biomedicine*, 13(5), 711–720. <https://doi.org/10.1109/TITB.2008.923773>
- Calhoun, V. D., Liu, J., & Adali, T. (2009, March). A review of group ICA for fMRI data and ICA for joint inference of imaging, genetic, and ERP data. *NeuroImage*. <https://doi.org/10.1016/j.neuroimage.2008.10.057>
- Carter, C., Braver, T., Barch, D., & Botvinick, M. (1998). Anterior cingulate cortex, error detection, and the online monitoring of performance. Retrieved from <http://science.sciencemag.org/content/280/5364/747.short>
- Cavanagh, J. F., & Frank, M. J. (2014, August). Frontal theta as a mechanism for cognitive control. *Trends in Cognitive Sciences*. <https://doi.org/10.1016/j.tics.2014.04.012>
- Cavanagh, J. F., & Shackman, A. J. (2015). Frontal midline theta reflects anxiety and cognitive

- control: meta-analytic evidence. *Journal of Physiology, Paris*, 109(1–3), 3–15. <https://doi.org/10.1016/j.jphysparis.2014.04.003>
- Chang, C., Liu, Z., Chen, M. C., Liu, X., & Duyn, J. H. (2013). EEG correlates of time-varying BOLD functional connectivity. *NeuroImage*, 72, 227–236. <https://doi.org/10.1016/J.NEUROIMAGE.2013.01.049>
- Chen, T., Kendrick, K. M., Feng, C., Yang, S., Wang, X., Yang, X., ... Luo, Y. (2014). Opposite effect of conflict context modulation on neural mechanisms of cognitive and affective control. *Psychophysiology*. <https://doi.org/10.1111/psyp.12165>
- Chen, X., Scangos, K. W., & Stuphorn, V. (2010). Supplementary motor area exerts proactive and reactive control of arm movements. *The Journal of Neuroscience : The Official Journal of the Society for Neuroscience*, 30(44), 14657–75. <https://doi.org/10.1523/JNEUROSCI.2669-10.2010>
- Cuffin, B. N. (1998). EEG dipole source localization. *IEEE Engineering in Medicine and Biology Magazine*, 17(5), 118–122. <https://doi.org/10.1109/51.715495>
- D'Ardenne, K., Eshel, N., Luka, J., Lenartowicz, A., Nystrom, L. E., & Cohen, J. D. (2012). Role of prefrontal cortex and the midbrain dopamine system in working memory updating. *Proceedings of the National Academy of Sciences*, 109, 19900–19909. <https://doi.org/10.1073/pnas.1116727109/-/DCSupplemental.www.pnas.org/cgi/doi/10.1073/pnas.1116727109>
- Dale, A. M., & Sereno, M. I. (1993). Improved Localization of Cortical Activity by Combining EEG and MEG with MRI Cortical Surface Reconstruction: A Linear Approach. *Journal of Cognitive Neuroscience*, 5(2), 162–176. <https://doi.org/10.1162/jocn.1993.5.2.162>
- Davis, T., LaRocque, K. F., Mumford, J. A., Norman, K. A., Wagner, A. D., & Poldrack, R. A. (2014). What do differences between multi-voxel and univariate analysis mean? How subject-, voxel-, and trial-level variance impact fMRI analysis. *NeuroImage*, 97, 271–83. <https://doi.org/10.1016/j.neuroimage.2014.04.037>
- Davison, A., & Hinkley, D. (1997). Bootstrap methods and their application. Retrieved from [https://books.google.de/books?hl=de&lr=&id=4aCDbm\\_t8jUC&oi=fnd&pg=PR7&dq=Davison,+A.C.,+Hinkley,+D.V.,+1997.+In:+Gill,+R.,+Ripley,+B.D.,+Ross,+S.,+Stein,+M.,+Williams,+D.+Eds.\),+Bootstrap+Methods+and+Their+Application.&ots=mY-1edW50b&sig=jxw58TcXmh8xA2pw0prXI6wPC4U](https://books.google.de/books?hl=de&lr=&id=4aCDbm_t8jUC&oi=fnd&pg=PR7&dq=Davison,+A.C.,+Hinkley,+D.V.,+1997.+In:+Gill,+R.,+Ripley,+B.D.,+Ross,+S.,+Stein,+M.,+Williams,+D.+Eds.),+Bootstrap+Methods+and+Their+Application.&ots=mY-1edW50b&sig=jxw58TcXmh8xA2pw0prXI6wPC4U)
- Debener, S., Makeig, S., Delorme, A., & Engel, A. K. (2004). What is novel in the novelty oddball paradigm? Functional significance of the novelty P3 event-related potential as revealed by independent component analysis. <https://doi.org/10.1016/j.cogbrainres.2004.09.006>
- Debener, S., Mullinger, K. J., Niazy, R. K., & Bowtell, R. W. (2008). Properties of the ballistocardiogram artefact as revealed by EEG recordings at 1.5, 3 and 7 T static magnetic field strength. *International Journal of Psychophysiology*, 67(3), 189–199. <https://doi.org/10.1016/j.ijpsycho.2007.05.015>
- Debener, S., Ullsperger, M., Siegel, M., & Engel, A. (2006). Single-trial EEG-fMRI reveals the dynamics of cognitive function. *Trends in Cognitive Sciences*. Retrieved from <http://www.sciencedirect.com/science/article/pii/S1364661306002725>
- Delorme, A., & Makeig, S. (2004). EEGLAB: an open source toolbox for analysis of single-trial EEG dynamics including independent component analysis. *Journal of Neuroscience Methods*. Retrieved from <http://www.sciencedirect.com/science/article/pii/S0165027003003479>
- Delorme, A., Palmer, J., Onton, J., Oostenveld, R., & Makeig, S. (2012). Independent EEG Sources Are Dipolar. *PLoS ONE*, 7(2), e30135. <https://doi.org/10.1371/journal.pone.0030135>
- Eichele, T., Calhoun, V. D., Moosmann, M., Specht, K., Jongsma, M. L. A., Quiroga, R. Q., ... Hugdahl, K. (2008). Unmixing concurrent EEG-fMRI with parallel independent component

- analysis. *International Journal of Psychophysiology*, 67(3), 222–234.
- Feldman, A. G. (1986). Once more on the equilibrium-point hypothesis ( $\lambda$  model) for motor control. *Journal of Motor Behavior*, 18(1), 17–54. <https://doi.org/10.1080/00222895.1986.10735369>
- Friston, K. J., Holmes, A. P., Worsley, K. J., Poline, J.-B., Frith, C. D., & Frackowiak, R. S. J. (1995). Statistical Parametric Maps in Functional Imaging : A General Linear Approach. *Human Brain Mapping*, 2(4), 189–210. Retrieved from <http://citeseerx.ist.psu.edu/viewdoc/download?doi=10.1.1.503.4426&rep=rep1&type=pdf>
- Fu, C. H. Y., & Costafreda, S. G. (2013). Neuroimaging-Based Biomarkers in Psychiatry: Clinical Opportunities of a Paradigm Shift. *The Canadian Journal of Psychiatry*, 58(9), 499–508. <https://doi.org/10.1177/070674371305800904>
- Gonçalves, S. I., De Munck, J. C., Pouwels, P. J. W., Schoonhoven, R., Kuijer, J. P. A., Maurits, N. M., ... Lopes Da Silva, F. H. (2005). Correlating the alpha rhythm to BOLD using simultaneous EEG/fMRI: Inter-subject variability. <https://doi.org/10.1016/j.neuroimage.2005.09.062>
- Gorgolewski, K., Burns, C. D., Madison, C., Clark, D., Halchenko, Y. O., Waskom, M. L., & Ghosh, S. S. (2011). NiPy: A Flexible, Lightweight and Extensible Neuroimaging Data Processing Framework in Python. *Frontiers in Neuroinformatics*, 5, 13. <https://doi.org/10.3389/fninf.2011.00013>
- Gramfort, A., Luessi, M., Larson, E., Engemann, D. A., Strohmeier, D., Brodbeck, C., ... Hämäläinen, M. (2013). MEG and EEG data analysis with MNE-Python. *Frontiers in Neuroscience*, 7, 267. <https://doi.org/10.3389/fnins.2013.00267>
- Gray, J. R. (2004). Integration of Emotion and Cognitive Control. *Current Directions in Psychological Science*, 13(2), 46–48. <https://doi.org/10.1111/j.0963-7214.2004.00272.x>
- Griesmayr, B., Berger, B., Stelzig-Schoeler, R., Aichhorn, W., Bergmann, J., & Sauseng, P. (2014). EEG theta phase coupling during executive control of visual working memory investigated in individuals with schizophrenia and in healthy controls. *Cognitive, Affective & Behavioral Neuroscience*, 14(4), 1340–55. <https://doi.org/10.3758/s13415-014-0272-0>
- Gutberlet, I. (2009). Did you know ...? MR Correction Dear Customers ,. *Analyzer*. Retrieved from [https://www.nitrc.org/docman/view.php/587/1140/Did\\_you\\_know\\_Compendium\\_001.pdf](https://www.nitrc.org/docman/view.php/587/1140/Did_you_know_Compendium_001.pdf)
- Harshman, R. a. (1970). Foundations of the PARAFAC procedure: Models and conditions for an “explanatory” multimodal factor analysis. *UCLA Working Papers in Phonetics*, 16(10), 1–84. Retrieved from <http://www.psychology.uwo.ca/faculty/harshman/wppffac0.pdf>
- Haynes, J. D. (2009). Decoding visual consciousness from human brain signals. *Trends in Cognitive Sciences*, 13(5), 194–202. <https://doi.org/10.1016/j.tics.2009.02.004>
- Helfrich, R. F., & Knight, R. T. (2016). Oscillatory Dynamics of Prefrontal Cognitive Control. *Trends in Cognitive Sciences*, 20(12), 916–930. <https://doi.org/10.1016/j.tics.2016.09.007>
- Helwig, N. (2017). Component Models for Multi-Way Data. *CRAN*.
- Henderson, D., Poppe, A. B., Barch, D. M., Carter, C. S., Gold, J. M., Ragland, J. D., ... MacDonald, A. W. (2012). Optimization of a goal maintenance task for use in clinical applications. *Schizophrenia Bulletin*, 38(1), 104–113. <https://doi.org/10.1093/schbul/sbr172>
- Henze, D., Borhegyi, Z., & Csicsvari, J. (2000). Intracellular features predicted by extracellular recordings in the hippocampus in vivo. *Journal Of*. Retrieved from <http://jn.physiology.org/content/84/1/390.short>
- Herrmann, C. S., & Debener, S. (2008). Simultaneous recording of EEG and BOLD responses: A historical perspective. *International Journal of Psychophysiology*, 67(3), 161–168. <https://doi.org/10.1016/j.ijpsycho.2007.06.006>

- Hervas, D. (2018). NPLS Regression with L1 Penalization. *CRAN*.  
[https://doi.org/10.1002/\(SICI\)1099-128X\(199601\)10:1%3C47::AID-CEM400%3E3.0.CO;2-C>](https://doi.org/10.1002/(SICI)1099-128X(199601)10:1%3C47::AID-CEM400%3E3.0.CO;2-C)
- Hox, J. J. (2010). Multilevel Analysis. <https://doi.org/10.4324/9780203852279>
- Hox, J. J., & Kreft, I. G. G. (1994). Multilevel Analysis Methods. *Sociological Methods & Research*, 22(3), 283–299. <https://doi.org/10.1177/0049124194022003001>
- Huettel, S., Song, A. W., & McCarthy, G. (2004). *Functional magnetic resonance imaging*. Retrieved from <https://pdfs.semanticscholar.org/b917/f1d5f55a44446d45a14f2f0192375108aa0e.pdf>
- Hunter, J. D. (2007). Matplotlib: A 2D Graphics Environment. *Computing in Science & Engineering*, 9(3), 90–95. <https://doi.org/10.1109/MCSE.2007.55>
- Huster, R. J., Debener, S., Eichele, T., & Herrmann, C. S. (2012). Methods for Simultaneous EEG-fMRI: An Introductory Review. *Journal of Neuroscience*, 32(18), 6053–6060. <https://doi.org/10.1523/JNEUROSCI.0447-12.2012>
- Huster, R. J., Eichele, T., Enriquez-Geppert, S., Wollbrink, A., Kugel, H., Konrad, C., & Pantev, C. (2011). Multimodal imaging of functional networks and event-related potentials in performance monitoring. *NeuroImage*, 56(3), 1588–1597. <https://doi.org/10.1016/j.neuroimage.2011.03.039>
- Hwang, K., Ghuman, A. S., Manoach, D. S., Jones, S. R., & Luna, B. (2016). Frontal preparatory neural oscillations associated with cognitive control: A developmental study comparing young adults and adolescents. *NeuroImage*, 136, 139–48. <https://doi.org/10.1016/j.neuroimage.2016.05.017>
- Iannotti, G. R., Pittau, F., Michel, C. M., Vulliemoz, S., & Grouiller, F. (2014). Pulse Artifact Detection in Simultaneous EEG-fMRI Recording Based on EEG Map Topography. *Brain Topography*, 28(1), 21–32. <https://doi.org/10.1007/s10548-014-0409-z>
- Ihalainen, T., Kuusela, L., Turunen, S., Heikkinen, S., Savolainen, S., & Sipilä, O. (2015). Data quality in fMRI and simultaneous EEG-fMRI. *Magnetic Resonance Materials in Physics, Biology and Medicine*, 28(1), 23–31. <https://doi.org/10.1007/s10334-014-0443-6>
- Im, C., Jung, H., & Fujimaki, N. (2005). fMRI-constrained MEG source imaging and consideration of fMRI invisible sources. *Human Brain Mapping*. Retrieved from <http://onlinelibrary.wiley.com/doi/10.1002/hbm.20143/full>
- Jann, K., Dierks, T., Boesch, C., Kottlow, M., Strik, W., & Koenig, T. (2009). BOLD correlates of EEG alpha phase-locking and the fMRI default mode network. *NeuroImage*, 45(3), 903–916. <https://doi.org/10.1016/J.NEUROIMAGE.2009.01.001>
- Johnstone, E. C., Ebmeier, K. P., Miller, P., Owens, D. G. C., & Lawrie, S. M. (2005). Predicting schizophrenia: findings from the Edinburgh High-Risk. *The British Journal of Psychiatry*, 186, 18–25. <https://doi.org/10.1192/bjp.186.1.18>
- Jones, E., Oliphant, T., & Peterson, P. (2014). {SciPy}: open source scientific tools for {Python}. Retrieved from <http://www.citeulike.org/group/19049/article/13344001>
- Kirmizi-Alsan, E., Bayraktaroglu, Z., Gurvit, H., Keskin, Y. H., Emre, M., & Demiralp, T. (2006). Comparative analysis of event-related potentials during Go/NoGo and CPT: Decomposition of electrophysiological markers of response inhibition and sustained attention. *Brain Research*, 1104(1), 114–128. <https://doi.org/10.1016/j.brainres.2006.03.010>
- Klem, G., Lüders, H., Jasper, H., & Elger, C. (1999). The ten-twenty electrode system of the International Federation. *Electroencephalography and Clinical Neurophysiology*, 102(2), 371–375. [https://doi.org/10.1016/0013-4694\(58\)90053-1](https://doi.org/10.1016/0013-4694(58)90053-1)
- Koles, Z. J. (1998). Trends in EEG source localization. *Electroencephalography and Clinical Neurophysiology*, 106(2), 127–137. [https://doi.org/10.1016/S0013-4694\(97\)00115-6](https://doi.org/10.1016/S0013-4694(97)00115-6)

- Krishnan, A., Williams, L. J., McIntosh, A. R., & Abdi, H. (2010). Partial Least Squares (PLS) methods for neuroimaging: A tutorial and review path modeling PLS Symmetric PLS Asymmetric PLS Task PLS Behavior PLS Seed PLS Multi-block PLS Multi-table PLS Canonical variate analysis Co-inertia analysis Multiple factor analysis STATIS Barycentric discriminant analysis Multiple factor analysis Common factor analysis. *NeuroImage*. <https://doi.org/10.1016/j.neuroimage.2010.07.034>
- Kyathanahally, S., Franco-Watkins, A., Zhang, X., Calhoun, V., & Deshpande, G. (2016). A realistic framework for investigating decision-making in the brain with high spatio-temporal resolution using simultaneous EEG/fMRI and joint ICA. *IEEE Journal of Biomedical and Health Informatics*, 21(4), 1–1. <https://doi.org/10.1109/JBHI.2016.2590434>
- Laufs, H. (2012). A personalized history of EEG–fMRI integration. *NeuroImage*. <https://doi.org/10.1016/j.neuroimage.2012.01.039>
- Lei, X., Xu, P., Luo, C., Zhao, J., Zhou, D., & Yao, D. (2011). fMRI functional networks for EEG source imaging. *Human Brain Mapping*, 32(7), 1141–1160. <https://doi.org/10.1002/hbm.21098>
- Lemieux, L., Allen, P. J., Franconi, F., Symms, M. R., & Fish, D. K. (1997). Recording of EEG during fMRI experiments: Patient safety. *Magnetic Resonance in Medicine*, 38(6), 943–952. <https://doi.org/10.1002/mrm.1910380614>
- Lesh, T. A., Niendam, T. A., Minzenberg, M. J., & Carter, C. S. (2011). Cognitive Control Deficits in Schizophrenia: Mechanisms and Meaning. *Neuropsychopharmacology*, 36(1), 316–338. <https://doi.org/10.1038/npp.2010.156>
- Li, Y. O., Adali, T., & Calhoun, V. D. (2006). Sample Dependence Correction for Order Selection in fMRI Analysis. *3rd IEEE International Symposium on Biomedical Imaging: Macro to Nano, 2006.*, 1072–1075. <https://doi.org/10.1109/ISBI.2006.1625107>
- Logothetis, N. K., Pauls, J., Augath, M., Trinath, T., & Oeltermann, A. (2001). Neurophysiological investigation of the basis of the fMRI signal. *Nature*, 412(6843), 150–157. <https://doi.org/10.1038/35084005>
- Logothetis, N. K., & Wandell, B. A. (2004). Interpreting the BOLD signal. *Annual Review of Physiology*, 66, 735–769. <https://doi.org/10.1146/annurev.physiol.66.082602.092845>
- Lopez-Garcia, P., Lesh, T. A., Salo, T., Barch, D. M., MacDonald, A. W., Gold, J. M., ... Carter, C. S. (2016). The neural circuitry supporting goal maintenance during cognitive control: a comparison of expectancy AX-CPT and dot probe expectancy paradigms. *Cognitive, Affective, & Behavioral Neuroscience*, 16(1), 164–175. <https://doi.org/10.3758/s13415-015-0384-1>
- Luck, S. (2005). An introduction to the event-related potential technique MIT press. *Cambridge, Ma*. Retrieved from [https://scholar.google.de/scholar?q=Luck%2C+S.+J.+%282005%29.+An+introduction+to+the+event-related+potential+technique.+Cambridge%2C+MA%3A+MIT+Press.&btnG=&hl=de&as\\_sdt=0%2C5](https://scholar.google.de/scholar?q=Luck%2C+S.+J.+%282005%29.+An+introduction+to+the+event-related+potential+technique.+Cambridge%2C+MA%3A+MIT+Press.&btnG=&hl=de&as_sdt=0%2C5)
- Maas, C. J. M., & Hox, J. J. (2004). Robustness issues in multilevel regression analysis. *Statistica Neerlandica*, 58(2), 127–137. <https://doi.org/10.1046/j.0039-0402.2003.00252.x>
- MacDonald, A. W., Cohen, J. D., Stenger, V. A., & Carter, C. S. (2000). Dissociating the role of the dorsolateral prefrontal and anterior cingulate cortex in cognitive control. *Science (New York, N.Y.)*, 288(5472), 1835–8. <https://doi.org/10.1126/SCIENCE.288.5472.1835>
- MacDonald, A. W., Goghari, V. M., Hicks, B. M., Flory, J. D., Carter, C. S., & Manuck, S. B. (2005). A convergent-divergent approach to context processing, general intellectual functioning, and the genetic liability to schizophrenia. *Neuropsychology*, 19(6), 814–21. <https://doi.org/10.1037/0894-4105.19.6.814>

- Magri, C., Schridde, U., Murayama, Y., Panzeri, S., & Logothetis, N. K. (2012). The Amplitude and Timing of the BOLD Signal Reflects the Relationship between Local Field Potential Power at Different Frequencies. *Journal of Neuroscience*, 32(4), 1395–1407.  
<https://doi.org/10.1523/JNEUROSCI.3985-11.2012>
- Martínez-Montes, E., Valdés-Sosa, P. A., Miwakeichi, F., Goldman, R. I., & Cohen, M. S. (2004). Concurrent EEG/fMRI analysis by multiway Partial Least Squares. *NeuroImage*, 22(3), 1023–1034. <https://doi.org/10.1016/j.neuroimage.2004.03.038>
- McGorry, P., Keshavan, M., Goldstone, S., Amminger, P., Allott, K., Berk, M., ... Hickie, I. (2014). Biomarkers and clinical staging in psychiatry. *World Psychiatry*, 13(3), 211–223.  
<https://doi.org/10.1002/wps.20144>
- McIntosh, A. R., Bookstein, F. L., Haxby, J. V., & Grady, C. L. (1996). Spatial pattern analysis of functional brain images using partial least squares. *NeuroImage*, 3(3 I), 143–157.  
<https://doi.org/10.1006/nimg.1996.0016>
- McIntosh, A. R., & Mišić, B. (2013). Multivariate Statistical Analyses for Neuroimaging Data. *Annual Review of Psychology*, 64(1), 499–525. <https://doi.org/10.1146/annurev-psych-113011-143804>
- McKinney, W. (2010). Data Structures for Statistical Computing in Python. *Proceedings of the 9th Python in Science Conference*, 1697900(Scipy), 51–56. Retrieved from <https://pdfs.semanticscholar.org/f6da/c1c52d3b07c993fe52513b8964f86e8fe381.pdf>
- Mento, G., Tarantino, V., Vallesi, A., & Bisiacchi, P. S. (2015). Spatiotemporal Neurodynamics Underlying Internally and Externally Driven Temporal Prediction: A High Spatial Resolution ERP Study. *Journal of Cognitive Neuroscience*, 27(3), 425–439. <https://doi.org/10.1162/jocn>
- Montague, P. R., Dayan, P., & Sejnowski, T. J. (1996). A framework for mesencephalic dopamine systems based on predictive Hebbian learning. *Journal of Neuroscience*, 16(5), 1936–1947.  
<https://doi.org/10.1.1.156.635>
- Moosmann, M., Schönfelder, V. H., Specht, K., Scheeringa, R., Nordby, H., & Hugdahl, K. (2009). Realignment parameter-informed artefact correction for simultaneous EEG–fMRI recordings. *NeuroImage*, 45(4), 1144–1150. <https://doi.org/10.1016/j.neuroimage.2009.01.024>
- Mullinger, K. J., Castellone, P., & Bowtell, R. (2013). Best Current Practice for Obtaining High Quality EEG Data During Simultaneous fMRI. *Journal of Visualized Experiments*, (76), e50283–e50283. <https://doi.org/10.3791/50283>
- Mullinger, K. J., Havenhand, J., & Bowtell, R. (2013). Identifying the sources of the pulse artefact in EEG recordings made inside an MR scanner. *NeuroImage*, 71, 75–83.  
<https://doi.org/10.1016/j.neuroimage.2012.12.070>
- Mumford, J. A., Davis, T., & Poldrack, R. A. (2014). The impact of study design on pattern estimation for single-trial multivariate pattern analysis. *NeuroImage*, 103, 130–138.  
<https://doi.org/10.1016/j.neuroimage.2014.09.026>
- Mumford, J. A., Turner, B. O., Ashby, F. G., & Poldrack, R. A. (2012). Deconvolving BOLD activation in event-related designs for multivoxel pattern classification analyses. *NeuroImage*, 59(3), 2636–43. <https://doi.org/10.1016/j.neuroimage.2011.08.076>
- Murayama, Y., Bießmann, F., Meinecke, F. C., Müller, K.-R., Augath, M., Oeltermann, A., & Logothetis, N. K. (2010). Relationship between neural and hemodynamic signals during spontaneous activity studied with temporal kernel CCA. *Magnetic Resonance Imaging*, 28(8), 1095–1103. <https://doi.org/10.1016/j.mri.2009.12.016>
- Murias, M., Swanson, J. M., & Srinivasan, R. (2007). Functional connectivity of frontal cortex in healthy and adhd children reflected in EEG coherence. *Cerebral Cortex*, 17(8), 1788–1799.  
<https://doi.org/10.1093/cercor/bhl089>

- Murta, T., Chaudhary, U., Tierney, T., Dias, A., & Leite, M. (2016). Phase-amplitude coupling and the BOLD signal: A simultaneous intracranial EEG (icEEG)-fMRI study in humans performing a finger-tapping task. Retrieved from <https://pdfs.semanticscholar.org/607e/b47f7442a24ce98f8ea8c222eeb160b2e679.pdf>
- Murta, T., Hu, L., Tierney, T., Chaudhary, U., & Walker, M. (2016). A study of the electro-haemodynamic coupling using simultaneously acquired intracranial EEG and fMRI data in humans. Retrieved from <https://pdfs.semanticscholar.org/45ab/8c992780e60a981a49bb7ab2f44ec569f420.pdf>
- Murta, T., Leite, M., Carmichael, D. W., Figueiredo, P., & Lemieux, L. (2015). Electrophysiological correlates of the BOLD signal for EEG-informed fMRI. *Human Brain Mapping*, 36(1), 391–414. <https://doi.org/10.1002/hbm.22623>
- Nouretdinov, I., Costafreda, S. G., Gammerman, A., Chervonenkis, A., Vovk, V., Vapnik, V., & Fu, C. H. Y. (2010). Machine learning classification with confidence: Application of transductive conformal predictors to MRI-based diagnostic and prognostic markers in depression. *NeuroImage*. <https://doi.org/10.1016/j.neuroimage.2010.05.023>
- Nunez, P. L., & Silberstein, R. B. (2000). On the Relationship of Synaptic Activity to Macroscopic Measurements: Does Co-Registration of EEG with fMRI Make Sense? *Brain Topography*, 13(2), 79–96. <https://doi.org/10.1023/A:1026683200895>
- Nunez, P. L., & Srinivasan, R. (2006). *Electric Fields of the Brain: The Neurophysics of EEG*, 2nd Edition: 9780195050387: Medicine & Health Science Books. Retrieved from [https://books.google.de/books?hl=de&lr=&id=fUv54as56\\_8C&oi=fnd&pg=PR11&dq=9.+Nunez+PL,+Srinivasan+R.+Electric+fields+of+the+brain:+the+neurophysics+of+EEG:+Oxford+University+Press,+USA%3B+2006.&ots=nYPj3VhMIS&sig=TAYLtt12NbS7ovqT4RHb1zY\\_S60](https://books.google.de/books?hl=de&lr=&id=fUv54as56_8C&oi=fnd&pg=PR11&dq=9.+Nunez+PL,+Srinivasan+R.+Electric+fields+of+the+brain:+the+neurophysics+of+EEG:+Oxford+University+Press,+USA%3B+2006.&ots=nYPj3VhMIS&sig=TAYLtt12NbS7ovqT4RHb1zY_S60)
- Nunez, P. L., Srinivasan, R., Westdorp, A. F., Wijesinghe, R. S., Tucker, D. M., Silberstein, R. B., & Cadusch, P. J. (1997). EEG coherency I: Statistics, reference electrode, volume conduction, Laplacians, cortical imaging, and interpretation at multiple scales. *Electroencephalography and Clinical Neurophysiology*. [https://doi.org/10.1016/S0013-4694\(97\)00066-7](https://doi.org/10.1016/S0013-4694(97)00066-7)
- Nunez, P., & Silberstein, R. (2000). On the relationship of synaptic activity to macroscopic measurements: does co-registration of EEG with fMRI make sense? *Brain Topography*. Retrieved from <http://link.springer.com/article/10.1023/A:1026683200895>
- Ollikainen, J. O., Vauhkonen, M., Karjalainen, P. A., & Kaipio, J. P. (1999). Effects of local skull inhomogeneities on EEG source estimation. *Medical Engineering & Physics*, 21(3), 143–54. [https://doi.org/10.1016/S1350-4533\(99\)00038-7](https://doi.org/10.1016/S1350-4533(99)00038-7)
- Pereira, F., Mitchell, T., & Botvinick, M. (2009). Machine learning classifiers and fMRI: a tutorial overview. *NeuroImage*, 45(1 Suppl), S199-209. <https://doi.org/10.1016/j.neuroimage.2008.11.007>
- Petermann, F. (2012). Wechsler Adult Intelligence Scale (WAIS-IV; deutsche Version).
- Phillips, C., Rugg, M. D., & Friston, K. J. (2002). Anatomically Informed Basis Functions for EEG Source Localization: Combining Functional and Anatomical Constraints. *NeuroImage*, 16(3), 678–695. Retrieved from [http://orbi.ulg.ac.be/bitstream/2268/84739/1/Phillipps\\_C\\_2002\\_Neuroimage\\_16\\_3\\_678.pdf](http://orbi.ulg.ac.be/bitstream/2268/84739/1/Phillipps_C_2002_Neuroimage_16_3_678.pdf)
- Phillips, C., Rugg, M. D., & Friston, K. J. (2002). Systematic Regularization of Linear Inverse Solutions of the EEG Source Localization Problem. *NeuroImage*, 17(1), 287–301. Retrieved from [http://orbi.ulg.ac.be/bitstream/2268/1356/1/Phillips\\_C\\_2002\\_Neuroimage\\_17\\_1\\_287.pdf](http://orbi.ulg.ac.be/bitstream/2268/1356/1/Phillips_C_2002_Neuroimage_17_1_287.pdf)
- Pisauro, M. A., Fouragnan, E., Retzler, C., & Philiastides, M. G. (2017). Neural correlates of evidence accumulation during value-based decisions revealed via simultaneous EEG-fMRI. <https://doi.org/10.1038/ncomms15808>

- Polich, J. (2007). Updating P300: an integrative theory of P3a and P3b. *Clinical Neurophysiology*. Retrieved from <http://www.sciencedirect.com/science/article/pii/S1388245707001897>
- Polich, J., & Criado, J. (2006). Neuropsychology and neuropharmacology of P3a and P3b. *International Journal of Psychophysiology*. Retrieved from <http://www.sciencedirect.com/science/article/pii/S0167876006000213>
- Popescu, V., Battaglini, M., Hoogstrate, W. S., Verfaillie, S. C. J., Sluimer, I. C., van Schijndel, R. A., ... Vrenken, H. (2012). Optimizing parameter choice for FSL-Brain Extraction Tool (BET) on 3D T1 images in multiple sclerosis. *NeuroImage*, 61(4), 1484–1494. <https://doi.org/10.1016/J.NEUROIMAGE.2012.03.074>
- Poppe, A. B., Barch, D. M., Carter, C. S., Gold, J. M., Ragland, J. D., Silverstein, S. M., & MacDonald, A. W. (2016). Reduced Frontoparietal Activity in Schizophrenia Is Linked to a Specific Deficit in Goal Maintenance: A Multisite Functional Imaging Study. *Schizophrenia Bulletin*, 42(5), 1149–1157. <https://doi.org/10.1093/schbul/sbw036>
- Porro, C. A., Francescato, M. P., Cettolo, V., Diamond, M. E., Baraldi, P., Zuiani, C., ... di Prampero, P. E. (1996). Primary motor and sensory cortex activation during motor performance and motor imagery: a functional magnetic resonance imaging study. *The Journal of Neuroscience : The Official Journal of the Society for Neuroscience*, 16(23), 7688–98. <https://doi.org/10.1523/JNEUROSCI.16-23-07688.1996>
- R Development Core Team. (2016). R: A language and environment for statistical computing. R Foundation for Statistical Computing, Vienna, Austria. 2014.
- Reuter, M., Schmansky, N. J., Rosas, H. D., & Fischl, B. (2012). Within-subject template estimation for unbiased longitudinal image analysis. *NeuroImage*, 61(4), 1402–18. <https://doi.org/10.1016/j.neuroimage.2012.02.084>
- Ritter, P., & Villringer, A. (2006). Simultaneous Eeg–fmri. *Neuroscience & Biobehavioral Reviews*. Retrieved from <http://www.sciencedirect.com/science/article/pii/S0149763406000534>
- Robinson, D. G., Woerner, M. G., Alvir, J. M. J., Geisler, S., Koreen, A., Sheitman, B., ... Lieberman, A. (1999). Predictors of Treatment Response From a First Episode of Schizophrenia or Schizoaffective Disorder. *Am J Psychiatry*, 1564. Retrieved from <https://ajp.psychiatryonline.org/doi/pdf/10.1176/ajp.156.4.544>
- Roesch, M. R., Calu, D. J., & Schoenbaum, G. (2007). Dopamine neurons encode the better option in rats deciding between differently delayed or sized rewards. *Nature Neuroscience*, 10(12), 1615–24. <https://doi.org/10.1038/nn2013>
- Rogers, R. L., Baumann, S. B., Papanicolaou, A. C., Bourbon, T. W., Alagarsamy, S., & Eisenberg, H. M. (1991). Localization of the P3 sources using magnetoencephalography and magnetic resonance imaging. *Electroencephalography and Clinical Neurophysiology*, 79(4), 308–321. [https://doi.org/10.1016/0013-4694\(91\)90126-O](https://doi.org/10.1016/0013-4694(91)90126-O)
- Rosa, M., Daunizeau, J., & Friston, K. (2010). EEG-fMRI integration: a critical review of biophysical modeling and data analysis approaches. *Journal of Integrative*. Retrieved from <http://www.worldscientific.com/doi/abs/10.1142/S0219635210002512>
- Rosen, B. R., Buckner, R. L., & Dale, A. M. (1998). Event-related functional MRI: past, present, and future. *Proceedings of the National Academy of Sciences of the United States of America*, 95(3), 773–80. <https://doi.org/10.1073/PNAS.95.3.773>
- Rothlübbers, S., Relvas, V., Leal, A., Murta, T., Lemieux, L., & Figueiredo, P. (2015). Characterisation and Reduction of the EEG Artefact Caused by the Helium Cooling Pump in the MR Environment: Validation in Epilepsy Patient Data. *Brain Topography*, 28(2), 208–220. <https://doi.org/10.1007/s10548-014-0408-0>
- Sadaghiani, S., & Kleinschmidt, A. (2016). Brain Networks and  $\alpha$ -Oscillations: Structural and

- Functional Foundations of Cognitive Control. *Trends in Cognitive Sciences*, 20(11), 805–817. <https://doi.org/10.1016/J.TICS.2016.09.004>
- Sanei, S., Chambers, J. A., Sanei, S., & Chambers, J. A. (2013). EEG Source Localization. In *EEG Signal Processing* (pp. 197–218). West Sussex, England: John Wiley & Sons Ltd. <https://doi.org/10.1002/9780470511923.ch5>
- Scheibe, C., Ullsperger, M., Sommer, W., & Heekeren, H. R. (2010). Effects of Parametrical and Trial-to-Trial Variation in Prior Probability Processing Revealed by Simultaneous Electroencephalogram/Functional Magnetic Resonance Imaging. *Journal of Neuroscience*, 30(49), 16709–16717. <https://doi.org/10.1523/JNEUROSCI.3949-09.2010>
- Schoffelen, J. M., & Gross, J. (2009). Source connectivity analysis with MEG and EEG. *Human Brain Mapping*. <https://doi.org/10.1002/hbm.20745>
- Schridde, U., Khubchandani, M., Motelow, J. E., Sanganahalli, B. G., Hyder, F., & Blumenfeld, H. (2008). Negative BOLD with large increases in neuronal activity. *Cerebral Cortex*, 18(8), 1814–1827. <https://doi.org/10.1093/cercor/bhm208>
- Shams, N., Alain, C., & Strother, S. (2015). Comparison of BCG artifact removal methods for evoked responses in simultaneous EEG–fMRI. *Journal of Neuroscience Methods*, 245, 137–146. <https://doi.org/10.1016/j.jneumeth.2015.02.018>
- Smith, S. M. (2006). BET: Brain Extraction Tool. *Review: Literature and Arts of the Americas*, 39(1), 25. <https://doi.org/10.1080/08905760600696445>
- Smith, S. M., Jenkinson, M., Woolrich, M. W., Beckmann, C. F., Behrens, T. E. J., Johansen-berg, H., ... Matthews, P. M. (2004). Advances in Functional and Structural MR Image Analysis and Implementation as FSL Technical Report TR04SS2. *Neuroimage*, 23(SI), 208–219. <https://doi.org/10.1016/j.neuroimage.2004.07.051>
- Sprooten, E., Rasgon, A., Goodman, M., Carlin, A., Leibu, E., Lee, W. H., & Frangou, S. (2017). Addressing reverse inference in psychiatric neuroimaging: Meta-analyses of task-related brain activation in common mental disorders. *Human Brain Mapping*, 38(4), 1846–1864. <https://doi.org/10.1002/hbm.23486>
- Srinivasan, R., Winter, W. R., Ding, J., & Nunez, P. L. (2007). EEG and MEG coherence: measures of functional connectivity at distinct spatial scales of neocortical dynamics. *Journal of Neuroscience Methods*, 166(1), 41. <https://doi.org/10.1016/J.JNEUMETH.2007.06.026>
- Sui, J., Adali, T., Yu, Q., Chen, J., & Calhoun, V. D. (2012). A review of multivariate methods for multimodal fusion of brain imaging data. *Journal of Neuroscience Methods*, 204(1), 68–81. <https://doi.org/10.1016/j.jneumeth.2011.10.031>
- Swann, N. C., Cai, W., Conner, C. R., Pieters, T. A., Claffey, M. P., George, J. S., ... Tandon, N. (2012). Roles for the pre-supplementary motor area and the right inferior frontal gyrus in stopping action: electrophysiological responses and functional and structural connectivity. *NeuroImage*, 59(3), 2860–70. <https://doi.org/10.1016/j.neuroimage.2011.09.049>
- Tang, Y.-Y., Posner, M. I., Rothbart, M. K., & Volkow, N. D. (2015). Circuitry of self-control and its role in reducing addiction. *Trends in Cognitive Sciences*, 19(8), 439–444. <https://doi.org/10.1016/j.tics.2015.06.007>
- Tchanturia, K., Davies, H., Roberts, M., Harrison, A., Nakazato, M., Schmidt, U., ... Morris, R. (2012). Poor Cognitive Flexibility in Eating Disorders: Examining the Evidence using the Wisconsin Card Sorting Task. *PLoS ONE*, 7(1), e28331. <https://doi.org/10.1371/journal.pone.0028331>
- Todorov, E., & Jordan, M. I. (1889). Optimal feedback control as a theory of motor coordination: Supplementary Notes. *Nature.Com*, 5(2), 82. <https://doi.org/10.2307/3752313>

- Todorov, E., & Jordan, M. I. (2002). A Minimal Intervention Principle for Coordinated Movement. *Advances in Neural Information Processing Systems*, 27–34. Retrieved from <http://papers.nips.cc/paper/2195-a-minimal-intervention-principle-for-coordinated-movement.pdf>
- Turner, B. M., Forstmann, B. U., Wagenmakers, E.-J., Brown, S. D., Sederberg, P. B., & Steyvers, M. (2013). A Bayesian framework for simultaneously modeling neural and behavioral data. *NeuroImage*, 72, 193–206. <https://doi.org/10.1016/j.neuroimage.2013.01.048>
- Turner, B. M., Rodriguez, C. A., Norcia, T. M., McClure, S. M., & Steyvers, M. (2016). Why more is better: Simultaneous modeling of EEG, fMRI, and behavioral data. *NeuroImage*, 128, 96–115. <https://doi.org/10.1016/j.neuroimage.2015.12.030>
- Turner, B. M., Sederberg, P. B., Brown, S. D., & Steyvers, M. (2013). A method for efficiently sampling from distributions with correlated dimensions. *Psychological Methods*, 18(3), 368–84. <https://doi.org/10.1037/a0032222>
- Ullsperger, M., & Debener, S. (2010). Simultaneous EEG and fMRI: recording, analysis, and application. Retrieved from [https://books.google.de/books?hl=de&lr=&id=yo4UDAAAQBAJ&oi=fnd&pg=PR9&dq=ullsperger+eeg+fmri&ots=aKzY5mtB6K&sig=RHDGHKnz5gQhFXe58\\_9zRbXJxiY](https://books.google.de/books?hl=de&lr=&id=yo4UDAAAQBAJ&oi=fnd&pg=PR9&dq=ullsperger+eeg+fmri&ots=aKzY5mtB6K&sig=RHDGHKnz5gQhFXe58_9zRbXJxiY)
- van der Walt, S., Colbert, S. C., & Varoquaux, G. (2011). The NumPy Array: A Structure for Efficient Numerical Computation. *Computing in Science & Engineering*, 13, 22–30. <https://doi.org/10.1109/MCSE.2011.37>
- Venkatasubramanian, G., & Keshavan, M. S. (2016). Biomarkers in Psychiatry - A Critique. *Annals of Neurosciences*, 23(1), 3–5. <https://doi.org/10.1159/000443549>
- Volkow, N. D., Wang, G.-J., & Baler, R. D. (2011). Reward, dopamine and the control of food intake: implications for obesity. *Trends in Cognitive Sciences*, 15(1), 37–46. <https://doi.org/10.1016/j.tics.2010.11.001>
- Voytek, B., Kayser, A. S., Badre, D., Fegen, D., Chang, E. F., Crone, N. E., ... D'Esposito, M. (2015). Oscillatory dynamics coordinating human frontal networks in support of goal maintenance. *Nature Neuroscience*, 18(9), 1318–24. <https://doi.org/10.1038/nn.4071>
- Waskom, M., Botvinnik, O., Hobson, P., Cole, J. B., Halchenko, Y., Hoyer, S., ... Allan, D. (2014). seaborn: v0.5.0 (November 2014). <https://doi.org/10.5281/ZENODO.12710>
- Whittingstall, K., Bartels, A., Singh, V., Kwon, S., & Logothetis, N. K. (2010). Integration of EEG source imaging and fMRI during continuous viewing of natural movies. *Magnetic Resonance Imaging*, 28(8), 1135–1142. <https://doi.org/10.1016/j.mri.2010.03.042>
- Wickham, H. (2009). ggplot2: Elegant Graphics for Data Analysis. *Springer New York*. <https://doi.org/10.1007/978-0-387-98141-3>
- Wiers, R. W., Gladwin, T. E., Hofmann, W., Salemink, E., & Ridderinkhof, K. R. (2013). Cognitive Bias Modification and Cognitive Control Training in Addiction and Related Psychopathology. *Clinical Psychological Science*, 1(2), 192–212. <https://doi.org/10.1177/2167702612466547>
- Wu, X., Wu, T., Zhan, Z., Yao, L., & Wen, X. (2016). A real-time method to reduce ballistocardiogram artifacts from EEG during fMRI based on optimal basis sets (OBS). *Computer Methods and Programs in Biomedicine*, 127, 114–125. <https://doi.org/10.1016/J.CMPB.2016.01.018>
- Xu, X.-L., Xu, B., & He, B. (2004). An alternative subspace approach to EEG dipole source localization. *Phys. Med. Biol.*, 49, 327–343. <https://doi.org/10.1088/0031-9155/49/2/010>
- Yan, W. X., Mullinger, K. J., Brookes, M. J., & Bowtell, R. (2009). Understanding gradient artefacts in simultaneous EEG/fMRI. *NeuroImage*, 46(2), 459–471. <https://doi.org/10.1016/J.NEUROIMAGE.2009.01.029>

- Yan, W. X., Mullinger, K. J., Geirsdottir, G. B., & Bowtell, R. (2010). Physical modeling of pulse artefact sources in simultaneous EEG/fMRI. *Human Brain Mapping*, 31(4), 604–620. <https://doi.org/10.1002/hbm.20891>
- Yeung, C. J., Susil, R. C., & Atalar, E. (2002). RF heating due to conductive wires during MRI depends on the phase distribution of the transmit field. *Magnetic Resonance in Medicine*, 48(6), 1096–1098. <https://doi.org/10.1002/mrm.10310>

## Appendix A: Forms and participant information

**NAME:****STUDIE:****GEBURTSDATUM:****GEWICHT:****KÖRPERGRÖSSE:**

### **Metallanamnese-Fragebogen**

Frage	ja	nein
1. Tragen Sie einen Herzschrittmacher?		
2. Hatten Sie jemals einen chirurgischen Eingriff? Was wurde operiert?		
3. Sind Sie schwanger oder vermuten Sie schwanger zu sein?		
4. Sind Sie jemals durch einen metallenen Fremdkörper verletzt worden (Geschoß, Granatsplitter, Metallsplitter usw.)?		
5. Haben oder vermuten Sie Metallobjekte im Auge (z.B. Prothese, Metallsplitter)? Tragen Sie Kontaktlinsen?		
6. Haben Sie Metallclips nach Gefäßoperationen? Wenn ja, wo (Gehirn, Herzkranzgefäß, Aneurysma, Transplantatniere)?		
7. Haben Sie eine Herzklappe aus Metall? Wenn ja, welcher Typ? (Herzklappenpass)		
8. Tragen Sie implantierte, elektrische Stimulationsgeräte (Biostimulatoren, Neurostimulatoren)? Anus-Praeter?		
9. Tragen Sie implantierte Medikamentenpumpen oder Infusionssysteme (z.B. Infusionspumpe, Ports)?		
10. Haben Sie eine Mittelohrprothese oder Cochlea-Implantat?		
11. Wurden bei Ihnen metallene Fremdkörper in die Blutgefäße oder den Verdauungstrakt implantiert (z.B. Stents, Cava-Filter, Spiralen)?		
12. Tragen Sie Gelenkprothesen aus Metall?		
13. Wurde bei Ihnen Osteosynthesematerial eingesetzt (z.B. Metallplatten, -stäbe, oder -schrauben) nach Knochenverletzungen?		
14. Tragen Sie einen Intrauterin-Pessar ("Spirale") aus Metall?		
15. Haben Sie herausnehmbaren metallenen Zahnersatz?		
16. Waren Sie jemals als Metallarbeiter tätig?		
17. Haben Sie Tätowierungen, Permanentmakeup oder Piercings? Haben Sie Implantate (z.B. Brust, Bauch etc.) ?		
18. Tragen Sie einen nicht herausnehmbaren Retainer/ Zahnpfanne? Haben Sie Akupunkturnadeln?		
19. Tragen Sie ein Medikamenten-Pflaster oder einen Verband?		
20. Leiden Sie an anderen chronischen oder akuten Krankheiten? (falls ja, bitte auf Rückseite erläutern)		
21. Nehmen Sie derzeit Medikamente? (falls ja, bitte auf Rückseite erläutern)		

**Ich habe die Fragen nach bestem Wissen und Gewissen beantwortet  
Mir ist bewusst, dass falsche Angaben meine Gesundheit gefährden können!**

**! ! ! Ich bestätige mit meiner Unterschrift, dass ich alle metallischen  
Gegenstände abgelegt habe ! ! !**

Marburg, den  
Uhrzeit:

.....

(Unterschrift)

**Philipps-Universität Marburg**  
 Klinik für Psychiatrie und Psychotherapie  
 Laboratory for Multimodal Neuroimaging  
 Rudolf-Bultmann-Straße 8  
 35039, Marburg

**Philipps-Universität Marburg**  
 Fachbereich 04 Psychologie  
 AE Neuropsychologie  
 Gutenbergstr. 18  
 35037, Marburg



**Probandeninformation für Forschungsvorhaben**  
**mit fMRT- und EEG-Untersuchung:**  
 „CognitiveCapture“

---

Projektleiter:	Dr. Jens Sommer
Untersuchungsleiter und Durchführung:	Peer Herholz
	Malte Rudo Güth

---

**Sehr geehrte Frau, sehr geehrter Herr,**

wir möchten Sie hiermit bitten, an unserer Untersuchung teilzunehmen. Im Folgenden erhalten Sie Informationen zur oben genannten Studie, zu den geplanten Untersuchungen, mögliche Risiken, zum Umgang mit sog. „Zufallsbefunden“, zum Umgang mit den erhobenen Daten und abschließend zu den Ausschlusskriterien für die Teilnahme an der Studie.

**Wozu dient diese Studie?**

Die Untersuchung findet im Rahmen einer Studie zur Erforschung von Zusammenhängen kognitiver Leistung und der mittels Elektroenzephalographie (EEG) und Funktioneller Magnet-Resonanz-Tomographie (fMRT) aufgezeichneten Gehirnaktivität statt. Ihre Teilnahme an der Studie hilft uns, grundlegende Mechanismen der Wahrnehmung und Bearbeitung von Aufgaben, bei denen Sie bestimmte Zielreize von anderen Reizen unterscheiden werden sollen, besser zu verstehen. Zum anderen soll die gleichzeitige Anwendung der genannten Methoden erprobt werden.

**Welche Kosten und welchen Nutzen habe ich von der Teilnahme? Gibt es Risiken?**

Es entstehen für Sie keine Kosten durch die Teilnahme. Für Ihre Teilnahme an dieser Studie haben Sie die Möglichkeit, Aufnahmen Ihres Gehirns zu erhalten.

Die MRT-Technologie ist für den Körper nach heutigem Erkenntnisstand unschädlich. Sie basiert auf mehr als 20 Jahren Erfahrung und wird weltweit, täglich in allen mittleren und größeren Kliniken eingesetzt. Bekannte Risiken ergeben sich ausschließlich durch metallische Gegenstände oder Stoffe mit magnetischen Eigenschaften, die sich am oder im Körper befinden. Diese können sich erhitzen und zu Verbrennungen führen. Lose Metallteile können durch das Magnetfeld beschleunigt werden und dann zu Verletzungen führen. Daher sind Personen von der Teilnahme an der Studie ausgeschlossen, die elektrische Geräte (z.B. Herzschrittmacher, Medikamentenpumpen) oder Metallteile (z.B. Schrauben nach Knochenbruch) im oder am Körper haben.

Risiken unabhängig von den Genannten sind bislang nicht bekannt. Abgesehen von

möglichen Unbequemlichkeiten, die vom stillen Liegen in der relativ engen MRT-Röhre resultieren, und der Lautstärke des MRT, sollten keine Beschwerden während der Untersuchung auftreten. Wir möchten sie allerdings darauf hinweisen, dass über mögliche langfristige Risiken bei wiederholten MRT-Messungen bisher keine wissenschaftlich abgesicherten Ergebnisse vorliegen.

Für die EEG-Untersuchung werden Messfühler (Elektroden) an Ihrem Kopf angebracht. Dies ist in der Regel schmerzfrei und mit keinerlei Risiken verbunden. Damit eine möglichst gute Signalqualität erreicht werden kann, wird der Kontakt zwischen den Elektroden und der Kopfhaut mit Hilfe eines speziellen salzhaltigen Gels verbessert. Dieses Gel lässt sich leicht wieder aus dem Haar auswaschen und ist mit keinerlei Nebenwirkungen verbunden. Auf Wunsch können Sie dies im Anschluss an die Untersuchung hier in den Laborräumen tun. Die Messung von elektrischen Gehirnignalen ist vollkommen ungefährlich. Es werden lediglich vom Gehirn produzierte, elektrische Signale in Form von geringen Potentialunterschieden erfasst. Weiterhin ist zu bemerken, dass kein Strom durch die Elektroden fließt.

#### Wie ist der Ablauf der Untersuchung?

Die Untersuchung beginnt mit dem Anbringen der Elektroden, welche zur Registrierung der elektrischen Gehirnaktivität notwendig sind. Dazu wird Ihnen eine elastische Kappe aufgesetzt, die mit einem elastischen Gurt unterhalb Ihres Kinns zugebunden wird. Zur Reduktion elektrischer Widerstände und zur Verbesserung der Signalqualität wird das bereits erwähnte Gel auf Ihre Kopfhaut aufgetragen. Das Anbringen der Messfühler nimmt zwischen 30 und 45 Minuten in Anspruch. Die Dauer kann aufgrund von individuellen Merkmalen wie der Kopfhaut, Frisur oder Dicke und Dichte der Haare variieren. Zuvor bitten wir Sie, einige Fragen zu beantworten, die der Erfassung allgemeiner Personendaten wie z.B. Alter oder Geschlecht dienen, und einen ca. fünfminütigen Vortest zur Konzentrationsleistung zu bearbeiten.

Daraufhin folgt die Lagerung im MRT, wofür ca. 5-10 Minuten benötigt werden. Anschließend wird eine Übersichtsaufnahme und eine hochauflöste Aufnahme von Ihrem Kopf erstellt. Dies dauert ca. 6 Minuten, in denen Sie lediglich ruhig liegen müssen.

Danach wird Ihnen die Aufgabe nochmals genau erläutert. Sie werden zwei aufeinanderfolgende Punktmuster sehen, die innerhalb eines Punktewürfels schnell aufblinken. Zuerst sehen Sie eines in Hellblau und nach einer kurzen Pause eines in Grau. Ihre Aufgabe wird darin bestehen, eine bestimmte Folge von Punktmustern zu erkennen. Im Anschluss an die Instruktion werden Sie in einigen Übungsdurchgängen die Aufgabe praktisch üben. Nach jedem Übungsblock wird Ihnen am Bildschirm eine Rückmeldung zu der Richtigkeit Ihrer Reaktion gegeben. Im Hauptteil der Untersuchung erhalten Sie keine Rückmeldung.

Insgesamt werden Sie vier Blöcke bearbeiten, die jeweils ca. sieben bis acht Minuten dauern. Nach jedem Block gibt es eine Pause von einer Minute. Mit Pausen wird die Bearbeitung der Aufgabe maximal 35 Minuten dauern.

Die Gesamtdauer der Untersuchung variiert und hängt von der Vorbereitung des EEG- und des MRT-Systems ab. In der Regel gehen wir von ca. 90 Minuten Gesamtdauer aus.

#### Was geschieht mit meinen Daten?

Die Datenerhebung erfolgt streng vertraulich. Alle die Studie durchführenden Personen sind zur Verschwiegenheit verpflichtet. Ihre Daten werden in anonymisierter Form auf einem gesicherten PC der Universität Marburg gespeichert und ausgewertet. Anonymisiert bedeutet, dass keine Angaben von Namen oder Initialen verwendet werden, sondern nur ein Code ohne Bezug zu Ihrer Person. Personenbezogene Informationen werden unabhängig von Ihren Versuchsdaten in einer Schlüsselliste gespeichert, welche nur dem Studienleiter zugänglich ist. Die Schlüsselliste wird nach Abschluss der Studie gelöscht. Bei der Datenverarbeitung werden die Bestimmungen des Datenschutzgesetzes eingehalten. Die Auswertung der Daten erfolgt ebenfalls anonymisiert und ausschließlich zu Studienzwecken. Ihre schriftlichen und elektronischen Unterlagen und Daten werden gemäß aktueller gesetzlicher Bestimmungen für eine Dauer von 10 Jahren nach Abschluss der Studie gespeichert. Der Abschnitt der Einverständniserklärung mit Ihrer Unterschrift wird hierbei getrennt von Ihren Daten verschlossen.

aufbewahrt. Zugriff auf die Daten haben nur die beteiligten Mitarbeiter des Forschungsprojektes. Eine Weitergabe von Daten findet nicht statt. Im Falle von Veröffentlichungen der Studienergebnisse bleibt die Vertraulichkeit der persönlichen Daten ebenfalls gewährleistet.

**Umgang mit Zufallsbefunden**

Bei der Studie handelt es sich um eine Forschungsstudie. Eine neuroradiologische Befundung der MRT-Bilder im Sinne einer klinisch orientierten Diagnostik findet daher nicht statt. Dennoch kann es vorkommen, dass in den MRT-Bildern Signalauffälligkeiten entdeckt werden, die eine mögliche klinische Relevanz haben („Zufallsbefund“). Falls sich bei der Untersuchung Anhaltspunkte für einen Zufallsbefund ergeben, die eine fachärztliche neuroradiologische Diagnostik empfehlenswert erscheinen lassen, würde Sie der Versuchsleiter persönlich darüber informieren und Ihnen eine fachärztlich neuroradiologische Diagnostik empfehlen. Falls Sie über einen Zufallsbefund nicht informiert werden wollen, stellt dies ein Ausschlusskriterium für die Teilnahme an der Studie dar.

**Teilnahme an der Studie und Beendigung der Teilnahme**

Ihre Teilnahme an der Studie ist freiwillig. Sollte Sie während der Untersuchung etwas körperlich oder seelisch zu stark beanspruchen, bitten wir Sie, uns dies sofort mitzuteilen. Sie können jederzeit und ohne Angabe von Gründen die Teilnahme beenden, ohne dass Ihnen dadurch Nachteile entstehen. In diesem Fall werden keine weiteren Daten von Ihnen erhoben. Die bisher gespeicherten Daten werden anonymisiert weiterverwendet, es sei denn Sie machen von Ihrem Recht Gebrauch, die sofortige Löschung aller bisher erhobenen Daten zu verlangen.

**Ausschlusskriterien**

Die Anwendung von Magnetfeldern bei der MRT-Untersuchung schließt die Teilnahme von Personen aus, die elektrische Geräte (z.B. Herzschrittmacher, Medikamentenpumpen usw.) oder Metallteile (z.B. Schrauben nach Knochenbruch, „Spirale“) im oder am Körper haben. Frauen, die schwanger sind, werden nicht als Probandinnen zugelassen. Probanden, die nicht über mögliche Zufallsbefunde informiert werden wollen, können ebenfalls nicht an der Studie teilnehmen.

Weitere Ausschlusskriterien sind vorbestehende neurologische und psychiatrische Erkrankungen und die aktuelle Einnahme von Psychopharmaka. Außerdem werden gute Deutschkenntnisse und gutes Sehvermögen vorausgesetzt.

**Wenn weitere Fragen bestehen, werden diese gerne vom Untersuchungsleiter beantwortet.**

**Einwilligungserklärung zur Teilnahme an dem Forschungsvorhaben**

Bei Ihrer Bereitschaft zur Teilnahme bitten wir Sie, die Einwilligungserklärung vor der Untersuchung vollständig auszufüllen und zu unterschreiben.

Ich bestätige hiermit, dass ich durch den Untersucher, Herrn Malte Güth, über Wesen, Bedeutung, Risiken und Tragweite der beabsichtigten Untersuchung aufgeklärt wurde und für meine Entscheidung genügend Bedenkzeit hatte. Ich habe die Probandeninformation gelesen. Ich fühle mich ausreichend informiert und habe verstanden, worum es geht. Der Untersucher hat mir ausreichend Gelegenheit gegeben, Fragen zu stellen, die alle für mich ausreichend beantwortet wurden. Ich hatte genügend Zeit, mich zu entscheiden.

Ich wurde darauf hingewiesen, dass es sich bei der Studie um eine Forschungsstudie handelt. Eine neuroradiologische Befundung der MR-Bilder im Sinne einer klinisch orientierten Diagnostik findet daher nicht statt. Dennoch kann es vorkommen, dass in den MR-Bildern Signalauffälligkeiten entdeckt werden, die eine mögliche klinische Relevanz haben („Zufallsbefund“). Mir ist bekannt, dass der Versuchsleiter mich informieren würde, falls sich bei der Untersuchung Anhaltspunkte für einen Zufallsbefund ergeben, die eine fachärztliche neuroradiologische Diagnostik empfehlenswert erscheinen lassen.

Ich habe verstanden, dass bei wissenschaftlichen Studien persönliche Daten und medizinische Befunde erhoben werden. Die Weitergabe, Speicherung und Auswertung dieser studienbezogenen Daten erfolgt nach gesetzlichen Bestimmungen und setzt vor Teilnahme an der Studie meine freiwillige Einwilligung voraus. Ich erkläre mich damit einverstanden, dass im Rahmen dieser Studie erhobene Daten auf Fragebögen und elektronischen Datenträgern aufgezeichnet und ohne Namensnennung zum Zwecke wissenschaftlicher Auswertung analysiert werden.

Ich habe eine Kopie der Probandeninformation und dieser unterschriebenen Einwilligungserklärung erhalten. Meine Einwilligung, an diesem Forschungsvorhaben als Proband teilzunehmen, erfolgt freiwillig. Ich wurde darauf hingewiesen, dass ich meine Einwilligung jederzeit ohne Angabe von Gründen und ohne Nachteile widerrufen kann.

Ich willige hiermit ein, als Proband an dem Forschungsvorhaben „CognitiveCapture“ teilzunehmen.

VOM PROBANDEN AUSZUFÜLLEN:

Name: .....

Geburtsdatum: .....

Datum: ..... Uhrzeit: .....

Ort: ..... Unterschrift: .....

VOM UNTERSUCHER AUSZUFÜLLEN:

Ich habe den Probanden über Wesen, Bedeutung, Reichweite und Risiken des Forschungsvorhabens aufgeklärt.

Datum: ..... Uhrzeit: .....

Ort: ..... Unterschrift: .....

## Appendix B: Interviews, protocol and pretest

Datum: \_\_\_\_\_

VP: \_\_\_\_\_

Vorinterview *CognitiveCapture* (2016/17)

1. Welches Geschlecht haben Sie?

weiblich

männlich

2. Wie alt sind Sie?

Ich bin \_\_\_\_\_ Jahre alt.

3. Welcher ist Ihr höchster Abschluss?

noch Schüler

Schule ohne Abschluss beendet

Hauptschule

Realschule / Mittlere Reife

Abgeschlossene Lehre

Fachabitur / Fachhochschulreife

Abitur / Hochschulreife

Fachhochschul- / Hochschulabschluss

Anderer Abschluss, nämlich:

---

4. Welche (Durchschnitts-)Note haben Sie erreicht? (bitte tragen Sie hier Ihre Note oder Punkte ein)

---

5. Wie ist Ihr Allgemeinbefinden während der letzten Zeit gewesen?

schlecht

eher schlecht

mittelmäßig

gut

sehr gut

Datum: \_\_\_\_\_

VP: \_\_\_\_\_

6. Wollen Sie über die Ergebnisse der Studie informiert werden?

Ja

Nein

7. Wenn ja, geben Sie bitte Ihre E-Mail-Adresse an:

Datum: \_\_\_\_\_

VP: \_\_\_\_\_

Protokollbogen *CognitiveCapture* (2016/17)

<b>Untersuchungsabschnitt</b>	<b>Zeit</b>	<b>Ereignis/Verhalten</b>
Begrüßung und Vortest		
EEG-Vorbereitung		
MRT-Vorbereitung		
Block 1.		
Block 2.		
Block 3.		
Block 4.		
Verabschiedung und Nachinterview		

**Zahlen-Symbol-Test**

1	2	3	4	5	6	7	8	9
L	D	A	-	II	H	C	L	H

Beispiel      Übung

6	8	3	9	5	4	1	7	2	1	4	8	2	7	6	9	3	5
8	3	1	9	2	5	6	4	3	7	2	9	8	1	4	7	6	5
9	1	2	4	7	2	5	6	9	5	8	6	4	3	1	7	8	3
1	3	9	6	3	9	7	5	1	4	2	8	7	2	8	5	6	4
7	6	4	1	3	2	8	1	7	9	2	5	3	4	8	6	5	9
8	1	9	5	1	4	2	6	9	8	7	3	5	6	4	7	2	3
3	6	8	9	1	8	4	7	5	2	9	6	7	1	5	2	3	4
6	4	1	9	5	7	3	6	8	3	2	7	5	8	4	2	9	1

Datum: \_\_\_\_\_

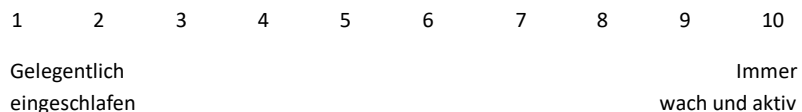
VP: \_\_\_\_\_

**Nachinterview *CognitiveCapture* (2016)**

1. Wie gut glauben Sie, ist Ihnen die Ausführung der Aufgabe auf einer Skala von 1 (gar nicht) bis 10 (sehr gut) gelungen?



2. Wie schätzen Sie Ihre Wachheit während des Experiments auf einer Skala von 1 bis 10 ein?



3. Konnten Sie alle Muster gut erkennen bzw. alle Instruktionen lesen?

Ja (1)  
Nein (2)

4. Was vermuten Sie, worum es ging?

---

---

5. Gibt es etwas, das sie zum Ablauf des Versuchs, den Versuchsleitern oder den Bedingungen (Raum, Temperatur, Licht, etc.) sagen möchten?

---

---

Datum: \_\_\_\_\_

VP: \_\_\_\_\_

6. Wollen Sie über die Ergebnisse der Studie informiert werden?

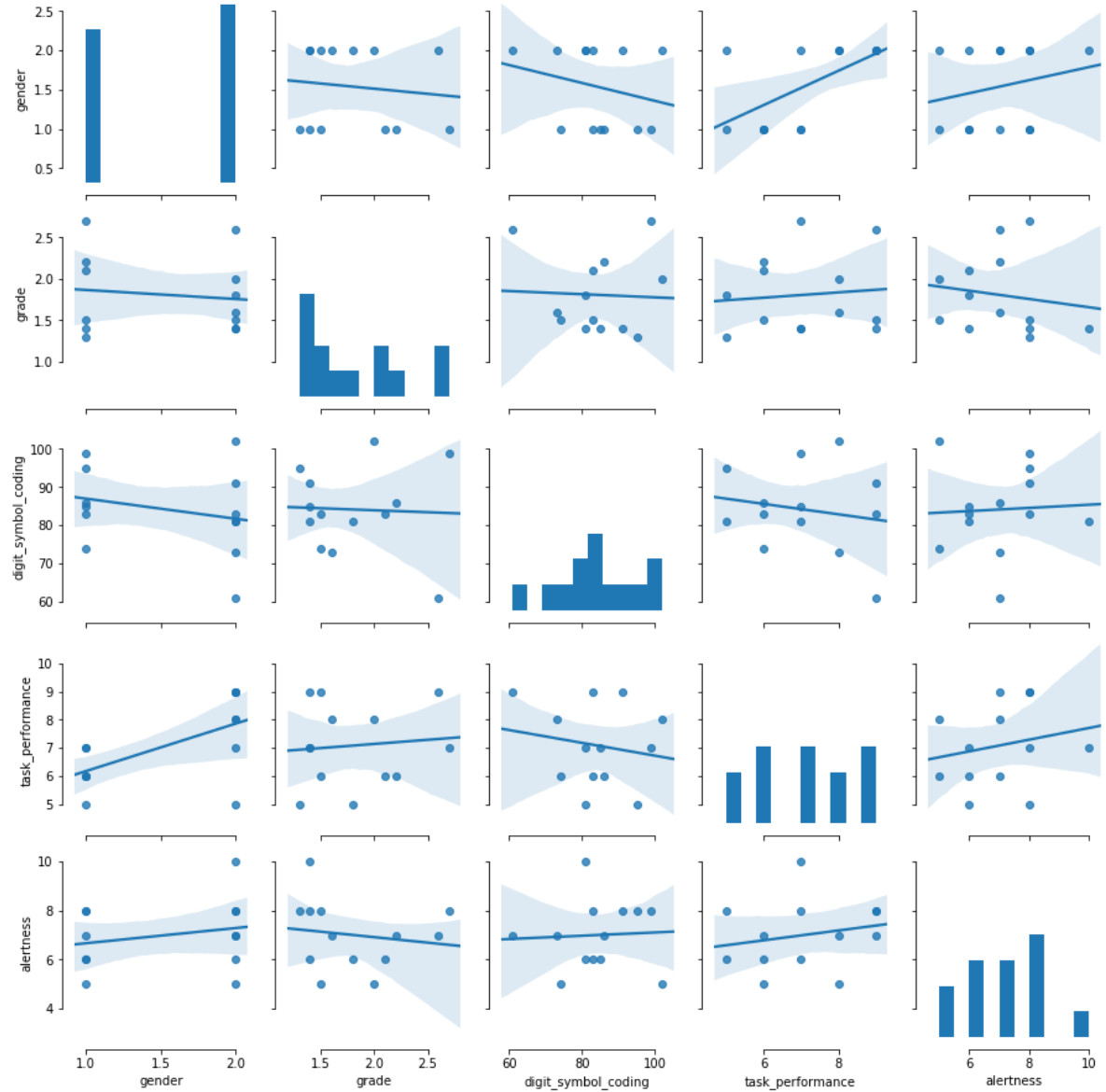
Ja

Nein

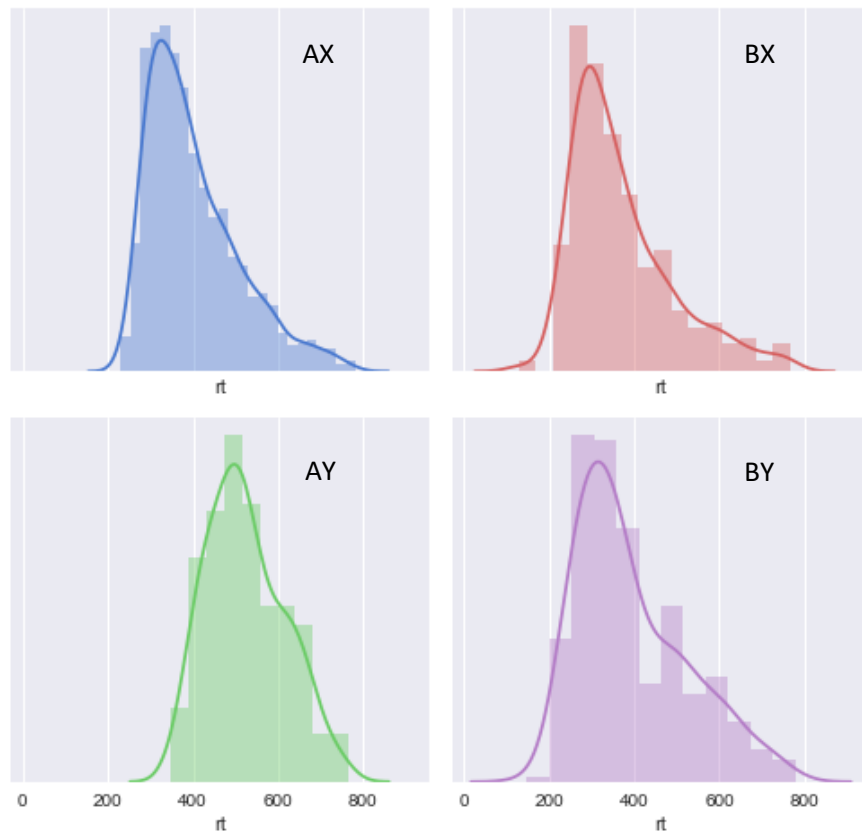
7. Wenn ja, geben Sie bitte Ihre E-Mail-Adresse an:

## Appendix C: Behavioral data

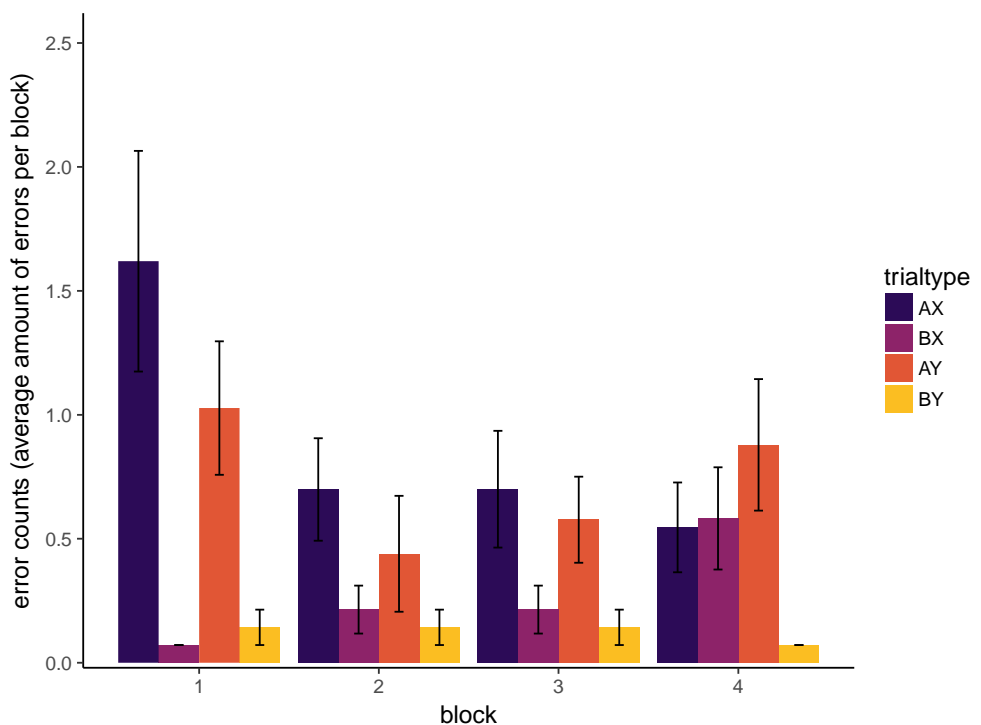
*Cross-correlations for demographic, cognitive performance and interview data. The variable gender is coded with male as 1 and female as 2.*



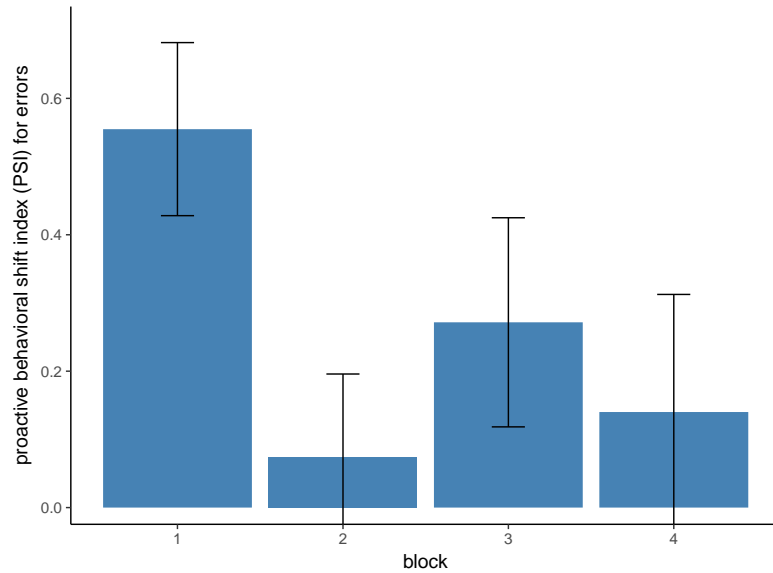
*Raw distributions of RT data divided by trialtypes AX (top left), BX (top right), AY (bottom left) and BY (bottom right).*



*Total error counts across blocks averaged over all subjects. Bars represent of  $\pm$  a single standard error of the mean.*

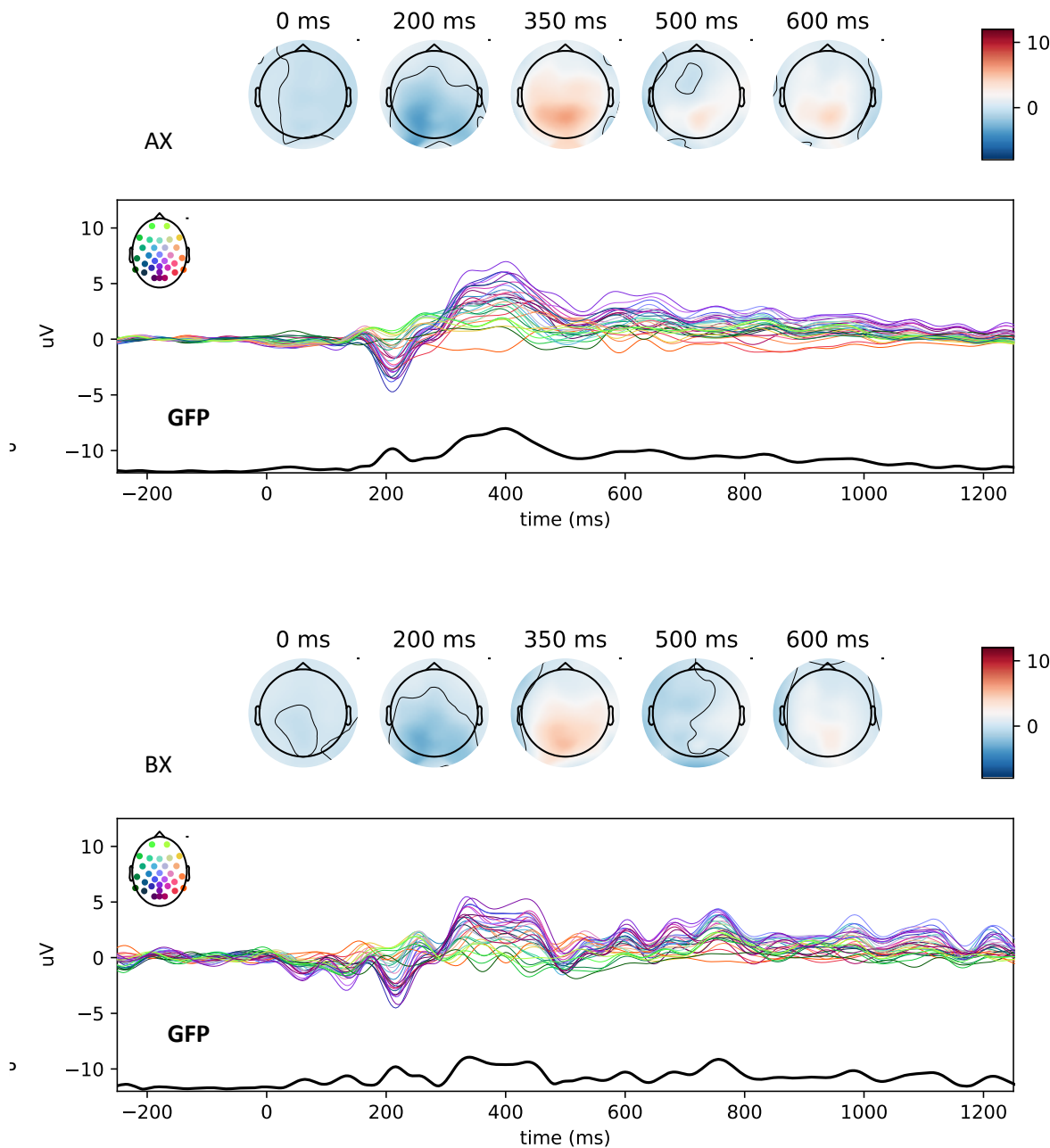


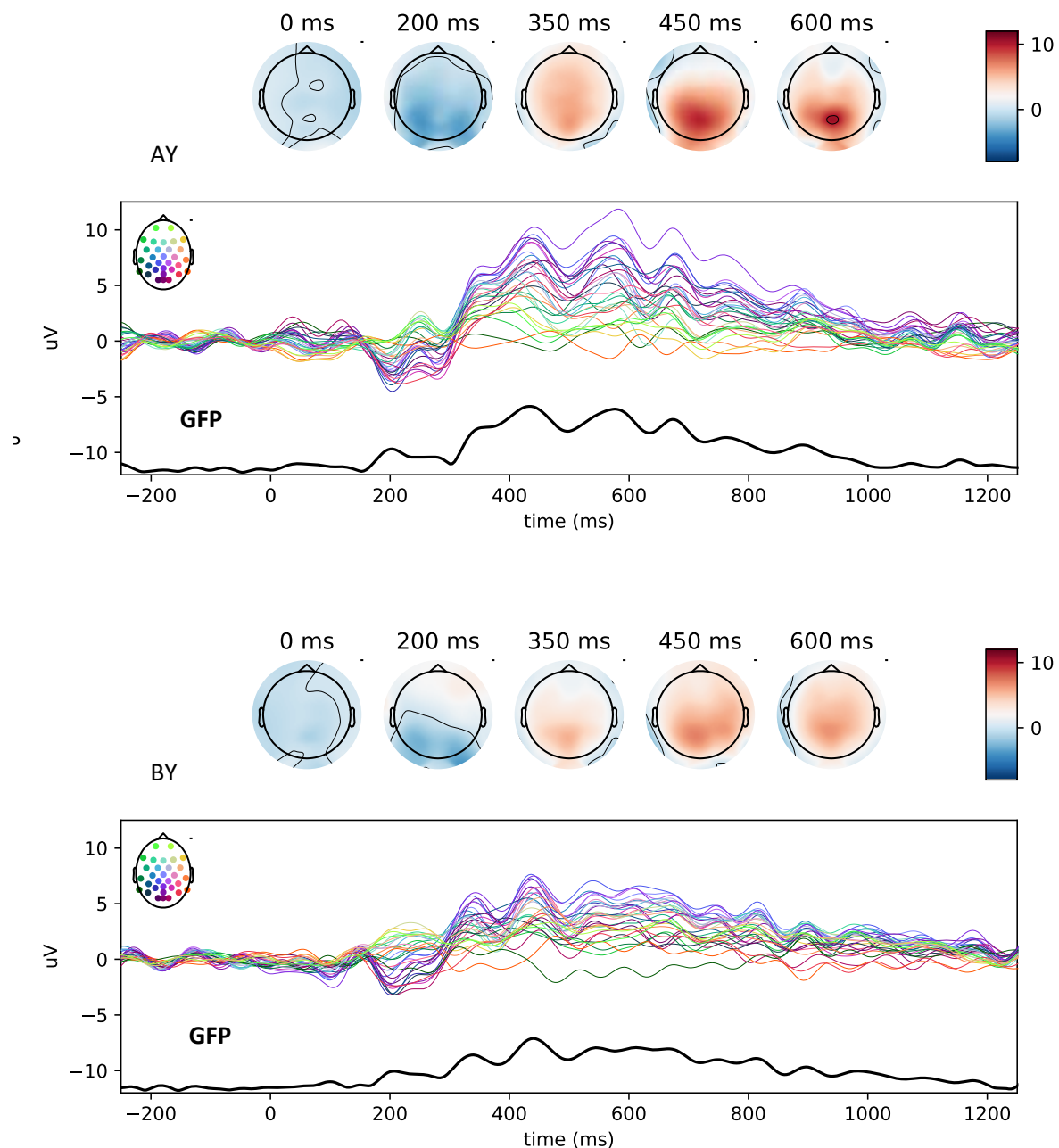
*PSI scores based on average error counts per block. Bars show the range of  $\pm$  a single standard error of the mean.*



## Appendix D: Supplementary ERP data

*Probe-locked ERPs for all channels.* ERPs were baseline corrected for the displayed time window of 250 ms before stimulus onset. Graphs show the 31 EEG channels color-coded for their spatial distribution across the scalp. A legend for spatial distribution of channels is provided with the colored head figure in the upper left corner of the ERP panel. The black graph depicts the GFP disregarding the ECG. Topographic maps on top show the averaged scalp distribution for an interval of 50 ms around the indicated time point.





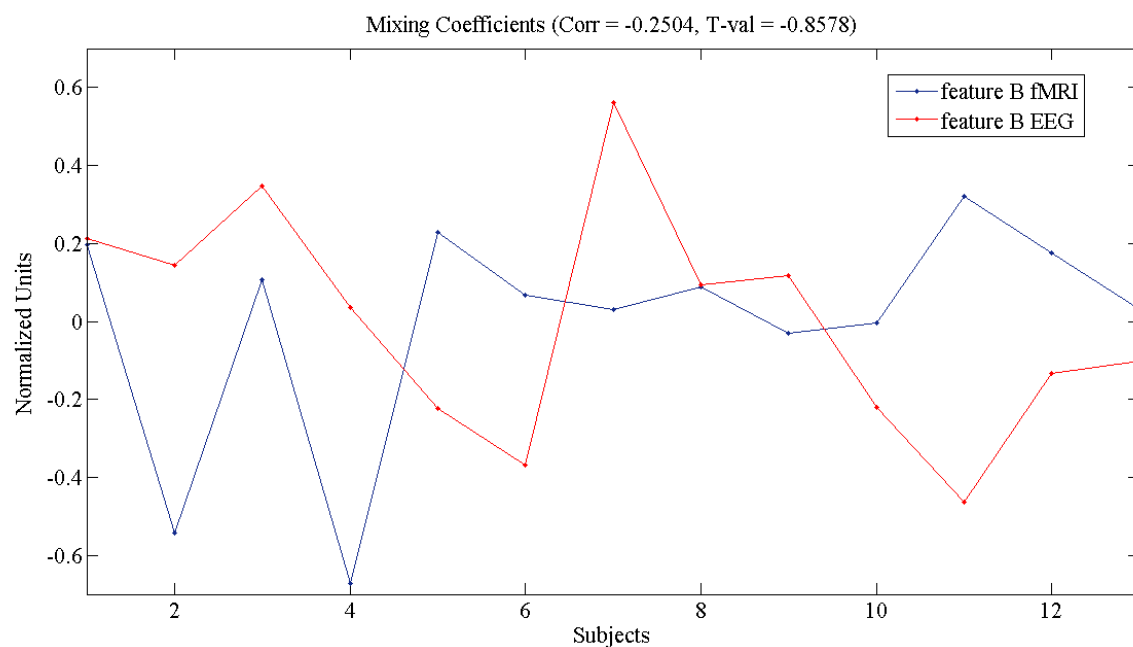
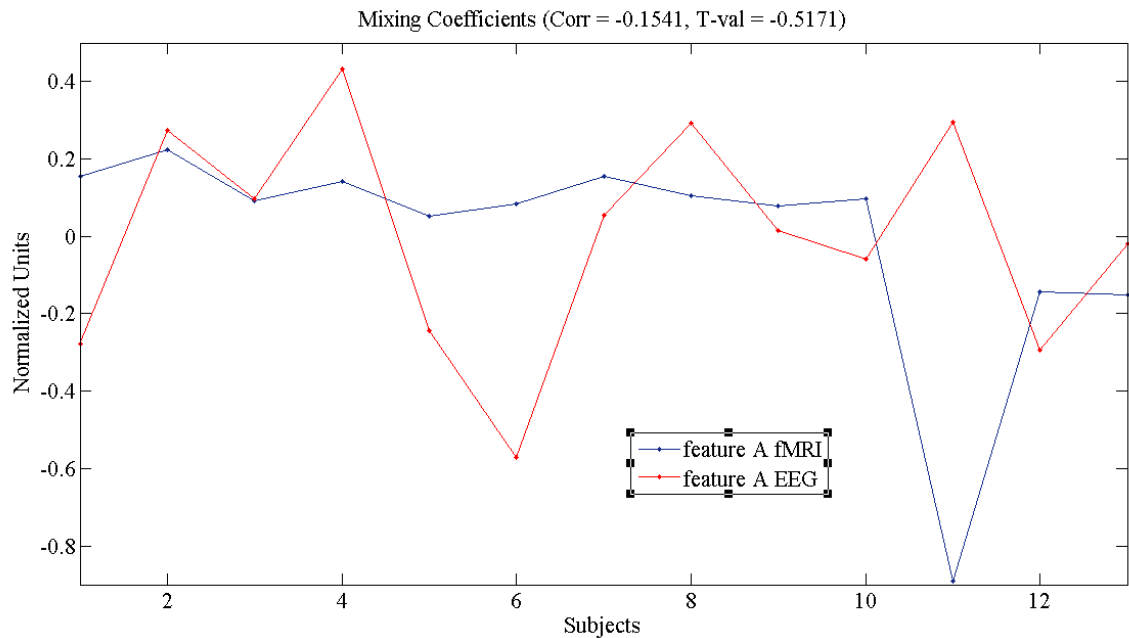
## Appendix E: Supplementary multimodal correlations

*Permutations tests of cross-correlation for all relevant univariate time series for cues.*

Variables	Theta	Alpha	Amplitude	IFG	MFG	Cingulate	PCG
<b>Cue A</b>							
Theta		-.4**	-.01	-.17*	-.13	-.15	-.12
Alpha			.04	.19*	.2*	.12	.04
Amplitude				.15	.18	.12	.12
IFG					.78**	.8*	.77*
MFG						.86*	.71**
Cingulate							.64**
PCG							
<b>Cue B</b>							
Theta		-.46**	.1	.48**	.42*	.43*	.4*
Alpha			.15	.1	.12*	.2	.01
Amplitude				-.01	-.05	-.2*	-.01
IFG					.89**	.72*	.65*
MFG						.8*	.68**
Cingulate							.7**
PCG							

*Note.* \* =  $p < .05$ , \*\* =  $p < .01$

*Correlations of mixing coefficient from the reported pICA components separated by cue (upper panel A, lower panel B). Red graphs show normalized values for mixing coefficient of the respective EEG feature and blue graphs those for the fMRI feature across all subjects. Correlation coefficients are Pearson correlations.*



## **Eigenständigkeitserklärung**

Hiermit versichere ich, dass ich die von mir eingereichte Masterarbeit selbstständig und ohne fremde oder unerlaubte Hilfe und ausschließlich mit den angegebenen Hilfsmitteln verfasst habe, ausgenommen Zitate aus publizierten Quellen, die eindeutig zitiert sind. Auch die Quellen von Abbildungen und Illustrationen so wie andere Materialien aus publizierten Werken sind angegeben.

14.05.2018, Marburg  
(Datum, Ort)

Malte Gräff, Malte Gräff  
(Name, Unterschrift)

## **Einverständniserklärung für die Veröffentlichung**

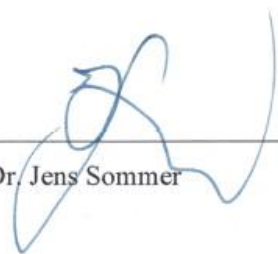
Ich, Malte Güth, erkläre mich damit einverstanden, dass die vorliegende Arbeit „The practicability of multimodal data fusion for simultaneous EEG-fMRI demonstrated on a cognitive control task“ in Bibliotheken allgemein zugänglich gemacht wird.

Dazu gehört, dass sie:

- von der Bibliothek der E
- +inrichtung, in der ich meine Arbeit angefertigt habe, zur Benutzung in ihren Räumen befreit gehalten wird;
- in konventionellen und maschinenlesbaren Katalogen, Verzeichnissen und Datenbanken verzeichnet wird;
- der UB für die lokale Benutzung und für Fernleihzwecke zur Verfügung steht;
- im Rahmen der urheberrechtlichen Bestimmungen für Kopierzwecke genutzt werden kann.

14.05.2018, Marburg  
(Datum, Ort)

Malte Güth



Dr. Jens Sommer

Prof. Dr. Dr. Martin Peper